SOUTHERN PLAINS
TRANSPORTATION CENTER

RESISTANCE OF ASPHALT COMPOSITES WITH RECYCLED MATERIALS TO WITHSTAND EXTREME TEMPERATURES

Rogelio Rodriguez, M.S.
Amit Bhasin, Ph.D., P.E.
Zahid Hossain, Ph.D., P.E.
Feroze Rashid, M.S.

SPTC14.1-30-F

Southern Plains Transportation Center
201 Stephenson Parkway, Suite 4200
The University of Oklahoma
Norman, Oklahoma 73019

DISCLAIMER

The contents of this report reflect the views of the authors, who are responsible for the facts and the accuracy of the information presented herein. This document is disseminated under the sponsorship of the Department of Transportation University Transportation Centers Program, in the interest of information exchange. The U.S. Government assumes no liability for the contents or use thereof. Mention of trade names or commercial products does not constitute endorsement or recommendations for use.

TECHNICAL REPORT DOCUMENTATION PAGE

1. REPORT NO.	2. GOVERNMENT ACCESSION NO.	3. RECIPIENTS CATALOG NO.
SPTC14.1-30-F		

4. TITLE AND SUBTITLE	5. REPORT DATE
Resistance of Asphalt Composites with Recycled Materials to withstand Extreme Temperatures	November 30, 2019
	6. PERFORMING ORGANIZATION CODE
7. AUTHOR(S)	8. PERFORMING ORGANIZATION REPORT
Rogelio Rodriguez, M.S., Amit Bhasin, Ph.D., P.E., Zahid Hossain, Ph.D., P.E., Feroze Rashid, M.S.	
9. PERFORMING ORGANIZATION NAME AND ADDRESS	10. WORK UNIT NO.
The University of Texas at Austin Arkansas State University	11. CONTRACT OR GRANT NO. DTRT13-G-UTC36
12. SPONSORING AGENCY NAME AND ADDRESS	13. TYPE OF REPORT AND PERIOD COVERED
Southern Plains Transportation Center 201 Stephenson Pkwy, Suite 4200 The University of Oklahoma Norman, OK 73019	Final June 2015 – May 2019
	14. SPONSORING AGENCY CODE

15. SUPPLEMENTARY NOTES

University Transportation Center

16. ABSTRACT

The asphalt industry has become particularly interested in the impact of recycled asphalt pavement (RAP)and additives such as rejuvenators on the behavior and performance of the material. The goal of this study was to evaluate the tensile strength characteristics of asphalt binders and composites in addition to their stiffness characteristics. The study was conducted in three parts: (1) the evaluation of tensile strength of asphalt binders with similar performance grades, (2) the evaluation of tensile strength of asphalt binders as a function of the amount of recycled asphalt binder added to the virgin binder as well field evaluation of binders with RAP, and (3) the influence of recycled asphalt and rejuvenators on the stiffness and tensile strength of asphalt mortars. In addition to these three objectives, this study also developed simplified methods to prepare and evaluate the tensile strength of asphalt binders and mortars as a material characterization tool to screen or evaluate the efficacy of RAP, rejuvenators, and other additives. Results show that similarly graded binders have a significant variability both in terms of their stiffness and strength and that rejuvenators can be used with RAP to achieve a balance of stiffness and strength. Finally, the proposed method using asphalt mortars can be used without extracting RAP binder to evaluate the relative performance of asphalt composites (as a screening tool) as a function of variables such as RAP content, RAP type, rejuvenator content, rejuvenator type, chemical additives, and binder source.

17. KEY WORDS	18. DISTRIBUTION STATEMENT
Recycled asphalt pavement (RAP), additives, binder, stiffness, strength	No restrictions. This publication is available at www.sptc.org and from the NTIS.

19. SECURITY CLASSIF. (OF THIS REPORT)	20. SECURITY CLASSIF. (OF THIS PAGE)	21. NO. OF PAGES	22. PRICE
Unclassified	Unclassified	165 + cover	

SI* (MODERN METRIC) CONVERSION FACTORS

APPROXIMATE CONVERSIONS TO SI UNITS

SYMBOL	WHEN YOU KNOW	MULTIPLY BY	TO FIND	SYMBOL
		LENGTH		
in	inches	25.4	millimeters	mm
ft	feet	0.305	meters	m
yd	yards	0.914	meters	m
mi	miles	1.61	kilometers	km
		AREA		
in^2	square inches	645.2	square millimeters	mm^2
ft^2	square feet	0.093	square meters	m^2
yd^2	square yard	0.836	square meters	m^2
ac	acres	0.405	hectares	ha
mi^2	square miles	2.59	square kilometers	km^2
		VOLUME		
fl oz	fluid ounces	29.57	milliliters	mL
gal	gallons	3.785	liters	L
ft^3	cubic feet	0.028	cubic meters	m^3
yd^3	cubic yards	0.765	cubic meters	m^3
		NOTE: volumes greater than 1000 L shall be shown in m^3		
		MASS		
oz	ounces	28.35	grams	g
lb	pounds	0.454	kilograms	kg
T	short tons (2000 lb)	0.907	megagrams (or "metric ton")	Mg (or "t")
		TEMPERATURE (exact degrees)		
°F	Fahrenheit	5 (F-32)/9 or (F-32)/1.8	Celsius	°C
		ILLUMINATION		
fc	foot-candles	10.76	lux	lx
fl	foot-Lamberts	3.426	candela/m^2	cd/m^2
		FORCE and PRESSURE or STRESS		
lbf	poundforce	4.45	newtons	N
lbf/in^2	poundforce per square inch	6.89	kilopascals	kPa

APPROXIMATE CONVERSIONS FROM SI UNITS

SYMBOL	WHEN YOU KNOW	MULTIPLY BY	TO FIND	SYMBOL
		LENGTH		
mm	millimeters	0.039	inches	in
m	meters	3.28	feet	ft
m	meters	1.09	yards	yd
km	kilometers	0.621	miles	mi
		AREA		
mm^2	square millimeters	0.0016	square inches	in^2
m^2	square meters	10.764	square feet	ft^2
m^2	square meters	1.195	square yards	yd^2
ha	hectares	2.47	acres	ac
km^2	square kilometers	0.386	square miles	mi^2
		VOLUME		
mL	milliliters	0.034	fluid ounces	fl oz
L	liters	0.264	gallons	gal
m^3	cubic meters	35.314	cubic feet	ft^3
m^3	cubic meters	1.307	cubic yards	yd^3
		MASS		
g	grams	0.035	ounces	oz
kg	kilograms	2.202	pounds	lb
Mg (or "t")	megagrams (or "metric ton")	1.103	short tons (2000 lb)	T
		TEMPERATURE (exact degrees)		
°C	Celsius	1.8C+32	Fahrenheit	°F
		ILLUMINATION		
lx	lux	0.0929	foot-candles	fc
cd/m^2	candela/m^2	0.2919	foot-Lamberts	fl
		FORCE and PRESSURE or STRESS		
N	newtons	0.225	poundforce	lbf
kPa	kilopascals	0.145	poundforce per square inch	lbf/in^2

*SI is the symbol for the International System of Units. Appropriate rounding should be made to comply with Section 4 of ASTM E380.
(Revised March 2003)

RESISTANCE OF ASPHALT COMPOSITES WITH RECYCLED MATERIALS TO WITHSTAND EXTREME TEMPERATURES

Final Report
November 2019

Rogelio Rodriguez, M.S.
and
Amit Bhasin, Ph.D., P.E.
The University of Texas at Austin

Zahid Hossain, Ph.D., P.E.
and
Feroze Rashid, M.S.
Arkansas State University

Southern Plains Transportation Center

ACKNOWLEDGMENTS

The authors acknowledge the financial support of the Southern Plains Transportation Institute for supporting this study. The authors would also like to acknowledge the Texas Department of Transportation and Arkansas Department of Transportation for their help in providing samples for this study, Prof. Adalberto Faxina from University of Sao Paulo, Sao Carlos for their collaboration and material samples on aspects related to the evaluation of rejuvenators, Cannon Instrument Company for loaning us the Bending Beam Rheometer (BBR) Pro that allows the testing of specimens until failure, and Dr. Delmar Salomon for his help with several parts of this study.

TABLE OF CONTENTS

List of Figures ix

List of Tables xiii

Chapter 1. Introduction 1

1.1 Problem Statement . . . 1
1.2 Motivation . . . 2
1.2.1 Recycled Materials . . . 2
1.2.2 Climate Change and Relevance to SPTC . . . 3
1.2.3 Drawbacks of Current Material Evaluation Methods . . . 4
1.3 Overview of this report . . . 6

Chapter 2. Background and Literature Review 7

2.1 Background on Performance Grading of Asphalt Binders . . . 7
2.2 Low Temperature Properties of Asphalt Binder . . . 8
2.2.1 Background . . . 8
2.2.2 Low temperature properties of asphalt binder . . . 10
2.3 Significance of Evaluating Mortar or FAM . . . 12
2.4 Summary and Scope . . . 13

Chapter 3. Laboratory and Field Performance of Recyled Binders 17

3.1 Introduction . . . 17
3.2 Objectives . . . 18
3.3 Background . . . 19
3.4 Materials . . . 21
3.5 Methodology . . . 23
3.6 Results and Discussion . . . 26
3.6.1 In-service Pavement Condition . . . 26
3.6.2 Construction Weather Condition . . . 29
3.6.3 Superpave Test Results . . . 31
3.6.3.1 Rotational Viscosity (RV) Test . . . 31
3.6.3.2 Dynamic Shear Rheometer (DSR) Test . . . 33

3.6.3.3 Bending Beam Rheometer (BBR) Test 38
3.6.4 AFM Test Results 44
3.6.5 Effect of Rejuvenator 47
3.7 Conclusion 51
3.7.1 Properties of RAP and Pavements 51
3.7.2 Superpave Test Results 52
3.7.3 AFM Test Results 53
3.7.4 Influence of Rejuvenator 53

Chapter 4. Specimen Fabrication and Test Method 54
4.1 Test Devices 54
4.1.1 Bending Beam Rheometer 54
4.1.2 Instron E1000 57
4.2 Specimen Fabrication 59
4.2.1 Specimen preparation for binders 59
4.2.2 Specimen fabrication for mortars 60
4.2.2.1 Direct compaction method 61
4.2.2.2 Superpave gyratory compactor method 67
4.2.3 Mortar Beam Specimen Preparation 70
4.3 Comparison of simple creep results from BBR to BBR-Pro 71
4.4 Summary 73

Chapter 5. Evaluation of Asphalt Binders and Mortars 74
5.1 Overview 74
5.2 Variation in Tensile Strength of Binders with Similar PG 75
5.2.1 Materials and Tests 75
5.2.2 Results and discussion 76
5.3 Variation in Tensile Strength of Binders with Change in Recycled Binder Content 93
5.3.1 Materials and Tests 93
5.3.2 Results and discussion 97
5.4 Evaluation of Influence of Recycling Agents and Recycled Binder on Properties of Asphalt Mortars 110
5.4.1 Materials and Tests 110
5.4.2 Results and discussion 113

5.5 Concluding Remarks 124

Chapter 6. Conclusions and Summary **131**

6.1 Fabrication of Mortar Specimens 131

6.2 Investigation of Binders with Similar PG 131

6.3 Influence of Recycling Agents and Recycled Binder on Properties of Asphalt Mortars 132

References **133**

Appendix A **139**

Appendix B **163**

Appendix C **167**

LIST OF FIGURES

Figure 3.1. Location of RAP Sampling Sites 22
Figure 3.2. Test Plan for RAP Blended Binder Characterization 24
Figure 3.3. Average IRI Values for RAP1 - RAP4 Pavement Sections 27
Figure 3.4. Average Rutting Depth for RAP1 - RAP4 Pavement Sections . . 29
Figure 3.5. Weather Data Plotted against Time for RAP1: a) Starting and b) Ending of the Construction Work 30
Figure 3.6. Viscosity of RAP1 Binder Blends 31
Figure 3.7. Comparative Status of Viscosities for RAP1-RAP4 Blends 32
Figure 3.8. DSR Test at High Temperatures for RAP1 Blends 33
Figure 3.9. DSR Test at Intermediate Temperatures for RAP1 Blends . . . 34
Figure 3.10. DSR Test at High Temperatures for RAP2 Blends 35
Figure 3.11. DSR Test at Intermediate Temperatures for RAP2 Blends . . . 36
Figure 3.12. DSR Test at High Temperatures for RAP3 Blends 37
Figure 3.13. DSR Test at Intermediate Temperatures for RAP3 Blends . . . 38
Figure 3.14. DSR Test at High Temperatures for RAP4 Blends 39
Figure 3.15. DSR Test at Intermediate Temperatures for RAP4 Blends . . . 40
Figure 3.16. BBR Test Data of Control 41
Figure 3.17. Different Phases of Asphalt Binders (PG 64-22) 44
Figure 3.18. Morphology of RAP3 Asphalt Blends: (i) - (iii) 25%, 40%, and 60% Unaged Blends, (iv) - (vi) 25%, 40%, and 60% RTFO-aged Blends, and (vii) - (ix) 25%, 40%, and 60% PAV-aged Blends, Respectively 45
Figure 3.19. Morphology of RAP4 Asphalt Blends: (i) - (iii) 25%, 40%, and 60% Unaged Blends, (iv) - (vi) 25%, 40%, and 60% RTFO-aged Blends, and (vii) - (ix) 25%, 40%, and 60% PAV-aged Blends, Respectively 46
Figure 3.20. Penetration Test Data of Rejuvenated Blends 48
Figure 3.21. Comparative Viscosity (mPa-s) Data of Rejuvenated Blends . . 49
Figure 3.22. Compaction and Mixing Temperatures for Rejuvenated Blends . 50
Figure 3.23. DSR Test Data of Rejuvenated RAP Blends 51
Figure 4.1. TE-BBR Pro Thermoelectric Bending Beam Rheometer 55
Figure 4.2. TE-BBR and TE-BBR Pro Three Point Loading System 56

Figure 4.3. TE-BBR Pro Four Point Loading System 57
Figure 4.4. Instron E1000 Plexiglass temperature chamber with added insulation 58
Figure 4.5. Instron E1000 Supports Used for Mortar Testing 59
Figure 4.6. Asphalt Binder Beam in Standard Molds Described in AASHTO T 313 60
Figure 4.7. Benchtop Sample Fabrication Setup for FAM Specimens 62
Figure 4.8. Compaction Mold Showing Separated Pieces and Sample Position 63
Figure 4.9. Constructed Compaction Mold with Compaction Plunger Used in Direction Compaction Method 64
Figure 4.10. Side View of SGC sample showing the slicing locations 68
Figure 4.11. Top View of SGC sample showing the slicing locations 69
Figure 4.12. Results from Creep Test Performed in the Standard BBR and BBR Pro 72
Figure 5.1. Typical Stress Results from Standard Creep Tests on Various PG Binders 77
Figure 5.2. Typical Strain Results from Standard Creep Tests on Various PG Binders 78
Figure 5.3. Typical Compliance Results from Standard Creep Tests on Various PG Binders 79
Figure 5.4. Compliance Results for a PG 64-22 Binder Tested at −12 °C . . 81
Figure 5.5. Typical Stress Results for Monotonic Load Test to Failure . . . 82
Figure 5.6. Typical Strain Results for Monotonic Load Test to Failure . . . 83
Figure 5.7. Average Tensile Strength for PG XX-22 Binders Tested at −6 °C 84
Figure 5.8. Average Tensile Strength for PG XX-22 Binders Tested at −12 °C 85
Figure 5.9. Average Tensile Strength for PG XX-22 Binders Tested at −18 °C 86
Figure 5.10. Average Tensile Strength for PG XX-28 Binders Tested at −12 °C 87
Figure 5.11. Average Tensile Strength for PG XX-28 Binders Tested at −18 °C 88
Figure 5.12. Average Tensile Strength for PG XX-28 Binders Tested at −24 °C 89
Figure 5.13. Average Tensile Strain for PG XX-22 Binders Tested at −6 °C . 91
Figure 5.14. Average Tensile Strain for PG XX-22 Binders Tested at −12 °C . 92
Figure 5.15. Average Tensile Strain for PG XX-22 Binders Tested at −18 °C . 93
Figure 5.16. Average Tensile Strain for PG XX-28 Binders Tested at −12 °C . 94
Figure 5.17. Average Tensile Strain for PG XX-28 Binders Tested at −18 °C . 95
Figure 5.18. Average Tensile Strain for PG XX-28 Binders Tested at −24 °C . 96

Figure 5.19. Average D_0-values With Respect to Increasing RAP Binder Content at −9 °C 99
Figure 5.20. Average D_0-values With Respect to Increasing RAP Binder Content at −12 °C 100
Figure 5.21. Average D_1-values With Respect to Increasing RAP Binder Content at −9 °C 101
Figure 5.22. Average D_1-values With Respect to Increasing RAP Binder Content at −12 °C 102
Figure 5.23. Average m-values With Respect to Increasing RAP Binder Content at −9 °C 103
Figure 5.24. Average m-values With Respect to Increasing RAP Binder Content at −12 °C 104
Figure 5.25. Average Tensile Strength for RAP Blended Binders of Varying Content at −9 °C 106
Figure 5.26. Average Tensile Strength for RAP Blended Binders of Varying Content at −12 °C 107
Figure 5.27. Average Tensile Strain for RAP Blended Binders of Varying Content at −9 °C 108
Figure 5.28. Average Tensile Strain for RAP Blended Binders of Varying Content at −12 °C 109
Figure 5.29. Typical Stress Results from Standard Creep Tests on Mortar Beams 114
Figure 5.30. Typical Strain Results from Standard Creep Tests on Mortar Beams 115
Figure 5.31. Typical Compliance Results from Standard Creep Tests on Mortar Beams 116
Figure 5.32. Flow Chart Illustrating the Standard Creep Analysis Process . . 117
Figure 5.33. Compliance Results from a Standard Creep Test Performed on a Mortar Beam at 6 °C 118
Figure 5.34. Average D_0-values With Respect to Temperature on Mortar Beams 119
Figure 5.35. Average D_1-values With Respect to Temperature on Mortar Beams 120
Figure 5.36. Average m With Respect to Temperature on Mortar Beams . . 121
Figure 5.37. Typical Stress Results from Monotonic Load Tests on Mortar Beams 122
Figure 5.38. Typical Strain Results from Monotonic Load Tests on Mortar Beams 123
Figure 5.39. Flow Chart Illustrating the Monotonic Load Analysis Process . . 124

Figure 5.40. Average Tensile Strength for Mortar Mixes with a 24.96 N min^{-1} Loading Rate 125
Figure 5.41. Average Tensile Strength for Mortar Mixes with a 12.48 N min^{-1} Loading Rate 126
Figure 5.42. Average Tensile Strength for Mortar Mixes with a 6.24 N min^{-1} Loading Rate 127
Figure 5.43. Average Tensile Strain for Mortar Mixes with a 24.96N/min. Loading Rate 128
Figure 5.44. Average Tensile Strain for Mortar Mixes with a 12.48N/min. Loading Rate 129
Figure 5.45. Average Tensile Strain for Mortar Mixes with a 6.24N/min. Loading Rate 130
Figure A.1. Weather Data for RAP1 (July, 2001). 143
Figure A.2. Weather Data for RAP1 (August, 2001). 144
Figure A.3. Weather Data for RAP1 (April, 2002). 145
Figure A.4. Weather Data for RAP1 (June, 2002). 146
Figure A.5. Weather Data for RAP2 (April, 2002). 147
Figure A.6. Weather Data for RAP2 (March, 2003). 148
Figure A.7. Weather Data for RAP2 (June, 2003). 149
Figure A.8. Weather Data for RAP2 (August, 2003). 150
Figure A.9. Weather Data for RAP2 (September, 2003). 151
Figure A.10. Weather Data for RAP2 (October, 2003). 152
Figure A.11. Weather Data for RAP2 (January, 2004). 153
Figure A.12. Weather Data for RAP3 (July, 2001). 154
Figure A.13. Weather Data for RAP3 (August, 2001). 155
Figure A.14. Weather Data for RAP3 (April, 2002). 156
Figure A.15. Weather Data for RAP3 (June, 2002). 157
Figure A.16. Weather Data for RAP4 (May, 2002). 158
Figure A.17. Weather Data for RAP4 (June, 2002). 159
Figure A.18. Weather Data for RAP4 (December, 2002). 160
Figure A.19. Weather Data for RAP4 (August, 2004). 161
Figure B.20. Viscosity of RAP2 Binder Blends. 163
Figure B.21. Viscosity of RAP3 Binder Blends. 164
Figure B.22. Viscosity of RAP4 Binder Blends. 165

LIST OF TABLES

Table 3.1. Type and Doses of the Rejuvenator in Application 21
Table 3.2. Information of Samples Used in this Study 23
Table 3.3. Laboratory Test Plan 25
Table 3.4. BBR Test data of the Control Binder 38
Table 3.5. Low PG Temperature from BBR and DSR Test (RAP1 and RAP2) 42
Table 3.6. Low PG Temperature from BBR and DSR Test (RAP3 and RAP4) 43
Table 4.1. Gradation Proportioning of Aggregate for FAM Mix 62
Table 4.2. Compaction Methods Used to Achieve Bulk Specific Gravity Goal 66
Table 5.1. Summary of Asphalt Binders Tested for Strength with Similar PG 76
Table 5.2. Test Matrix for Simple Creep Tests Performed on Recycled Binder Specimens 97
Table 5.3. Composition of the Mortar Mixes Used in This Study 111
Table 5.4. Mortar Mix Testing Regimen 113
Table A.1. Calculation of Rutting and Roughness Data for RAP1 139
Table A.2. Calculation of Rutting and Roughness Data for RAP2 140
Table A.3. Calculation of Rutting and Roughness Data for RAP3 141
Table A.4. Calculation of Rutting and Roughness Data for RAP4 142
Table C.5. Calculation of Low PG Temperature for 25% RAP1 168
Table C.6. Calculation of Low PG Temperature for 40% RAP1 169
Table C.7. Calculation of Low PG Temperature for 60% RAP1 170
Table C.8. Calculation of Low PG Temperature for 25% RAP2 171
Table C.9. Calculation of Low PG Temperature for 40% RAP2. 172
Table C.10. Calculation of Low PG Temperature for 60% RAP2 173
Table C.11. Calculation of Low PG Temperature for 25% RAP3 174
Table C.12. Calculation of Low PG Temperature for 40% RAP3 175
Table C.13. Calculation of Low PG Temperature for 60% RAP3 176
Table C.14. Calculation of Low PG Temperature for 25% RAP4 177
Table C.15. Calculation of Low PG Temperature for 40% RAP4 178
Table C.16. Calculation of Low PG Temperature for 60% RAP4 179

EXECUTIVE SUMMARY

The Performance Grading or PG system used to specify the properties of asphalt binder prescribes an operational temperature range within which the binder is expected to perform satisfactorily without resulting in rutting, fatigue cracking or thermal cracking as a distress. On the low-temperature and thermal cracking end, this system uses both a metric related to stiffness and rate of relaxation (m value) to establish a low temperature grade for a given asphalt binder. Although these parameters provide some information on the rate of relaxation and overall stiffness of the asphalt binder they do not include an evaluation of the tensile strength of the asphalt binder. The tensile strength of the binder is critical to understanding and modeling its resistance to cracking including thermal cracking.

The asphalt industry has become particularly interested in the impact of recycled asphalt pavement (RAP) and additives such as rejuvenators on the behavior and performance of the material. The goal of this study was to evaluate the tensile strength characteristics of asphalt binders and composites in addition to their stiffness characteristics. The study was conducted in three parts: (1) the evaluation of tensile strength of asphalt binders with similar performance grades, (2) the evaluation of tensile strength of asphalt binders as a function of the amount of recycled asphalt binder added to the virgin binder as well field evaluation of binders with RAP, and (3) the influence of recycled asphalt and rejuvenators on the stiffness and tensile strength of asphalt mortars. In addition to these three objectives, this study also developed simplified methods to prepare and evaluate the tensile strength of asphalt binders and mortars as a material characterization tool to screen or evaluate the efficacy of RAP, rejuvenators, and other additives. Results show that similarly graded binders have a significant variability both in terms of their stiffness and strength and that rejuvenators can be used with RAP to achieve a balance of stiffness and strength. Finally, the proposed method using asphalt mortars can be used without extracting RAP binder to evaluate the relative performance of asphalt composites (as a screening tool) as a function of variables such as RAP content, RAP type, rejuvenator content, rejuvenator type, chemical additives, and binder source.

CHAPTER 1. INTRODUCTION

1.1 PROBLEM STATEMENT

Recycled asphalt pavements and shingles (RAP or RAS) are increasingly being incorporated in the production of asphalt mixtures for pavement construction and preservation purposes. For brevity the term RAP is used through the remainder of this proposal although such recycled materials may include RAS. A study of the climate in the south central states (TX, OK, AR, LA, MI, TN) reported that that there has been an increase in the number of extreme cold days over the past century (Henderson and Muller, 1997). Also, several geographic areas within the Southern Plains Transportation Center (SPTC) region are susceptible to extreme diurnal temperature changes. It is well recognized that mixtures containing RAP or RAS may have an increased susceptibility to low-temperature cracking. Unless, proper design and performance evaluation tools are put into practice, the increased occurrence of extreme cold days and diurnal temperature changes combined with an increase in the use of RAP mixes will increase the risk of pavement failure in the years ahead.

A national pooled fund study (Marasteanu et al., 2007) has recognized the need for a simple test method to identify asphalt mixtures susceptible to low temperature cracking. Typical Superpave tests conducted solely on the pure asphalt binder do not accurately reflect the low temperature cracking resistance of asphalt mixtures because of the missing aggregate mineral - asphalt binder interaction effects. Also, tests on pure asphalt binders are difficult to execute while evaluating mixtures with RAP and/or RAS, since this would require binder recovery from RAP/RAS mixes. On the other extreme, tests conducted on full asphalt mixtures require much longer time and resources (e.g., manpower, equipment, etc.). The objective of this study was use low-temperature tests on asphalt binders as well as mortars with and without RAP and RAS (binder or as is) as a surrogate to determine the resistance of the asphalt materials to low temperature cracking. The use of mortars as a surrogate for low-temperature evaluation has several advantages:

- it is less resource intensive to test compared to full mixtures,
- it evaluates the matrix where most of the cracking is concentrated,
- it captures the influence of mineral - binder interaction,
- it can be used to test separated fines from fractionated RAP or RAS to evaluate

the influence of RAP or RAS, and
- it can be evaluated using devices similar to or already being used to evaluate asphalt binders.

The anticipated deliverable from this research is an easy to use test method and a simplified analysis approach that can be used by material and pavement engineers to evaluate cracking resistance of asphalt materials.

The findings from this research are particularly relevant to ensure durability of pavements in the SPTC region. The states within this region are not only facing a general increase in the number of extreme low temperature days but there are many regions within the SPTC that also experience very rapid diurnal changes in temperature. The SPTC region states will benefit from the technology delivered by this research by ensuring durability of asphalt mixtures that are increasingly incorporating higher percentages of RAP.

1.2 MOTIVATION

1.2.1 Recycled Materials

According to the National Asphalt Paving Association (NAPA) based on a survey conducted by the Federal Highway Administration (FHWA), the amount of RAP used in asphalt pavement was approximately 56 million tons in 2009, 62 million tons in 2010, and 68 million tons in 2012 (National Asphalt Paving Association). While this number is only expected to grow over time, several states are also concerned about the potential affect of RAP on the durability of asphalt pavements. For example, several state DOTs do not allow for more than approximately 20 to 25% RAP without extensive testing, evaluation and design of asphalt mixtures.

It is well established that owing to the highly oxidized binder in RAP materials, mixtures containing RAP have relatively higher stiffness and reduced rates of relaxation compared to mixtures without any RAP. Consequently, RAP mixtures have an increased resistance to permanent deformation or rutting. However, the increased stiffness and reduced rates of relaxation also translate into a higher accumulation of thermal stresses as the pavement temperature cools. Ultimately, the material fails in tension if these stresses were to exceed the tensile strength of the mix. It is important to emphasize that both stiffness and strength of the material play a role in dictating the cracking resistance of the asphalt materials (Marasteanu et al., 2007). On the other hand, recent studies have also shown

that although recycled or aged binders have a higher stiffness and reduced rates of relaxation, these binders also show an increase in the fatigue or fracture resistance (Arega Z.Z. et al., 2013; Sultana et al., 2014). Therefore, it is possible to design durable asphalt mixtures containing higher amount of RAP. The missing link to do so, is the ability to characterize the relaxation modulus as well as the strength of the material as a function of temperature. Also, when these basic material properties are known it is possible for the end user to estimate the fracture temperature for any given cooling profile or rate of cooling.

1.2.2 Climate Change and Relevance to SPTC

There are two environmental characteristics that govern low temperature cracking: (i) the lowest pavement temperature, and (ii) the cooling rate of the pavement. While the states within the SPTC may not be regarded as regions with extreme low temperatures in the United States, these states do in fact experience high fluctuations in the diurnal temperatures. Such fluctuations translate into higher rates of cooling, which results in reduced relaxation in flexible pavements and a concomitant build up of thermal stresses and susceptibility to cracking. For example, climate data from a weather station in Pierce, Texas suggests that it is not unusual to have up to 13 °C to 14 °C variation in the daily temperature during the winter season (Leathers et al., 1998). In fact, according to the National Oceanic and Atmospheric Administration, Texas and Oklahoma Panhandles experience diurnal temperature changes of approximately 20 °C. In addition to the extreme diurnal changes in the temperature, there is also a gradual increase in the extreme low temperature days. For example, a study of the climate in the south central states (TX, OK, AR, LA, MI, TN) reported that that there has been an increase in the number of extreme cold days over the past century (Henderson and Muller, 1997). Another study that evaluated the climate change trends in the United States and other countries reported that although the mean minimum temperatures have generally increased over the years, there has also been a consistent increase in the extreme minimum seasonal temperatures with little or no increase in the maximum temperature (Karl et al., 1991). In summary, there is an increasing trend in terms of the extreme cold temperature days as well as extreme changes in daily temperatures. This trend in combination with an increased use of RAP and current practice for material selection, that is largely based on asphalt binders without recycled materials, is very likely to result in a scenario where states may be facing

much shorter than expected pavement service lives.

1.2.3 Drawbacks of Current Material Evaluation Methods

Most of the current methods used to evaluate the low-temperature cracking resistance of asphalt mixtures (with or without RAP) are focused on either evaluating the asphalt binder or the asphalt mixture. For example, the current performance grade (PG) specification to evaluate asphalt binders is primarily based on the use of the Bending Beam Rheometer (BBR). The BBR is an excellent tool to measure the low temperature stiffness (S) and rate of relaxation (m-value) of the asphalt binder. In rare cases when the stiffness value meets to fail the requirements, the specification allows for a strength test (DTT or direct tension test). The metrics obtained using the BBR are useful in estimating the tensile stresses being developed in the material as the pavement temperature falls. Higher stiffness or lower m-value are indicators of higher thermal stresses. However, failure only occurs when the thermal stresses (in combination with external load related stresses), exceed the tensile strength of the material. The BBR does not provide a measure for the strength of the material. Also, in order to use the BBR to evaluate binder in the RAP mixtures, one would have to (i) recover the binder from the RAP material and (ii) blend the recovered binder with the virgin binder and assuming that complete comingling also occurs in the mixture. Finally, according to the findings from a national pooled fund study, the type of aggregate also affects the low temperature cracking resistance of the asphalt binder (Marasteanu et al., 2007). From the point of view of a purchase specification, it is not possible to eliminate the need for an exclusive binder test. However, from the performance prediction point of view, relying on binder specifications as a measure of low-temperature cracking resistance has three major drawbacks summarized from the discussion above: (i) it does not measure the strength of the binder, which is a completely different attribute and can be significantly different especially for RAP modified binders, (ii) it cannot be adapted for use with mixtures containing RAP without the tedious process of recovering the binder from the RAP and assuming that complete co-mingling of RAP and virgin binder occurs, and (iii) it does not take into account the influence of mineral - binder interactions, if any.

Another method that is used to evaluate the low-temperature cracking resistance of an asphalt mixture is to evaluate the full asphalt mixture as a whole. The most common test in this regard is the thermal stress restrained specimen test (TSRST) method. In this test, the test specimen is cooled at a specific rate while restricting any thermal strains

and measuring the corresponding thermal stress that develops. The temperature, at which the sample breaks, is called fracture temperature and corresponding stress is termed as fracture strength. Due to the simplicity of the test, TSRST has been widely used for predicting low temperature cracking potential of an asphalt mix. However, there are several serious limitations of the TSRST method. For example, material heterogeneity of asphalt concrete, minor misalignments or asymmetry of specimens can lead to rotation of end plates (even when the specimen is properly centered) resulting in non-uniform stress distribution and inaccurate results (Velásquez et al., 2009). It has also been noted that specimen size can alter fracture temperature. The TSRST test is conducted at a constant cooling rate of $10\,^{\circ}\mathrm{C\,h^{-1}}$, which might not represent the actual field scenario. Other studies have also shown that the TSRST does not accurately reflect the performance of asphalt mixtures containing polymer modified binders (Roy and Hesp, 2001). Finally, non-technical drawbacks of the TSRST are that (i) it requires specialized capital equipment to conduct the test, (ii) it also requires a constant supply of a coolant such as liquid nitrogen to control the temperature of the test temperature, and (iii) the specimen preparation takes a very long time (fabrication and gluing).

Ongoing research studies have tried to overcome the limitations of the binder and mixture test methods discussed above to develop a simple and easy to use method that can predict the low temperature cracking resistance of asphalt binders and/or mixtures. For example, Hesp and co-workers have developed a double edged notch test (DENT) test to evaluate the low-temperature cracking resistance of asphalt binders (Kodrat et al., 2007). While results from the DENT test correlate well with the field performance, it would still require specialized capital equipment and extensive effort to test RAP binders using this approach. Marasteanu and co-workers have evaluated the use of the BBR with small slivers of asphalt mixtures to evaluate low-temperature cracking resistance of asphalt mixtures (Falchetto et al., 2014). However, this test method has been critiqued for its use of test specimens that are considerably smaller than the largest particle size in the mixture. Behnia et al. have developed the use of an acoustic based method to evaluate the low-temperature cracking resistance of asphalt mixtures (Behnia and Dave, 2011). However, they have also concluded that this method must be used in conjunction with mechanical tests to evaluate the low-temperature cracking resistance of asphalt mixtures.

One of the main goals of this study was to overcome some of the aforementioned limitations of the asphalt binder- and mixture-based test methods by using asphalt mortar as a surrogate to measure the low-temperature cracking resistance of the asphalt materials

(with or without RAP). The proposed method is not only easy to conduct and execute by state DOTs but will also add to the body of knowledge directly towards a more mechanistic approach to design asphalt mixtures. The test method will also serve as a valuable tool to evaluate different rejuvenators and chemical additives that can be used to design asphalt mixtures with RAP and promote the increase in RAP content in asphalt mixtures. It is important to recognize that the use of mortars or fine aggregate matrix (FAM) proposed in this study is not in lieu of mixture testing. Rather tests at this length scale can serve as a preliminary valuable screening tool to identify affects or material combinations that are of the most interest for further examination using mixture tests.

1.3 OVERVIEW OF THIS REPORT

This report covers the findings from the aforementioned research study. Specifically, Chapter 2 of this report presents a more detailed review of the current binder grading system, its limitations particularly in the context of low temperature properties, and a more detailed review of the relevance of testing mortars or FAM. Chapter 3 covers results from the part of the study that related to PG evaluation of asphalt binders, with and without RAP as well as a fundamental examination of the influence of RAP on the asphalt binder microstructure. Chapters 4 and 5 cover the more unconventional tests and methods that focus on both the stiffness and strength of asphalt binders and mortars. Chapter 4 covers a description of the testing devices, test methods, and specimen fabrication procedures. Standard devices and methods used in the PG system are not covered. Emphasis is placed on the newer devices and/or method variations that were developed as a part of this study. Chapter 5 presents the findings from tests conducted using asphalt binders and mortars. Specifically, this chapter examines the variability in the stiffness and strength of binders with similar PG without the addition of RAP. This chapter also examines the influence of RAP on both the stiffness and strength of asphalt binders using two different test methods. Finally, Chapter 5 presents an overview of the influence of RAP and several different rejuvenator combinations on the stiffness and strength of asphalt mortars.

CHAPTER 2. BACKGROUND AND LITERATURE REVIEW

2.1 BACKGROUND ON PERFORMANCE GRADING OF ASPHALT BINDERS

In the United States, grading systems are established by organizations such as the Federal Highway Administration (FHWA), the American Society for Testing and Materials (ASTM), and Departments of Transportation, as a means to specify the quality of binder used for pavement construction as well as to serve as a purchase specification. The first asphalt binder grading system that was implemented in the United States was the penetration grading system in 1931 (Roberts et al., 1996). This grading system was based around the Penetrometer. The Penetrometer uses a standard needle and 100 g weight to penetrate an asphalt binder for 5 s at 25 °C. The separate penetration categories were designed to help delineate binders for certain climate conditions (Roberts et al., 1996). The penetration grading system, that was implemented and used widely around the U.S. and is still being used in various parts of the world, incorporates other properties such as softening point, the flash point, the ductility, and the solubility of the asphalt binder in addition to the penetration.

In an attempt to enhance the penetration grading system, a viscosity test was developed, which eventually lead to a shift towards the viscosity grading system. The viscosity grading system is similar to that of the penetration grading system in that it incorporates many of the same tests. A significant difference between the two grading systems is the viscosity test, which measures the viscosity of asphalt binder at two temperatures 60 °C and 135 °C (Roberts et al., 1996). The viscosity grading system was advantageous in that it used a more fundamental property, viscosity, to determine the grade of the binder (Roberts et al., 1996). Subsequent improvements to the viscosity grading system included incorporating the influence of aging on the performance of the asphalt binder using aged residue or AR.

The penetration, viscosity, and AR grading systems all provided important information for asphalt binders but they have their limitations as well. These grading systems were highly empirical and do not reflect the fundamental engineering properties that explain the distress evolution in asphalt mixtures. These limitations were addressed in the subsequent system for grading binders, referred to as the Peformance Grading or PG system, which was developed as a part of the Strategic Highway Research Program (SHRP) in the 1990s

(Kennedy et al., 1994).

The PG system uses grades based on an average maximum pavement design temperature and a minimum pavement design temperature (Kennedy et al., 1994). For example, a binder grade could be specified as PG 64-16, in which the maximum design pavement temperature is 64 °C and the minimum design temperature is −16 °C. An important difference, as compared to older grading systems, is that rather than grading the asphalt binder on different property requirements, the requirements stay the same but must be met in a specific temperature range (Kennedy et al., 1994). Aging of the asphalt binder is also largely taken into consideration; the binder is evaluated for critical distresses under unaged, short-term aged, and long-term aged conditions.

In the PG system, asphalt binder properties are tested using a Bending Beam Rheometer (BBR), Direct Tension Tester (DTT), and Dynamic Shear Rheometer (DSR). The BBR performs low temperature creep stiffness tests obtaining both a stiffness and the rate of relaxation at a specific point in time referred to as the m value. A load controlled flexural test is performed on a beam cast of asphalt binder in a low temperature bath within the BBR. The DTT also performs a low temperature test but for obtaining fracture properties (Kennedy et al., 1994). A strain controlled test is performed on a dog bone shaped sample until failure occurs in order to obtain a maximum strain at failure. Lastly, the DSR is used to apply a cyclic torsion on a small cylindrical sample at intermediate and high temperatures in order to obtain the shear stiffness and phase angle of the asphalt binder (Kennedy et al., 1994). Using the properties obtained from these tests at specific temperatures both a high temperature and low temperature grade can be established. This performance grading system is now being used across the U.S. and in several other countries around the world.

2.2 LOW TEMPERATURE PROPERTIES OF ASPHALT BINDER

2.2.1 Background

Low temperature cracking is one of two forms of distresses induced primarily due to the temperature conditions; the other form of distress is thermal fatigue. Although low temperature cracking is the main focus of this study, some of the properties measured and mechanisms discussed are also applicable to thermal fatigue resistance of asphalt binders.

As the pavement temperature begins to decrease, both the aggregate and asphalt binder experience thermal contraction. Owing to the constraint boundary conditions, the

material cannot contract but instead develops stresses referred to as thermally induced stresses. Within the asphalt mixture composite, aggregate due to its elastic constitutive behavior cannot relax or relieve any thermally induced stress. At the same time these aggregate particles are being held together by the asphalt binder in a confined condition (Anderson et al., 2011). Confinement plays a large role in initiating the internal thermal stresses by placing the asphalt binder in tension between aggregate particles as the asphalt binder contracts due to the low temperature event. As these internal stresses increase due to a decrease in temperature as the pavement cools further, the asphalt binder tries to relax and relieve these stresses due to its viscoelastic nature. However, the rate of relaxation competes against the rate at which stresses build up due to the decreasing temperature. In a scenario where the binder stiffness is high or the rate of relaxation is low, the relaxation may not adequately offset the stress buildup causing stresses to approach the strength of the material and resulting in the formation of cracks. From this mechanism, it is evident that not only is the magnitude of low temperature or decrease in pavement temperature important but also the rate at which the pavement cools. This mechanism is also applicable to thermal fatigue with the only difference being that the thermally induced stresses do not exceed the strength in a single catastrophic event but rather the stresses cycle every day due to diurnal temperature changes.

While the occurrence of low temperature cracking or thermal fatigue is primarily driven by the material properties, this distress may be exacerbated by stresses induced from traffic. In this sense, low temperature cracking is primarily a phenomenon driven by material properties and particularly the properties of the binder because only the binder has the ability to relax and relieve stresses, failing which, this is also the component where cracking initiates (with some minor exceptions in mixes with very low durability aggregates). Therefore, the screening and evaluation of asphalt binders is particularly critical to ensure that the pavement does not experience low temperature cracking.

The two main tests used the measure the susceptibility of asphalt binders to low temperature cracking are the BBR (Bending Beam Rheometer) creep test and the DTT (Direct Tension Test) fracture test. The BBR is typically used to measure the stiffness and the m value or rate of relaxation of the binder at a specific point in time during the creep test. These values are used to screen asphalt binders based on their ability to resist low temperature cracking. Specific values for the stiffness and m value are set by the performance grading system and will be discussed in further detail in the following section. Not every asphalt binder is tested using the DTT. This test is only performed under certain

circumstances when the BBR requirements may not have been met. The DTT measures the strain at fracture at a specific temperature to help characterize the behavior of the asphalt binder in low temperature conditions. Both of these tests are specified in the SHRP asphalt binder section for low temperature cracking characterization. Based on informal data collected from industry and agency representatives, it appears that binders are currently being designed to avoid the use of DTT altogether.

In the case of asphalt mixtures, the data obtained via the BBR using the asphalt binder as well as an indirect tensile test conducted on the asphalt mixture are used to assess the mixtures' resistance to low temperature cracking. The indirect tensile test is performed on a cylindrical mixture sample by applying a compressive force down its diametral axis (Kennedy et al., 1994). Due to the mechanics of the test, even though a compressive load is being applied, a tensile stress is achieved along this diametral axis, which is in turn monotonically increased until failure to determine the tensile strength of the mixture. This test is typically performed at three temperatures 0 °C, −10 °C, and −20 °C to help predict the mixtures performance when exposed to a low temperature event (Kennedy et al., 1994). In addition to this test, the thermal stress restrained specimen test (TSRST) is also used to screen asphalt mixtures for their resistance to low temperature cracking. As briefly discussed in Chapter 1, this empirical test measures the temperature at which a prismatic asphalt mixture specimen that is constrained from movement along its length experiences fracture when the temperature is lowered at a fixed rate.

While both the inherent properties of the binder as well as the properties of the mixture, such as aggregate type or gradation, play a role in dictating low temperature cracking, the scope of this study was limited to asphalt binders and mortars with the primary goal of developing a material screening tool.

2.2.2 Low temperature properties of asphalt binder

As mentioned earlier the low temperature characteristics of asphalt binder are important to specify and screen asphalt binders for specific applications. These properties are typically measured using a BBR and DTT. The PG system gives guidelines and requirements for the measured values as well as the testing procedure. Both the BBR and DTT are specified in the PG system guidelines but the use of the DTT is contingent on the values obtained using the BBR, therefore the BBR tends to be more heavily used.

A discussion of the testing procedure and measured values using the BBR is necessary

to better understand the rationale and methods used in this study. The BBR test associated with the PG system specifies the use of an asphalt binder beam of 125 mm in length, 12.5 mm in width, and 6.25 mm in thickness (Kennedy et al., 1994). The beam is placed in a bath of ethanol or methanol and conditioned at a temperature 10 °C higher than the minimum pavement temperature which is also the lower grade of the binder (Kennedy et al., 1994). Once the asphalt binder beam has been conditioned for 60 minutes, it is placed on the supports and the contact load is applied (AASHTO T313-12, 2015). After the contact load has been correctly applied then the test is performed; a static load of 980 mN is applied for 240 seconds and both the stiffness and m value are measured at 60 seconds using the data obtained.

The stiffness is calculated using the dimensions of the beam as well as the applied load and deflection of the beam at 60 seconds. A maximum value of 300 MPa is specified in the PG system as the limiting for creep stiffness for any given asphalt binder (AASHTO M320, 2015). Another important measurement made is that of the m value at 60 seconds, which is determined using the slope of the creep stiffness versus time on a log-log scale. According to the PG specifications, a binder shall not have an m value lower than 0.3 when tested at 10 °Cabove the minimum pavement temperature and at 60 seconds (AASHTO M320, 2015). Both the stiffness and m value are the two main asphalt binder characteristics measured and used to quantify the low temperature cracking resistance. In situations when the creep stiffness is greater than 300 MPa, the direct tension test is recommended to be performed (AASHTO M320, 2015).

The DTT uses a dog bone shaped specimen while applying tension at a constant rate of 1 mm min^{-1} until the sample experiences failure. Effective gauge length and change in length are used to calculate the failure strain (Kennedy et al., 1994). According to the PG system the minimum allowable failure strain is one percent (AASHTO M320, 2015). If the asphalt binder has a creep stiffness value greater than 300 MPa but less than 600 MPa then the DTT value can be used instead to grade the binder. It was originally envisioned that the DTT would be used mostly for modified binders that tend to have high stiffness values but large failure strains owing to their enhanced ductility (Kennedy et al., 1994). The PG system specified the use of the DTT to gain failure properties of the asphalt binder which would be a very useful characteristic to obtain. Despite the significance of the failure properties of a binder, the DTT hasn't gained very much acceptance within the asphalt community (Hesp et al., 2009). This is a very important shortcoming because stiffness and m value represent the undamaged properties of the binder and dictate the

rate at which the binder relaxes versus accumulates thermal stresses. However, failure occurs only when the stresses in the binder exceed its strength. Without DTT, there is no measure of strength in the current system. This study aims to address this gap and demonstrate the importance of stiffness, rate of relaxation and strength in material evaluation and screening.

2.3 SIGNIFICANCE OF EVALUATING MORTAR OR FAM

Along with characterizing the low temperature properties of binder, this study will also include a section on characterizing the properties of asphalt mortars or fine aggregate matrix (FAM). Asphalt mixtures are composite of asphalt binders with aggregates of various sizes. Asphalt mixtures can be evaluated at four different length scales: asphalt binders, asphalt mastics, asphalt mortars or FAM and full asphalt mixtures. FAM is the material scale right below that of a full asphalt mixture and right above that of asphalt mastic. FAM consists of asphalt binder, filler, and fine aggregates; fine aggregates within a FAM mix are generally defined to pass a No. 16 sieve (1.18 mm) while the mineral filler are defined as fines that pass a No. 200 sieve (0.075 mm).Asphalt FAM differs from that of a full mix in that it excludes the coarse aggregate that a full hot mix asphalt mixture incorporates. The FAM scale sets it self apart from asphalt mastic by incorporating fine aggregates as well as filler, whereas mastics only consist of two parts asphalt binder and mineral filler.

Evaluating asphalt materials as a FAM has several advantages, which also explains its recent popular use in several different studies to investigate fatigue and moisture induced damage (Masad et al., 2008; Zollinger, 2005; Vasconcelos et al., 2010). Experiments that involve FAM usually involve smaller samples, which take less time to prepare and require less material. These time and material savings can be significant when a large test matrix is being implemented for a large research project that aims at evaluating the impact of several different additive and material combinations on expected performance, particularly related to thermal or traffic load related cracking. Evaluation of FAM provides much more insight into the expected mixture behavior (at least in terms of relative performance of several different material - additives combinations at the binder and filler level) compared to evaluation of asphalt binders. This is on account of the following reasons:

1. FAM incorporates the complex physico-chemical interactions between the binder, minerals from the high surface area fines, fine aggregate particles, and additives on

the overall mechanical response of the composite.

2. For a given coarse aggregate structure and type, distresses such as cracking (thermal or fatigue) are localized in the mortar or FAM portion of the mix. By using FAM one is able to focus more on this fraction where such damage originates.
3. FAM being close in material scale to a full mixture can also be used to predict (with appropriate modeling) stiffness and strength of the desired mixture.
4. Another advantage of FAM, particularly in the context of this study, is that it allows the incorporation of recycled asphalt pavement (RAP) into mixes, this would allow for easy addition and quantification of impact on various mixes. Adding RAP at a particular sieve size would be easier as well as more efficient than having to go through the long arduous process of extracting the RAP binder from a deconstructed mixture. In addition to adding RAP to FAM, additives such as softening agents or rejuvenators could be included in FAM mixes to determine the extent of their impact on various mixes.

Finally, it should be emphasized that using FAM to quantify the impact of the additives within a particular test matrix cuts down on the time and material being used, compared to similar evaluation of full mixture samples. For these reasons the use of FAM can be beneficial and is the subject of further characterization.

2.4 SUMMARY AND SCOPE

The asphalt industry has benefited from the incorporation of several new technologies in the past few decades. In each case, the technology has helped solve certain engineering and/or economic challenges. However, each new technology has added to the list of variables in terms of materials, additives or technologies that can be used to design an asphalt mixture.

For example, warm mix asphalt (WMA) was developed to reduce the high temperatures needed when producing and placing hot mix asphalt. A reduction in production temperature also corresponds to a decrease in energy consumption for the plant as well as lowering of production costs. Since the WMA is being produced at a lower temperature less emissions are produced from the burning of fuels to heat the production equipment. Emissions from the heating of asphalt binder and additives in the form of fumes and odors experience a decrease due to the lowering of the production temperature.Less emissions during the production and placing process decrease the total amount of pollution due to

asphalt production as well as create better working conditions for those employed by the industry. The reasoning for using WMA is positive but the production process adversely effects the overall performance of the product as well. WMA requires additives that effect the viscosity of the binder that allow a lower production and placing temperature. These additives can interact with binders and mineral aggregates in many different ways and influence the overall long term performance of the mix. The use of FAM provides an efficient tool to address such questions.

Another example that has recently been implemented is the use of industrial by-products as extenders in asphalt binders such as recycled engine oil bottoms (REOB). REOB is a waste product that is captured from the distilling process of used motor oil.Large quantities of REOB are produced and sold to asphalt producers for a minimal cost as a modifier. Adding this waste material to asphalt mixtures is one application that can help decrease the amount of waste to be placed in a landfill or disposed of in other ways, but when used incorrectly REOB can have detrimental effects on the asphalt mixture. REOB effects the temperature grade given to the binder using the PG system, which may lead to premature failures.Ongoing studies are still being done to help quantify the effects of REOB on asphalt binder and mixtures and once again mortars or FAM can be used as a tool for such evaluation.

The third example is the increased use of recycled asphalt pavement in asphalt mixtures. As asphalt producers look for more economical and sustainable production practices, the use of ground up recycled asphalt pavement (RAP) has increased in popularity. Implementing the use of recycled asphalt pavement helps make full asphalt mixes and roadway projects more economical since obtaining and using recycled material is a simpler process than obtaining virgin high quality materials.Emissions would also decrease with the use of RAP because the asphalt plant wouldn't have to process as much virgin material for a specific job site.Implementation of significant quantities of RAP into mixes would help decrease the rate at which high quality virgin materials were being used. The asphalt binder surrounding the aggregate in RAP has been oxidized due to the age of the material which makes it stiffer than new virgin material. Adding RAP can then lead to the mixture having a higher stiffness depending on the quantities added to the mixture.A higher stiffness can impact the long term performance of the pavement, so to counter this increased stiffness, rejuvenators can be added to the mixture to soften the mix. This means that not only can RAP be added in significant quantities but a chemical rejuvenator can be added as well, these additives can have substantial effects on the overall quality and performance

of the asphalt mixture. As RAP provides economical and environmental benefits it can also considerably impact the mixture, which is why this particular technology was chosen for this study.

In summary, new technologies provide a sustainability factor to the asphalt industry but can also make the prediction of performance of an asphalt mixture difficult. This becomes even more challenging considering the variability and less predictable nature of the operating climatic conditions in which the pavement is constructed and expected to be of service. The reasoning and application of the techniques described can provide positive effects on pollution and sustainability in the asphalt industry but need to be weighed against the impact they have on a pavements performance and design life. As mentioned before, the PG system was established to predict the performance of asphalt binders but with all of these new additives that task has become more challenging. With pavement performance and sustainability in mind this study aimed to develop a method to evaluate the material properties as well as tensile strength of asphalt binders and FAM. The following Chapter evaluates the influence of RAP on the properties of asphalt binder, both in terms of current PG metrics as well as a more fundamental examination of the binder microstructure and its changes due to the presence of RAP and rejuvenators. In the subsequent chapters the following subjects will be discussed:

- A description of each testing device and the procedures used to fabricate the test specimens included in this study
- Comparison of standard creep results between two similar testing devices used in this study in order to ensure that results produced by each machine were compliant with one another
- Standard creep and monotonic load tests to failure were performed on various binders of the same PG to compare behavior and failure properties of similar asphalt binders
- Standard creep and monotonic load tests to failure were performed on asphalt binders with varying contents of recycled binder in order to observe the impact of recycled materials on behavior and failure properties
- Standard creep and monotonic load tests to failure were performed on asphalt mortar samples of various components for comparing the impact of recycling agents and recycled asphalt pavement on behavior and failure properties

CHAPTER 3. LABORATORY AND FIELD PERFORMANCE OF RECYLED BINDERS

3.1 INTRODUCTION

The evaluation of construction materials under different service conditions is very important to ensure an economical and good quality pavement. Asphalt consists thousands of chemical components, whose proportions vary from one source to another. The composition of asphalt also varies with its age. The characterization of asphalt binder in different environment and service conditions has always been a challenge to pavement professionals. In addition to that, addition of new materials or chemicals with virgin binder alters the chemical composition as well as the structural orientation of the binder, resulting in an essentially new material. RAP binders are actually highly aged binders and possess a different set of characteristics than those of the neat binders. Hence, after addition of the RAP, the properties of the neat binder are expected to change. The chemical process in the blend may change the molecular structures of the base binder, introducing high stiffness and low rate of relaxation compared to the virgin binder. Consequently, asphalt mixes containing RAP may be susceptible to low temperature cracking. The low temperature cracking is a result of both the low temperature and the rate of lowering the temperature of the pavement. With the help of proper design and performance evaluation tools, the maximum use of RAP in new pavement construction can be ensured with a low risk of pavement failure due to environmental factors.

The Superpave test methods are developed on the basis of unmodified asphalt binders and mixes. Several researchers have reported limitations of the Superpave test protocols over last several years. Bouldin et al. (Bouldin et al., 2001) reported that the representative field behaviors of asphalt mixes are not captured completely by the Superpave tests. Bahia et al. (Bahia et al., 2010) documented that the Superpave asphalt binder specification has limited effectivity in predicting fatigue behavior of asphalt materials. These authors suggested adoption of new test methods to characterize fatigue behavior of asphalt in low temperatures. The necessity of new test methods to measure the fatigue behavior of asphalt mixes was also stated by Abbas et al. (Abbas et al., 2013). These specifications also fail to predict asphalt materials' field performances when those are modified with dif-

[0]This chapter summarizes the work conducted at the Arkansas State University

ferent polymer or non-polymer additives (?). On the other hand, current tests in practice on asphalt mixtures are time consuming and resource intensive (manpower, equipment, etc.). This study is aimed at developing a simple and ready to implement test method to characterize low temperature cracking resistance of asphalt mixtures. In this study, four types of RAP binders have been blended with a base binder at different percentages (25%, 40%, and 60% by weight). The blends are aged in short- and long-term conditions. All the samples have been tested by following selected Superpave test protocols (Rotational viscosity, Dynamic Shear Rheometer, and Bending Beam Rheometer). The mechanistic behaviors of these RAP-blended asphalts are then correlated with the actual field performance of the RAP sites. While correlating the field performance of pavements with laboratory results, the construction weather conditions and in-service pavement distress types are also taken in to consideration.

3.2 OBJECTIVES

The objective of this part of the study was to characterize RAP blended asphalt binders of different origin with the Superpave test methods (Rotation Viscosity Test, Dynamic Shear Rheometer Test, and Bending Beam Rheometer Test) and correlate the results with the field performance and distress data of the RAP pavement sites. An Atomic Force Microscope (AFM) was also used to observe the changes in the morphologies of different RAP blends at different proportions and aging conditions. The major steps that were carried out to achieve this objective are summarized below.

- RAP samples were collected to obtain RAP binders from the field core samples; these binders were then used to prepare test RAP blends (25%, 40%, and 60% of RAP by weight). The construction weather data and in-service pavement distress data was collected and analyzed to evaluate the influence of the weather on the pavement performance.
- Selected Superpave (Rotation Viscosity, Dynamic Shear Rheometer, and Bending Beam Rheometer) tests were conducted on the unaged, short-, and long-term aged binder blends to record the rheological properties of different proportioned RAP blends.
- AFM tests were conducted on the RAP blends of different ages. The AFM test was intended to obtain the morphology for the binder set.
- The changes in the high proportion RAP blended asphalt samples due to addition

of a rejuvenator were observed using both the Superpave and AFM tests.

3.3 BACKGROUND

Previous researchers used different laboratory tests to predict the behavior of asphalt pavements under service conditions. As this study focuses on characterizing RAP blending asphalt blends, existing literature was reviewed to assimilate the current practices and reported behaviors of asphalt binders tested by different tests.

Hossain et al. (Hossain et al., 2012) studied the effects of high percentage of RAP when used in base and surface courses of flexible pavements in Oklahoma. In Oklahoma, the maximum allowable RAP in surface course is 0% and that in base course is 25%. These researchers used 10% RAP in the surface and 40% RAP in the base along with the maximum allowable RAP percentages to get a comparable data. It was found that the PG grading of asphalt binder increased due to the addition of the RAP, but the PG grading was not affected by adding a 0.5% anti-stripping agent. The authors concluded that the addition of RAP could improve the fatigue performance of asphalt mixes.

Mannan et al. (Mannan et al., 2015) aimed at evaluating the effects of loading frequency and strain level using RAP and non-RAP mixes on the fatigue behavior of asphalt mixes and binders. Their study also focused on finding correlations between the binder fatigue test results with mixture test results for different loading frequencies. From the statistical analyses of the results, the authors suggested the time sweep and Linear Amplitude Sweep (LAS) tests to be performed to investigate fatigue behavior as they provided reliable results and were less time consuming than the beam fatigue test.

Wang et al. (Wang et al., 2012) investigated the fatigue behavior of asphalt binder, mastic (mixture of binder and filler) and fine aggregate mixture at low temperatures by means of Direct Tension Test (DTT), a newly developed fatigue test method, X-ray analysis, and finite element analysis of the materials. They reported that the additional fine aggregates did not have impact on improvement of fatigue resistance, but it enhanced the mix strength compared to fresh asphalt cement. The authors suggested that the developed fatigue test simulation methodology to be used as a basis for further fatigue research.

Mahmoud et al. (Ma et al., 2010) used a modified Bending Beam Rheometer (BBR) to evaluate RAP without the extraction and recovery processes. These researchers aimed to characterize low temperature cracking behavior of RAP binders while avoiding the possible

effects of different solvents used during the recovery process. The study suggested using aggregates retaining on Sieve #100 sieve and 20% RAP binder to be used in the proposed modified BBR test.

ValdÃ©s et al. (Valdés et al., 2011) studied mechanical behavior of asphalt mixes containing 40% and 60% of RAP. These researchers used the stiffness test, IDT, Fenix Test (a new direct tensile test), and fatigue test to characterize the asphalt mix for this study. The authors reported a higher stiffness value for 60% RAP mixture, whereas the average modulus of 40% RAP mixture was little lower than the others.

Sabouri et al. (Sabouri, 2014) studied the RAP percentage and total asphalt content of the mixture with different amounts of the base binder. These researchers used a simplified viscoelastic continuum damage model for the fatigue characterization, and the Triaxial Stress Sweep (TSS) test method to determine the rutting behavior. The RAP content more than 20% worsened the result, which could be mitigated by using a softer base binder, as suggested by the authors. The authors found that the optimum binder for the mix would be the amount that would not cause excess rutting or make the mix susceptible to fatigue crack. It was also reported that a higher RAP content increased the stiffness, whereas the increasing binder content resulted in opposite findings.

To mitigate the drawbacks of using RAP in asphalt mixes, the use of a soft base binder or the application of a rejuvenator has been suggested by previous researchers. Shen et al. (Shen et al., 2007a) used an oil based rejuvenating agent (the name was not mentioned) with RAP containing Superpave mix to observe its performance against softer neat binders. Blending charts established by DSR and BBR test (Shen and Ohne, 2002) yielded 12.5% of rejuvenator by weight of the RAP binder (2-3% of the weight of the mixture containing 30-50% RAP) to be used for test samples. The literature was reviewed for the type and the optimum amount of the rejuvenator to be used in the RAP blends for this study. The findings are summarized in Table 3.1.

According to the suggestion a practicing engineer from the Oklahoma Department of Transportation (ODOT), the rejuvenator for this study was selected to be EvoflexÂ®, which was an oil based rejuvenator. In this case, 12.5% of the rejuvenator by weight of the RAP binder was selected to be the design rejuvenator dosage for the RAP blends. No further study on the optimum rejuvenator dose was done under the scope of this study.

An AFM has also been used by pavement professionals to observe the changes in the asphalt binder before and after modification by different agents. An AFM works based on the van der Waals attraction force, which is the intermolecular residual attractive or

Table 3.1. Type and Doses of the Rejuvenator in Application

Authors	Dosage	Rejuvenator
Shen et al. (Shen et al., 2007a)	12.5% (wt.) of RAP binder	Oil type
Shen et al. (Shen et al., 2007b)	2% - 7.4% of the binder	Not mentioned
Boyer (Boyer and Engineer, 2000)	0.12 gallons per sq. yd.	Reclamite
	0.15 gallons per sq. yd.	Koppers BP
Karlsson and Isacsson (Karlsson and Isacsson, 2006)	20% of the total binder	Not mentioned
GarcÃa et al. (García et al., 2010)	7% of the total binder (Shen et al. 2007a)	Not Mentioned
Brownridge (Brownridge, 2010)	—	Reclamite

repulsive forces other than those arise from a covalent bond or electrostatic interaction. The AFM can capture nanometer level data that provides the morphology of the surface of the asphalt binders as well as the nanomechanical properties such as elastic modulus, hardness, adhesion, and energy dissipation. Multiple studies (De Moraes et al., 2010; Masson et al., 2006; Dourado et al., 2012) have estimated mechanical properties of asphalt binders using different AFM systems. In this study, an AFM (Dimension Icon from Bruker) has been used to observe the morphological changes in binder blends after mixing with different RAPs and at different aging conditions.

3.4 MATERIALS

This is an extension of a related study that was started by surveying existing (in-service) pavements in Arkansas. With the help of the AHTD officials, nine (9) pavement sites on I-30 and I-40 were selected based on the physical appearance, developed rutting, presence of distress types, etc. Among these nine sites, four (4) sections have been selected for the current study. Two of the selected sites were performing well and were identified as "GOOD"; whereas the other two were identified as "POOR" performance pavement sections with potential temperature related transverse cracking. The geographical locations of RAP collection sites are shown in Figure 3.1.

As shown in Figure 3.1, three of four sites are on I-40 with another site on I-30; all of

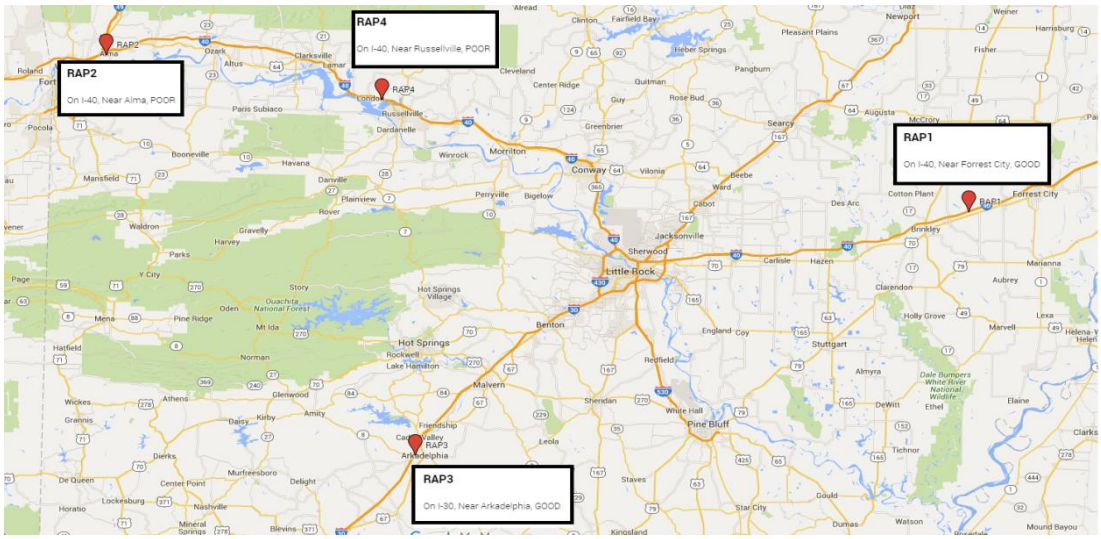

Figure 3.1. Location of RAP Sampling Sites

them are in high traffic areas with an average annual daily traffic (AADT) ranging from 25000 to 31000. The detailed information of all five samples, including the base binder, is given in Table 3.2.

Table 3.2. Information of Samples Used in this Study

Sample	Sample Description	Source of Materials	Remarks
Control	PG 64-22, base binder	Ergon, Memphis, TN	Unmodified
RAP-1	25%, 40%, and 60%	I-40, Forest City, AR	GOOD
RAP-2	25%, 40%, and 60%	I-40, Alma, AR	POOR
RAP-3	25%, 40%, and 60%	I-30, Arkadelphia, AR	GOOD
RAP-4	25%, 40%, and 60%	I-40, Russellville, AR	POOR

RAP samples were collected in the form of cylindrical cores with the help of the AHTD personnel as part of the Transportation Research Council (TRC) 1404 (Chowdhury et al., 2015) project of AHTD. The RAP binders were extracted from these core samples to blend in different percentages with the base binder for further testing.

3.5 METHODOLOGY

The first task of this study was to search for existing information relevant to this study to duplication of effort in this study. A review of the literature was done for established

procedures to remove the chance of getting non-relevant results, and reach the goal of this research without unnecessary efforts. Based on the literature review, a test methodology was been developed as illustrated in Figure 3.2.

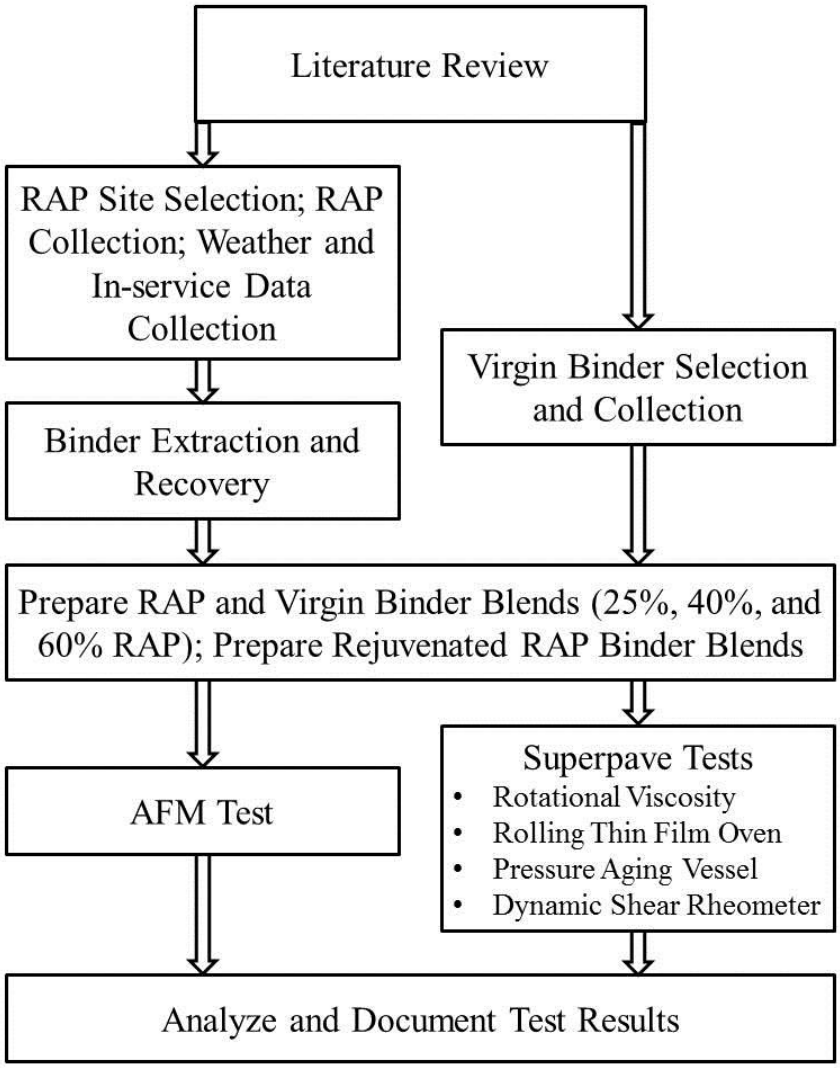

Figure 3.2. Test Plan for RAP Blended Binder Characterization

The RAP core samples were collected from in-service pavements as discussed earlier. The in-service pavement distress data was collected from the AHTD. A performance grade base binder (PG 64-22) was collected from a local refinery to blend with the RAP binder recovered from the field core samples. The binder extraction and recovery process for all RAP samples was done in the laboratory according to AASHTO T 164 and ASTM D5404, respectively. Different blends (25%, 40%, and 60% by weight) of RAP and

virgin binders were prepared following a manual blending protocol suggested by Hossain et al. (Hossain et al., 2012). In accordance with this procedure, both the base and RAP binders were heated and required amounts were poured into an aluminum container. Then the container was heated at 163 °C for nine minutes in an oven. After nine minutes of heating, the binders were stirred using a pre-cleaned and pre-heated glass rod for one minute. Afterwards, the container was placed into the oven for another nine minutes of heating. The 10 minutes heating and stirring procedure was repeated for a total of six times, allowing one hour of blending time per blend. This process is expected to simulate the plant mixing of asphalt concrete.

The rejuvenated RAP blends were also prepared following the same protocol as above. The binder blends were aged in short- and long-term conditions in accordance with AASHTO T 240 and AASHTO R 28 specifications, respectively. The unaged, short and long term aged binder blends were tested by following conventional Superpave test protocols and with an AFM. The heat cast approach of the AFM sample preparation technique (Tarefder and Zaman, 2009; Hossain et al., 2016; Rashid and Hossain, 2016) was adopted to prepare test specimens for the AFM test for each of the blends. A series of laboratory tests were done on the prepared RAP blends of different ages. Table 3.3 shows the detailed laboratory test plans at a glance.

The main focus of this study was to evaluate the RAP blends of different origins and proportions by following the Superpave test protocols. The Rotational Viscosity (RV) test was done on the unaged binder blends of all RAP types by following the AASHTO T 316 method. A Brookfield Rotational Viscometer (DV-II+Pro) device was used in this study for RV tests. The Dynamic Shear Rheometer (DSR) test was done on unaged, RTFO and PAV aged binders of all RAP blends. AASHTO T 315 provided directions to characterize asphalt binder having dynamic shear modulus in between 100 Pa and 10.000 Pa, which was typical for asphalt binders from 40 °C to 88 °C at an oscillatory speed of 10 rad s^{-1}. For this study, grading of asphalt binder was the main purpose; hence the tests were done until the test specimen failed due to increase in temperature. The Superpave rutting parameter $|G^*|/\sin\delta$ and the fatigue related parameter $|G^*|\sin\delta$ were considered as the governing criteria for the high service temperature (unaged and RTFO-aged binders) and the intermediate service temperature (PAV-aged binders) test verification, respectively. The Bending Beam Rheometer (BBR) was used to determine the low temperature stiffness and relaxation properties of asphalt binders. The BBR test was used to determine the minimum temperature up to which the binder could be used in its service condition.

Table 3.3. Laboratory Test Plan

Test Type	Name of the Test	AASHTO Specification	Test Samples
Sample Simulation	RTFO	AASHTO T 240	PG 64-22 and RAP1-RAP4 blends
	PAV	AASHTO R 28	
Sample Preparation	Blending	N/A	PG 64-22 and RAP1-RAP4 blends
	Heat Cast	N/A	
Mechanistic Tests	Rotational Viscosity	AASHTO T 316	PG 64-22 and RAP1-RAP4 blends
	Dynamic Shear Rheometer	AASHTO T 315	PG 64-22 and RAP1-RAP4 blends
	Bending Beam Rheometer	AASHTO T 313	PG 64-22 and RAP1-RAP4 blends
Emerging Technology	Atomic Force Microscopy	Tapping Mode	PG 64-22 and RAP3-RAP4 blends

AASHTO T 313 provided the standard practices for BBR test while AASHTO PP 42 was used mainly to determine the low PG temperature of asphalt binders in the laboratory. The BBR test for this study was done in the research partner institution, The University of Texas at Austin.

To investigate the influence of weather conditions on the performance of the pavement, specific weather data was collected for each of the selected sites ranging in date from the start of construction to the finishing date of the job. Weather data was collected from a weather forecasting website (**?**). The data included maximum and minimum temperatures, humidity, and total amount of rainfall for each day of the construction period. Pavement distress data was also collected for all the RAP sites for their respective service periods. Most of the North American highway agencies have automated methods of pavement distress data collection (Chowdhury, 2015), although step by step collection and evaluation methods may vary from state to state. The AHTD uses Automated Road Analyzer (ARAN) vehicles to collect pavement distress data in a regular basis. The ARAN vehicle collects the rutting data and International Roughness Index (IRI) data of the pavement on which it rolls (Yang et al., 2015). The AHTD's Pavement Management

Division collects, processes, analyzes, and reports the pavement performance data for the entire highway network. The collected ARAN data are analyzed using computer software named Multimedia Highway Information System (MMHIS). This software allows its user to analyze raw data as well as visualize the pavement surface based on its integrated multipurpose output system. The ARAN data for the selected pavements analyzed in this study includes pavement distress information from 2001 to 2014. At the end of the study, collected information and test results were analyzed to draw conclusions about the research questions of this study.

3.6 RESULTS AND DISCUSSION

RAP samples from four different sources have been collected from the interstate system in Arkansas. The RAP binders have been recovered and blended with a neat binder at different percentages (25%, 40%, and 60%). A variety of tests have been conducted over a two year period to characterize asphalt materials of different ages. The outcomes of Superpave tests (Rotational Viscosity, Dynamic Shear Rheometer, and Bending Beam Rheometer) on control, RAP blended, and rejuvenated RAP blended asphalt binders are discussed in this section.

3.6.1 In-service Pavement Condition

Surface conditions of the pavement have been a major indication of the quality of the overall pavement. The ride quality of the pavement mostly depends on the surface roughness as the "variation in the surface elevation produces vibration in oncoming vehicles" (Sayers, 1986). Hence, the roughness of the pavement surface is considered as the most popular way to assess the pavement quality. Apart from the riding comfort, a large value of roughness indicates higher pavement deformation which might have an impact on the storm water drainage as well as driving safety of the pavement. Lin et al. (Lin et al., 2003) reported International Roughness Index (IRI) as a perfect indication of pavement distress condition from their neural network analysis. The IRI values for all four of the pavement sections of this study have been collected. The average IRI of any specific point (log mile) of any section has been calculated from the Right Wheel Path (RWP) and the Left Wheel Path (LWP). The calculated average IRI values for RAP1 through RAP4 pavement sections are presented in Figure 3.3.

From the basics of the IRI model, a higher IRI value is an indication of poor performing

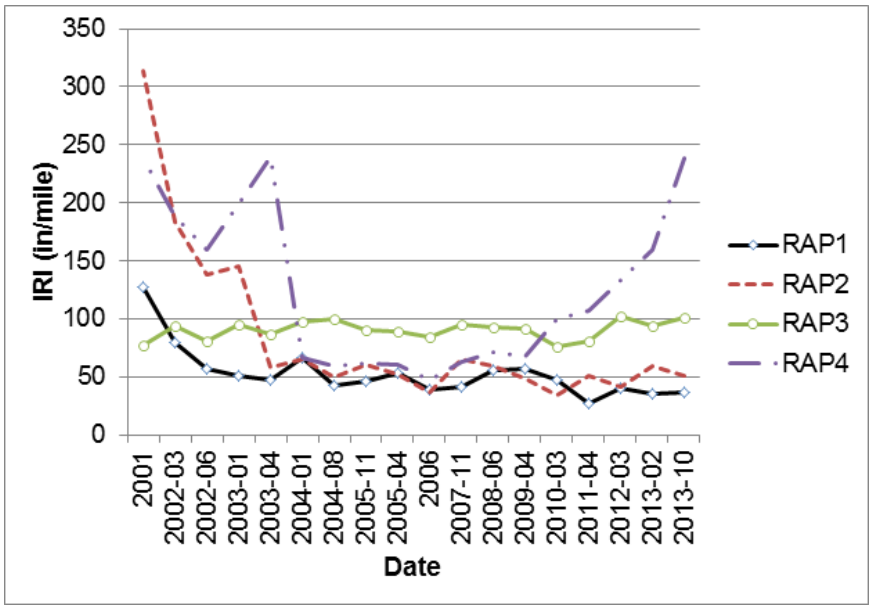

Figure 3.3. Average IRI Values for RAP1 - RAP4 Pavement Sections

pavement surface. Although poor performing sections (RAP2 and RAP4) were expected to show higher values of roughness at the end of their service lives, they did not show such a trend as shown in Figure 3.3. For the poor performing sections, the initial IRI values were quite high; it reduced over time with a steady value around 0.8 mm km^{-1} after three years of construction. Continuous friction between the vehicle wheels and the pavement might have reduced the roughness of the surface. There might have been some patching work in 2003 and 2004. Initial high value of the roughness might be the indication of premature failure of RAP2 and RAP4 (Poor performing) sections. Although the roughness of RAP2 section remained steady for the rest of the study duration, IRI of RAP4 started to increase in mid of year 2009 to reach up to 3.8 mm km^{-1} by the end of 2013. On the other hand, the roughness of good performing sections (RAP1 and RAP3) was nearly constant over the lifetime of both of those pavements. RAP3 showed a steady value around 1.6 mm km^{-1} whereas this value stuck around 0.8 mm km^{-1} for RAP1 for 12 years of their service period. The field performance for RAP1 and RAP3 were reflected by the IRI profile over the course of the time. Another important distress type to indicate the pavement quality was the accumulated rut depth developed on the surface of the pavement. Rutting could occur in any of the pavement surface, aggregate base, subgrade layer, or in combination of these layers (Tarefder et al., 2003). Hence, rut depth on the surface should be considered as the overall reflection of the section on the pavement

surface. The processed rutting data for all four pavement sections are presented in Figure 3.4.

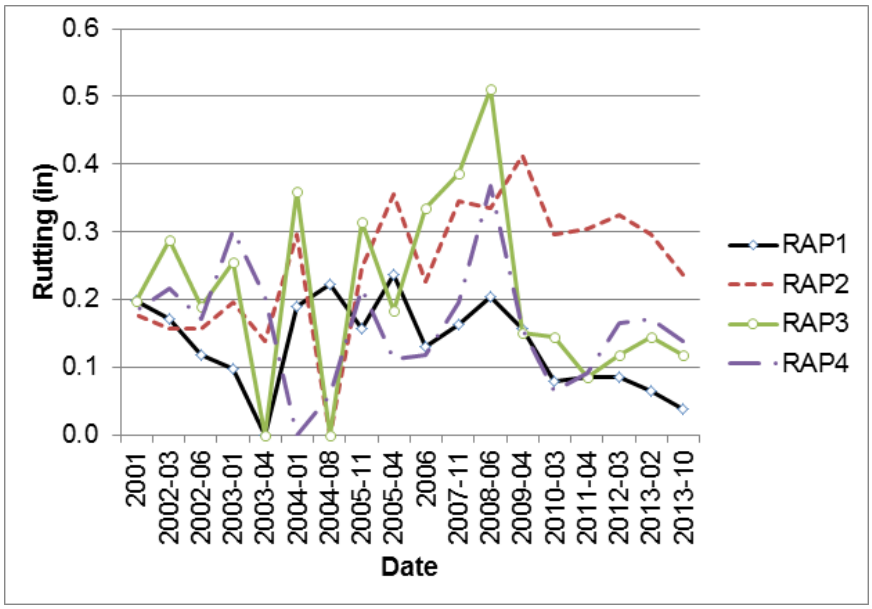

Figure 3.4. Average Rutting Depth for RAP1 - RAP4 Pavement Sections

To correlate field performance of different pavement sections, the expectation for high rut depth of RAP2 and RAP4 were not reflected in Figure 3.4. In fact, all four sections (both good and poor performing) of pavements showed similar kind of rutting values up to 10.2 mm over the lifetime. The RAP2 section showed initial high rutting of 7.6 mm which was not seen for the other three pavements. However, the application of rutting depth as an assessment criterion for overall pavement performance might need further detailed adjustments as it appears to fail to correlate the current in-service statuses. From a related study, (Chowdhury, 2015) there was also a discussion about the applicability of ARAN data or data collection methods for pavement quality assessment.

3.6.2 Construction Weather Condition

The environmental factors during the construction of the pavement play an important role in long term performance and durability of the roadway (Rada, 2013). To investigate whether the environmental factors were responsible for performance issues of pavements under study, maximum temperature, minimum temperature, moisture, and precipitation data throughout the construction period have been collected from nearby weather station.

Construction related information such as starting of base course, starting of surface course, and finishing of pavement layers have been collected from AHTD's records. As an example, weather and construction data for RAP1 (Forest city, AR) pavement section have been presented in Figure 3.5.

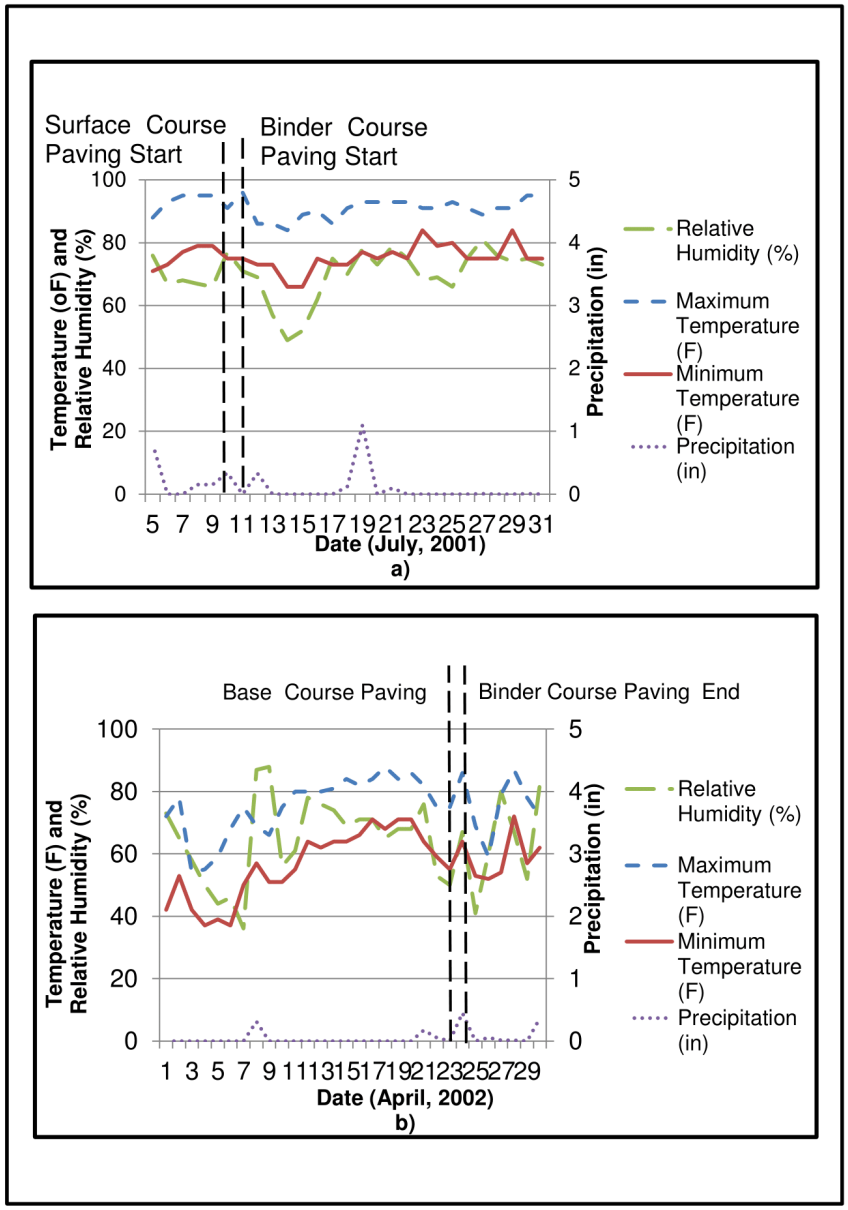

Figure 3.5. Weather Data Plotted against Time for RAP1: a) Starting and b) Ending of the Construction Work

In Figures 3.5-a and 3.5-b maximum and minimum temperatures in Fahrenheit and

relative humidity has been plotted in the left Y-axis; the precipitation data (in) is shown in the right Y-axis. Figure 3.5-a shows weather data for July 2001 when paving of that section was started. The paving work ended in April 2002 (Figure 3.5-b). As can be seen from these figures, there was almost zero rainfall during construction. The temperature varied from 26.7 °C to 32.2 °C (80 to 95^{o}F) with about 75% relative humidity over the period. Although, only two months' data are presented here, the weather information was collected and analyzed throughout the construction duration. The weather conditions were very consistent over the construction period of 10 months, especially when the surface course of the pavement was laid down. Climatic data for RAP2 —RAP4 sections are provided in Appendix A. An observation of climatic data for poor performing sections (RAP2 and RAP4 in Alma and Russellville, respectively) suggests that no abrupt changes happened during the paving operations of base, binder, surface courses of these pavements. Hence, the poor performance is less likely due to the weather condition during construction period for these sections.

3.6.3 Superpave Test Results

The RAP binders from all four RAP samples were extracted and recovered to prepare 25%, 40%, and 60% by weight blends with a PG 64-22 (base) binder. This section describes the results from the selected Superpave tests (RV, DSR, and BBR) conducted on differently aged binder blends with varying RAP.

3.6.3.1 Rotational Viscosity (RV) Test

The pavement with RAP1 served for more than 10 years. The RAP1 binder can be considered as a highly aged binder and is expected to increase the viscosity of the binder blends. This trend is shown in Figure 3.6 for RAP1 binder blends.

For RAP2, RAP3, and RAP4 binder blends, a similar trend of increased viscosity is noticed. The changes in viscosity with temperature for RAP2, RAP3, and RAP4 blends are shown in Appendix B. Different RAP blends showed different trends of viscosities at different temperatures. At 135 °C the magnitude of viscosity for different RAP varied from as high as 3200 mPa s(RAP2) to as low as 1300 mPa s(RAP3) for 60% RAP blend sets. Such a high viscosity data of 60% RAP2 modified binder makes it ineligible as an asphalt as per Superpave specifications. The comparative status of viscosities of different RAP blends is shown in Figure 3.7.

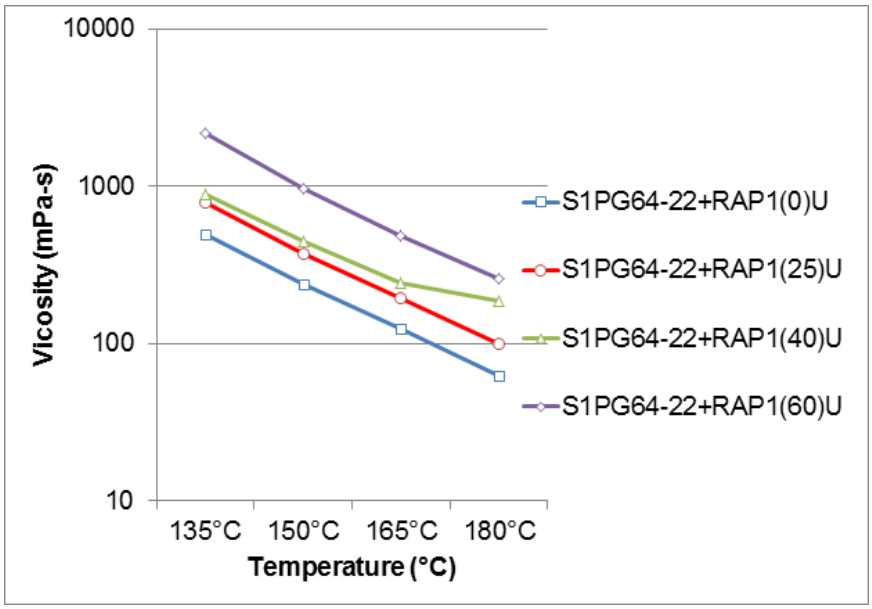

Figure 3.6. Viscosity of RAP1 Binder Blends

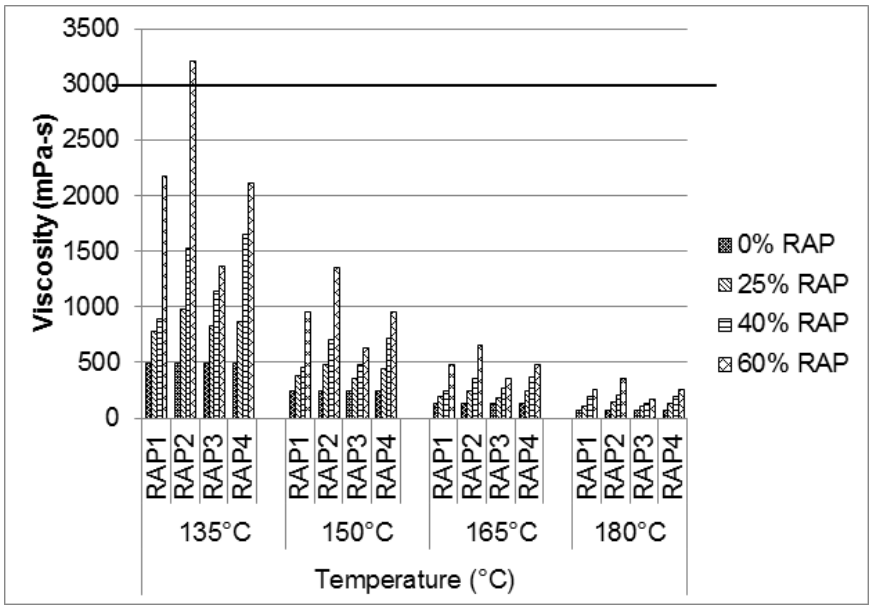

Figure 3.7. Comparative Status of Viscosities for RAP1-RAP4 Blends

While RAP1 and RAP4 showed similar magnitudes and trends in terms of viscosity, RAP3 maintained a low viscous profile over the temperature range. Looking at the field performance for these sections, RAP2 and RAP4 were noted as poor performing sections. A high viscosity RAP2 blend could be an indicator of the premature pavement failure of

the pavement. A low viscosity profile for RAP1 and RAP3 are considered to meet the expectation to correlate their in-service performance rating.

3.6.3.2 Dynamic Shear Rheometer (DSR) Test

The results of DSR test on unaged and RTFO-aged binder blends at high temperatures and at intermediate temperatures on PAV-aged binder blends are shown in 3.8 through 3.15.

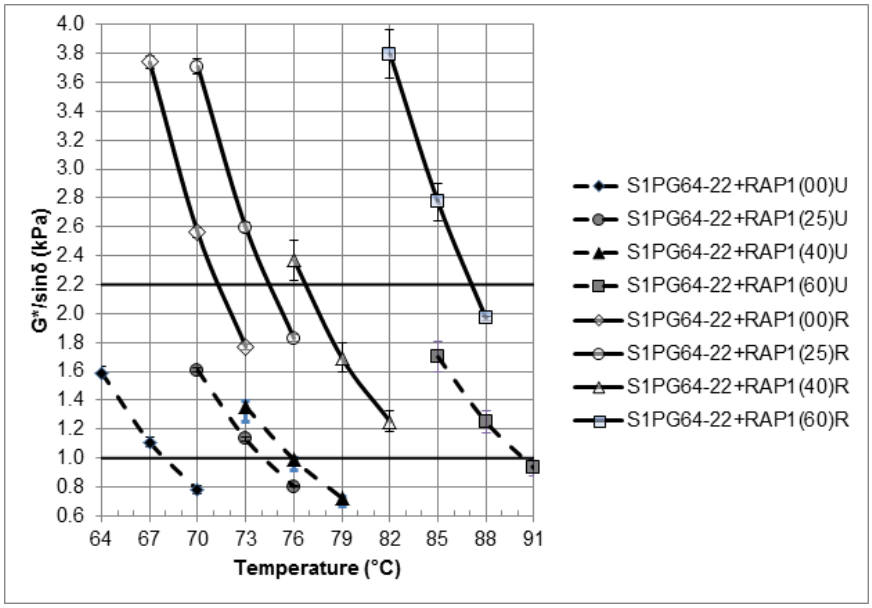

Figure 3.8. DSR Test at High Temperatures for RAP1 Blends

Figure 3.8 shows the DSR test results of unaged and RTFO-aged binder blends of RAP1. According to the Superpave specification, the failure temperatures were the temperatures at which the rutting parameters were 1.0 kPa and 2.2 kPa for unaged and RTFO-aged binders, respectively. The least of these two temperatures was taken as the high PG temperature for any specific blend. As can be seen from the figure, the base binder (S1PG64-22+RAP1(00)) passed 64 °C temperature as expected for both the unaged and RTFO-aged conditions. For both aging conditions, addition of RAP increased the PG temperature. While the increase in the temperature from 25% RAP1 to 40% RAP1 was around 30 °C, this difference in temperatures for 40% RAP1 to 60% RAP1 was 9 °C (unaged) and 12 °C (RTFO-aged). The failure temperature for PAV-aged binders at intermediate temperature could be seen from Figure 3.9. A fatigue parameter value of 5 MPa

was considered as the passing criteria for intermediate temperature of tested blends. However, DSR at intermediate temperature could not alone determine the low PG temperature of any binder blend. The test results from BBR play role in this regard. For this reason, the DSR test results at intermediate temperatures only are presented here. The DSR test along with the BBR test results will be used at the end of this chapter to determine the low PG temperature for the blends. The addition of RAP1 influenced the low PG temperatures of the base binder as well, which was also reflected on the intermediate temperatures of the blends, as can be seen from Figure 3.9.

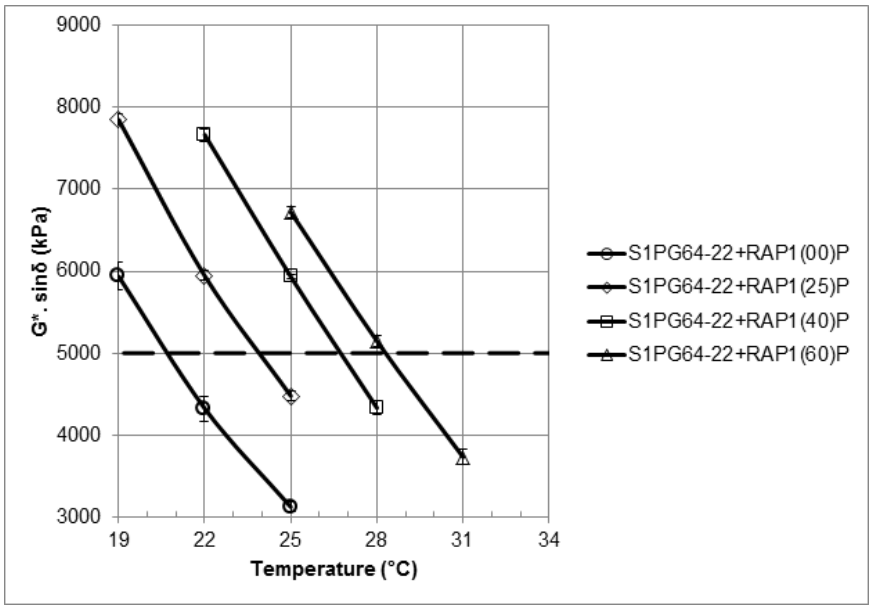

Figure 3.9. DSR Test at Intermediate Temperatures for RAP1 Blends

For 25%, 40%, and 60% RAP1 blended PAV-aged samples, the fatigue failure temperatures increased gradually. Such an increase in fatigue failure temperatures may have adverse effects on the high RAP modified asphalts. As mentioned earlier, the BBR test results are also required to describe the quantitative effects of RAP on the base binder, which is done at the end of this section.

Figures 3.10 and 3.11 show the DSR test results at the high and intermediate temperatures for RAP2 blends. For RAP2 blends, the trend of increasing high PG temperatures along with RAP amount was seen similar to RAP1 blends, but with a higher magnitude. Both the unaged and RTFO-aged binders passed at 91 °C for 60% RAP content which was 24 °C higher than the control. The 40% blend also showed 15 °C increase in temperature from the control sample. From these data, it was obvious that RAP2 binder was stiffer

than RAP1, which was also seen from the viscosity data. The observations can be related with the premature failure of RAP2 section in service conditions.

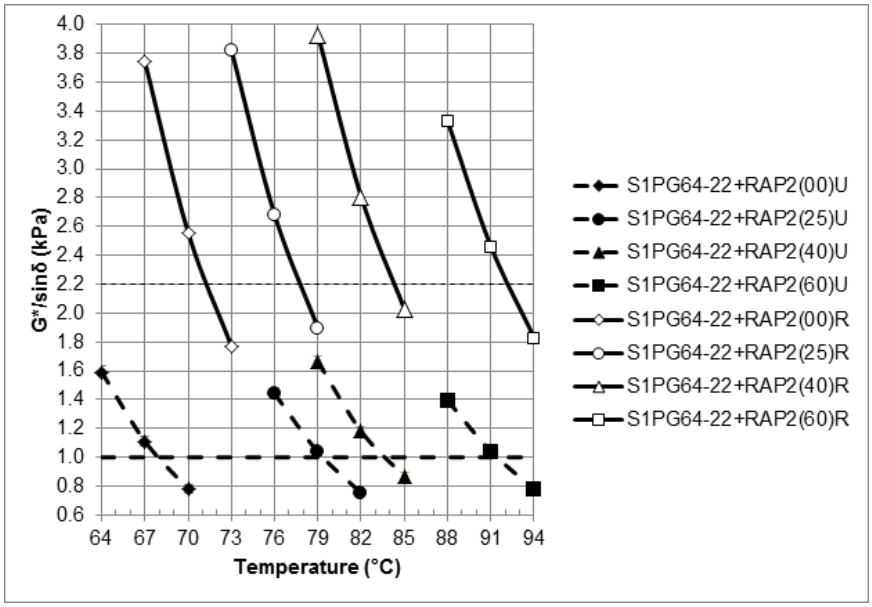

Figure 3.10. DSR Test at High Temperatures for RAP2 Blends

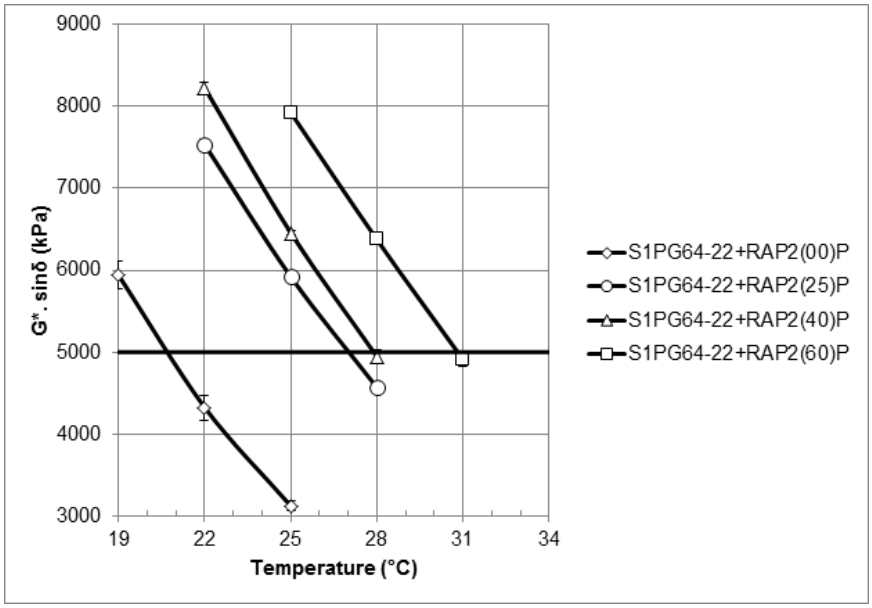

Figure 3.11. DSR Test at Intermediate Temperatures for RAP2 Blends

The phenomenon of increase in the low PG temperature of asphalt blend after the

addition of RAP was also observed strongly in case of RAP2 binders from PAV-aged binders, which is shown in Figure 3.11. Although RAP3 increased the stiffness, as indicated by high PG temperatures from DSR tests, the increment was not as much as it was for RAP2. The test results of DSR test at high PG temperatures are shown in Figure 3.12.

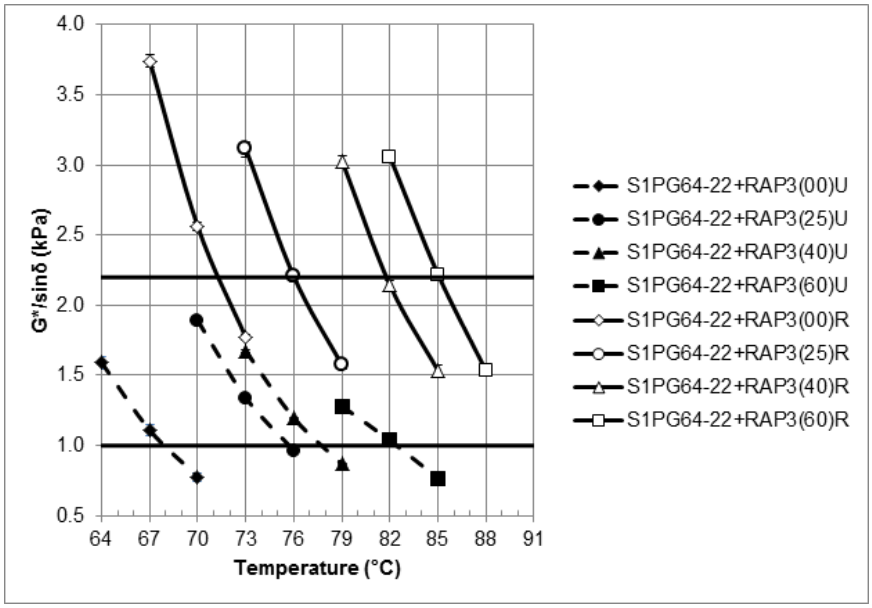

Figure 3.12. DSR Test at High Temperatures for RAP3 Blends

For RAP3 blends, 60% RTFO-aged binder showed 13 °C higher PG than the control. For a similar set of conditions, RAP2 showed 24 °C higher temperature than the unaged control binder. To correlate with the field performance, it can be said that, RAP3 was not as stiff as RAP2; hence the change in the high temperature showed lower magnitude in the case of RAP3 blends. The original binder used in RAP3 construction maintained its properties up to the design expectation which was reflected in its "good" field performance. The PAV-aged RAP3 blends showed increase (Figure 3.13) in intermediate temperature as well, from which, it can be inferred that this RAP also affected the low PG temperature of the base binder similar to the previous RAP binders. The outcome of these changes in intermediate temperature will be combined with BBR test results to determine the ultimate changes in the low PG temperature of the blends.

Figures 3.14 and 3.15 represent the DSR test outcomes of RAP4 blends. The maximum temperature noticed for RAP4 blends was 90 °C for RTFO-aged 60% RAP blends, but for unaged condition this temperature was 85 °C. The temperature graphs were equally spaced which indicates that the increase of RAP content from 25% to 40% is equivalent

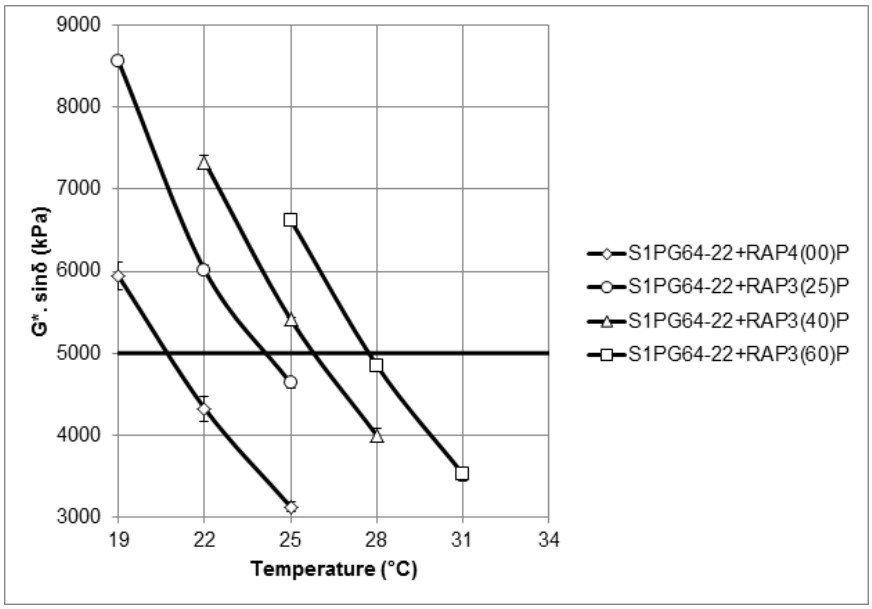

Figure 3.13. DSR Test at Intermediate Temperatures for RAP3 Blends

to that of 40% to 60% unlike RAP1.

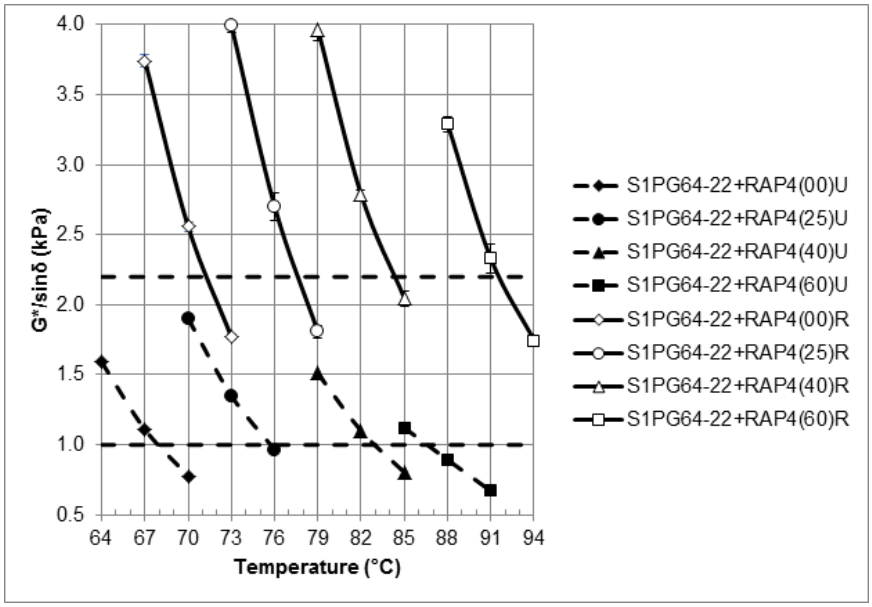

Figure 3.14. DSR Test at High Temperatures for RAP4 Blends

Looking at the PAV-aged binders (Figure 3.15) of RAP4 blends, not much difference was noted compared to RAP3 blends. The changes in the intermediate temperatures

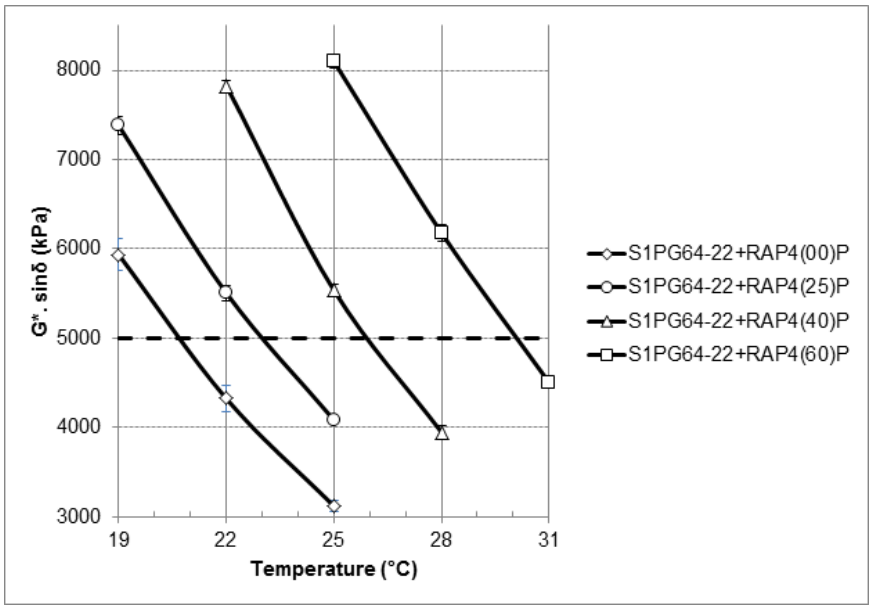

Figure 3.15. DSR Test at Intermediate Temperatures for RAP4 Blends

followed the same trend and magnitude (19 to 28°C).

3.6.3.3 Bending Beam Rheometer (BBR) Test

The BBR tests were done on PAV-aged samples of four different RAP blends. Table 3.4 shows the BBR test data of PG 64-22 (control) binder at −9 °C and −12 °C .

Table 3.4. BBR Test data of the Control Binder

Test Temp. (°C)	Average m value	Stiffness at 60 seconds (MPa)
-9	0.35	91.2
-12	0.33	143.5

The AASHTO specification suggested an m value lower than 0.300 and a stiffness value higher than 300 MPa as failure criteria of BBR test. So, it is evident that the test samples did not fail at either of these two test temperatures (−9 °C or −12 °C). Based on the available data, liner extrapolations were done to find out the failure temperatures. Figure 3.16 shows the m value and stiffness data plot for this binder along with the regression analysis.

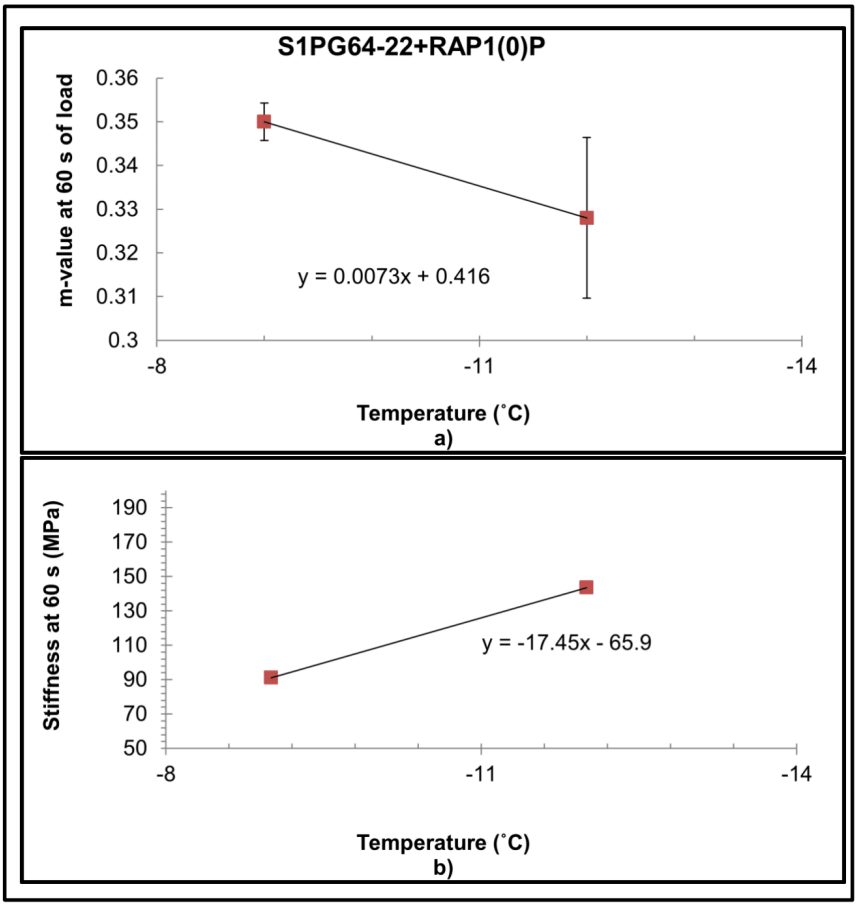

Figure 3.16. BBR Test Data of Control

From extrapolation, the failure temperature (which is 10 °C below the test temperature) comes out as −25.82 °C based on m value and −30.96 °C based on stiffness criterion. The higher of these two (−25.82 °C) was taken as low PG temperature for tested binder. All RAP blends of four RAP types were tested with the BBR for their low PG temperature. Detailed calculations for those blends are given in the Appendix C, while the results are summarized in Tables **??** and 3.6.

The intermediate temperatures were calculated based on the BBR test result. For example, the intermediate temperature for S1PG64-22+RAP1(25)P is (74-21.88)/2+4 = 30 °C. Then the fatigue failure temperature was noted to compare with the intermediate temperature for each blend. As can be seen from Table 3.5, the low temperature grade for all RAP blended binders were increased up to 2 °C. In general, 25% RAP1 and RAP2 blends can be graded as PG 70-16 and PG 76-16 binders, respectively. If any specific

Table 3.5. Low PG Temperature from BBR and DSR Test (RAP1 and RAP2)

Sample	Test temp. (°C)	Stiff-ness	m Value	Fail temp.(°C)	Inter. Temp. (°C)	Fatigue critical temp. (°C)
S1PG64-22 +RAP1(00)P	-9	89.7	0.347	-25.82	25	20
		92.6	0.353			
	-12	145	0.315			
		142	0.341			
S1PG64-22 +RAP1(25)P	-9	124	0.329	-21.88	30.5	23
		127	0.319			
	-12	188	0.3			
		184	0.298			
S1PG64-22 +RAP1(40)P	-6	107	0.337	-20.7	32	26
		104	0.321			
	-9	148	0.312			
		146	0.309			
S1PG64-22 +RAP1(60)P	-6	160	0.334	-20.47	37.5	28
		145	0.333			
	-9	240	0.309			
S1PG64-22 +RAP2(25)P	-9	129	0.321	-21.83	32	26
		125	0.343			
	-12	186	0.302			
		188	0.294			
S1PG64-22 +RAP2(40)P	-6	137	0.303	-19.69	36	27
		136	0.305			
	-9	187	0.289			
		184	0.282			
S1PG64-22 +RAP2(60)P	-6	145	0.328	-20.41	39.5	30
		149	0.296			
	-9	239	0.289			
		235	0.284			

mix design requires a binder of a low PG in case of the high temperature, a softer base binder (for example, PG 58-28) could be used to get the target PG blend. While the BBR test provides the low PG temperature, the DSR test on PAV aged binder checked the probability of fatigue failure temperature for any PG binder. For both RAP1 and RAP2, the intermediate temperatures were higher than the fatigue failure temperatures found from DSR test. Hence, it can be said that, for RAP1 and RAP2, as high as 60% RAP binder can be used with a PG 64-22 binder considering both the rutting and fatigue resistance of the pavement mix. However, the BBR test results of RAP3 and RAP4 (Table 3.6) vary significantly than those of RAP1 and RAP2 blends.

The 25% RAP3 blend showed very low PG temperature, which decreased the intermediate temperature than the fatigue failure temperature, as can be seen from Table 3.6. While, 40% RAP3, 60% RAP3, 25% RAP4 blends showed low PG temperature around $-20\,^{\circ}\mathrm{C}$, it reduced to $-16\,^{\circ}\mathrm{C}$ for the cases of 40% RAP4 and 60% RAP4 blends. From this observation, it can be said that, out of all the RAP blends, 40% and 60% of RAP4 with a virgin binder stiffens the blend most. The field performance and the viscosity data indicated that RAP4 was stiffer than RAP3, which was also seen from the BBR test data.

Table 3.6. Low PG Temperature from BBR and DSR Test (RAP3 and RAP4)

Sample	Test temp. (°C)	Stiff-ness	m Value	Fail temp.(°C)	Inter. Temp. (°C)	Fatigue critical temp. (°C)
S1PG64-22 +RAP1(00)P	-9	89.7	0.347	-25.82	25	20
		92.6	0.353			
	-12	145	0.315			
		142	0.341			
S1PG64-22 +RAP1(25)P	-9	124	0.329	-21.88	30.5	23
		127	0.319			
	-12	188	0.3			
		184	0.298			
S1PG64-22 +RAP1(40)P	-6	107	0.337	-20.7	32	26
		104	0.321			
	-9	148	0.312			
		146	0.309			
S1PG64-22 +RAP1(60)P	-6	160	0.334	-20.47	37.5	28
		145	0.333			
	-9	240	0.309			
		227	0.313			
S1PG64-22 +RAP2(25)P	-9	129	0.321	-21.83	32	26
		125	0.343			
	-12	186	0.302			
		188	0.294			
S1PG64-22 +RAP2(40)P	-6	137	0.303	-19.69	36	27
		136	0.305			
	-9	187	0.289			
		184	0.282			
S1PG64-22 +RAP2(60)P	-6	145	0.328	-20.41	39.5	30
		149	0.296			
	-9	239	0.289			
		235	0.284			

3.6.4 AFM Test Results

A Dimension Icon AFM system, procured from Bruker Inc., was used to test RAP3 and RAP4 binder blends. The primary target for the AFM test was to observe the changes in the morphology due to addition of RAP and aging. Jäger et al. (Jäger et al., 2004) stated that different chemical compositions resulted in different microstructures and morphologies of asphalt binders. Hence, the differences in the morphology of the asphalt can be examined as a representation of the changes in the chemical compositions of asphalt binders. Differently aged RAP3 and RAP4 blends (25%, 40%, and 60% RAP by weight) were examined with a scan area of 10 µm × 10 µm area using the tapping mode of AFM. Common phases in the morphology of asphalt binder are presented in Figure 3.17.

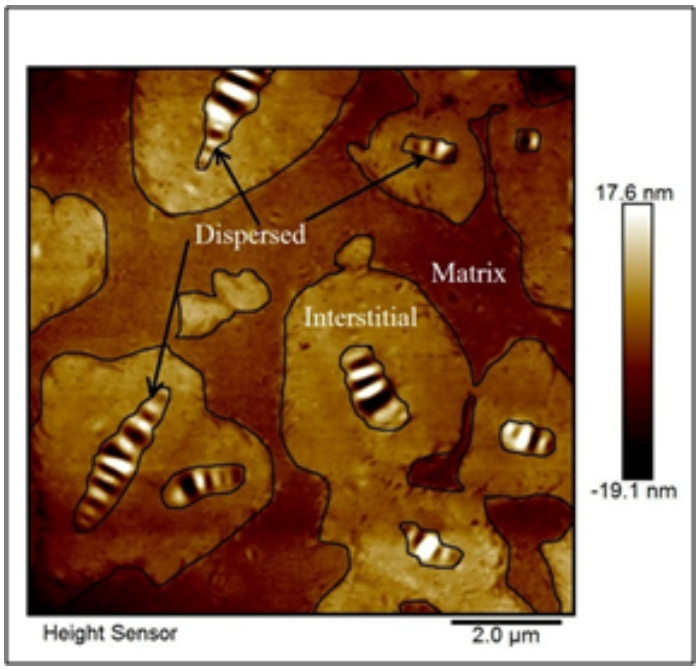

Figure 3.17. Different Phases of Asphalt Binders (PG 64-22)

The morphologies of tested binder blends are presented in Figures 3.18 and 3.19. Figure 3.17 shows the AFM result for the control sample. The control (PG 64-22) was tested in unaged condition only. In the control sample, three distinct phases, namely dispersed, interstitial, and matrix, were observed. These phases are sometimes referred to as the Catana, Peri-phase, and Perpetua phase, respectively in the literature.

It is clear from Figure 3.17 that the interstitial phase covers more area than the dispersed or the matrix. Relevant studies (Rashid and Hossain, 2016; Rashid, 2016) show

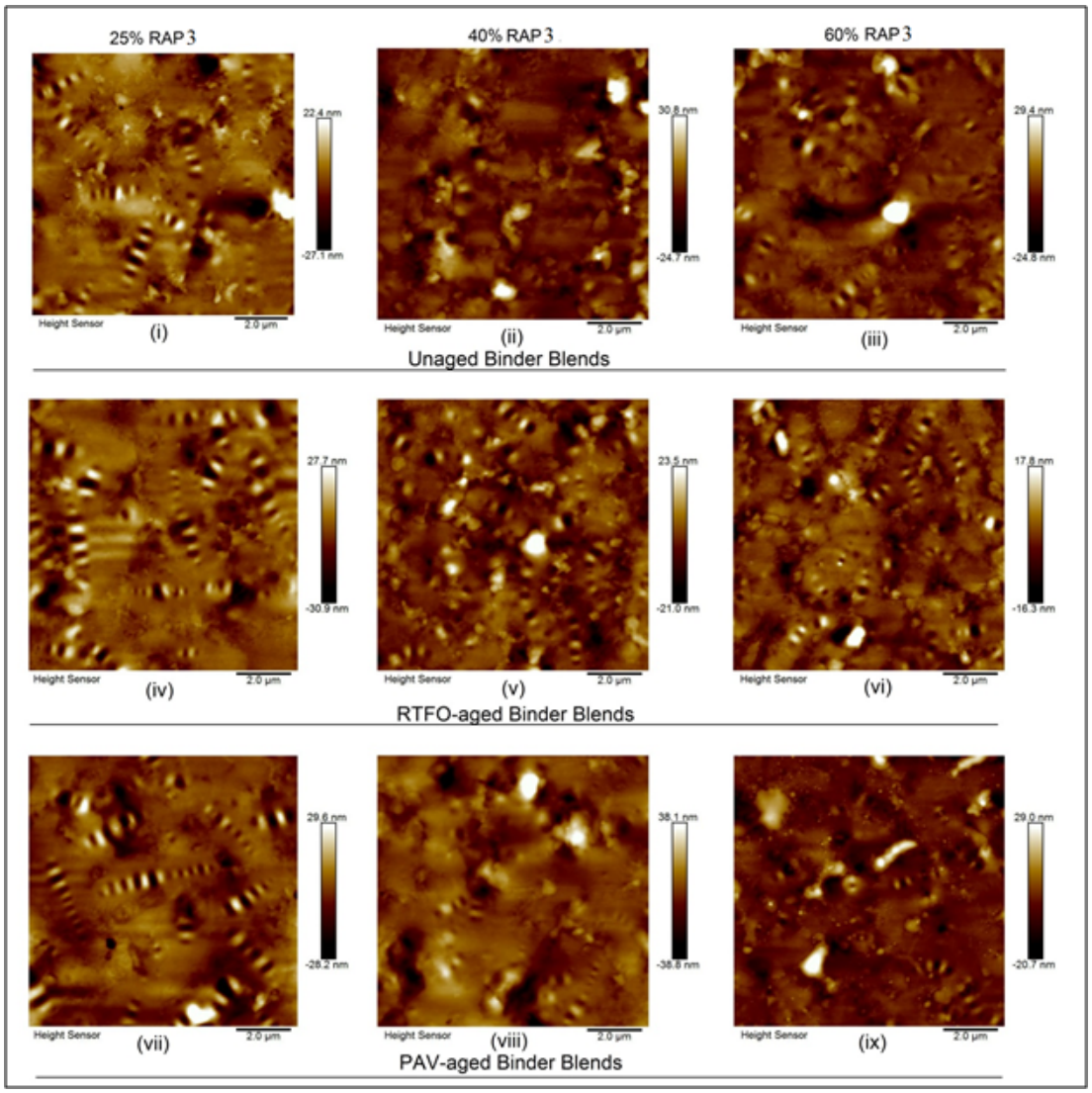

Figure 3.18. Morphology of RAP3 Asphalt Blends: (i) - (iii) 25%, 40%, and 60% Unaged Blends, (iv) - (vi) 25%, 40%, and 60% RTFO-aged Blends, and (vii) - (ix) 25%, 40%, and 60% PAV-aged Blends, Respectively

that different phases of asphalt binder possess different mechanical properties. From Figure 3.18, the morphology maps of RAP3 modified asphalt binders with different aging conditions and blend proportions can be seen. In Figure 3.18, each row represents samples of unaged, RTFO-aged, and PAV-aged binders, while each column represents proportions of 25%, 40%, and 60% RAP by the weight of the total blend. It is clear that 25% RAP3 binders of all aging conditions showed the dispersed, interstitial, and matrix phases in the morphology, although the dividing lines between interstitial and matrix were not as

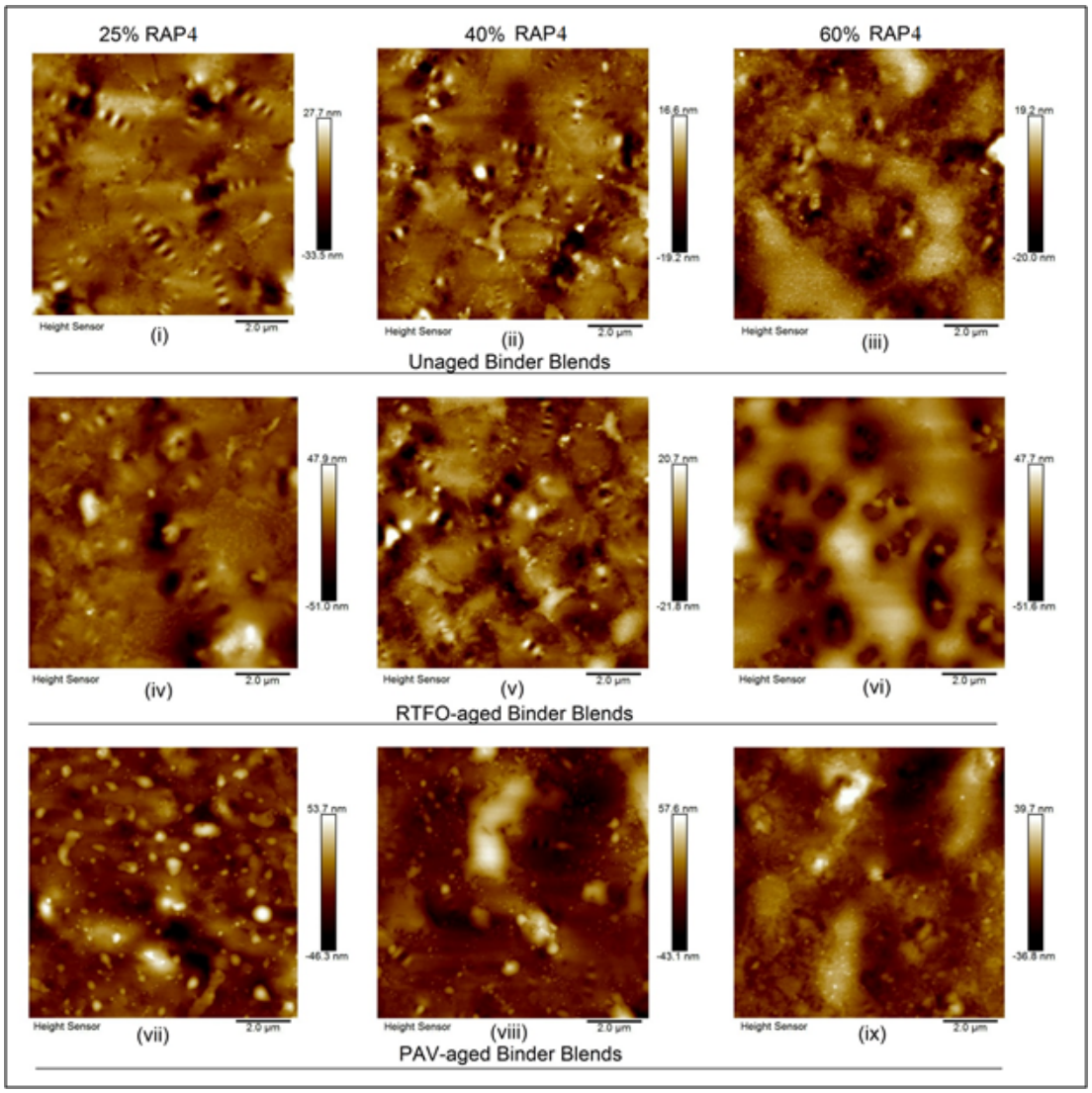

Figure 3.19. Morphology of RAP4 Asphalt Blends: (i) - (iii) 25%, 40%, and 60% Unaged Blends, (iv) - (vi) 25%, 40%, and 60% RTFO-aged Blends, and (vii) - (ix) 25%, 40%, and 60% PAV-aged Blends, Respectively

clear as the control. As the binders were aged, the "bee" structures changed noticeably both in numbers and sizes. In the PAV-aged blends, the number of "bees" was fewer than the unaged blends with a diminishing trend along with aging of asphalt. Recently, it has been revealed that "bee" structures seen on surface are correlated with smaller sized "ant" structures in the bulk (Ramm et al., 2016); so the phenomenon observed on the surface is somewhat of an amplified view of what happens in the bulk. The morphological images of RAP4 modified binders of different blend proportions and aging conditions can be seen

in Figure 3.19. For the 25% RAP4 blends, the unaged sample showed all three phases as the control. But it seemed that the dispersed phase was diminishing in RTFO-aged samples, which finally turned into small protrusions in PAV aged binders. The changes in "bees" were also seen in 40% RAP4 blends irrespective to the aging conditions. For the 60% blends, the bees were almost absent in the unaged sample; in RTFO- and PAV-aged samples, the changes in morphology were significantly different from the 25% blends.

3.6.5 Effect of Rejuvenator

The effect of rejuvenator on the RAP blended asphalt binders was evaluated in this study. The 40% RAP blend for all four types were chosen to be rejuvenated for this study. Based on the suggestion of a practicing engineer from the Oklahoma Department of Transportation (ODOT), a commercial rejuvenator named as Evoflex®was selected to rejuvenate the RAP blends. All rejuvenated blends were subjected to the Penetration test, RV test, and DSR test in unaged condition. The results of rejuvenated blends and corresponding RAP blends are discussed in this section.

The comparative result of the Penetration tests of rejuvenated RAP blends and RAP blends are presented in Figure 3.20. Four types of RAP binders, 40% RAP blends, and rejuvenated 40% RAP blends were considered from the penetration test. The RAP binders showed low penetration values (lower than 10) whereas blending of RAP binder in the base binder increased those values up to 30. A lower value of penetration indicated high stiffness of binders. The RAP binders were more than 10 years of age, hence they were expected to show low penetration value. The blending of RAP binders with the neat binder reduced the stiffness of the RAP binder, which is reflected in the penetration values of 40% RAP blends. The addition of rejuvenator further increased the penetration values of the blends. RAP3 showed the maximum penetration value of 65 after the rejuvenation while RAP2 showed the lowest increase (40) in the penetration result. RAP1 and RAP4 blends showed similar values around 50 after the rejuvenation. A similar set of results were seen in the case of RV test of RAP blends. RAP1 and RAP4 blends showed increasing trend in viscosity values at different test temperatures while RAP2 and RAP3 showed lower magnitudes of increase in viscosity values. The RV tests were done on rejuvenated RAP blends and compared with the corresponding blends in Figure 3.21.

In Figure 3.21 the viscosity test data of original RAP binder are also included to observe the effect of rejuvenator on the RAP blends. The mixing and compaction temperatures

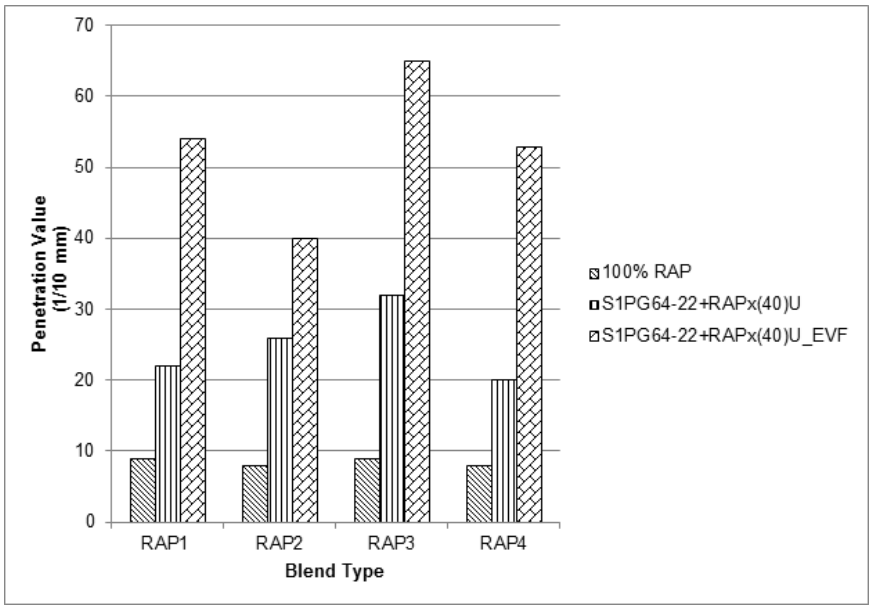

Figure 3.20. Penetration Test Data of Rejuvenated Blends

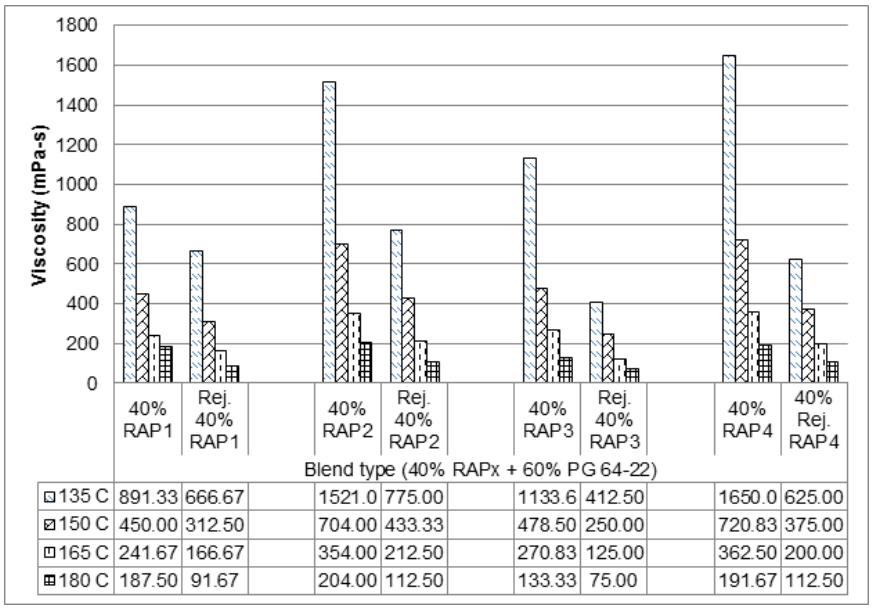

	40% RAP1	Rej. 40% RAP1	40% RAP2	Rej. 40% RAP2	40% RAP3	Rej. 40% RAP3	40% RAP4	40% Rej. RAP4
	Blend type (40% RAPx + 60% PG 64-22)							
135 C	891.33	666.67	1521.0	775.00	1133.6	412.50	1650.0	625.00
150 C	450.00	312.50	704.00	433.33	478.50	250.00	720.83	375.00
165 C	241.67	166.67	354.00	212.50	270.83	125.00	362.50	200.00
180 C	187.50	91.67	204.00	112.50	133.33	75.00	191.67	112.50

Figure 3.21. Comparative Viscosity (mPa-s) Data of Rejuvenated Blends

for rejuvenated blends can be observed from Figure 3.22. According to AASHTO T 312, the mixing and compaction temperatures of HMA are expressed in ranges of temperature based on asphalt blend viscosities. The viscosity values for mixing and compaction are suggested as 170 $\pm$ 20 mPa-s and 280 $\pm$ 30 mPa-s, respectively. In this study, The ASTM

D 2493 method was adopted to determine the mixing and compaction temperatures of the binder blends. As can be seen from Figure 3.22, the 40% RAP blends were so viscous that they would require mixing temperatures higher than 180°C, which would require special consideration. The application of rejuvenator helps solve this problem. The rejuvenated blends were found to have lower viscosities at each tested temperature. Based on the viscosity requirement of mixing HMA ingredients, Figure 3.22 suggested a mixing temperature range of 157°C - 173°C for rejuvenated 40% RAP blends. The compaction temperature range was found to be 144°C - 162°C. Hence, it can be said that the rejuvenated blends can be mixed at 165°C $\pm$ 8°C and compacted at 153°C $\pm$ 9°C. These mixing and compaction temperatures confirms to the temperatures suggested in TxDOT Report No. 1250-5 (Yildirim et al., 2006).

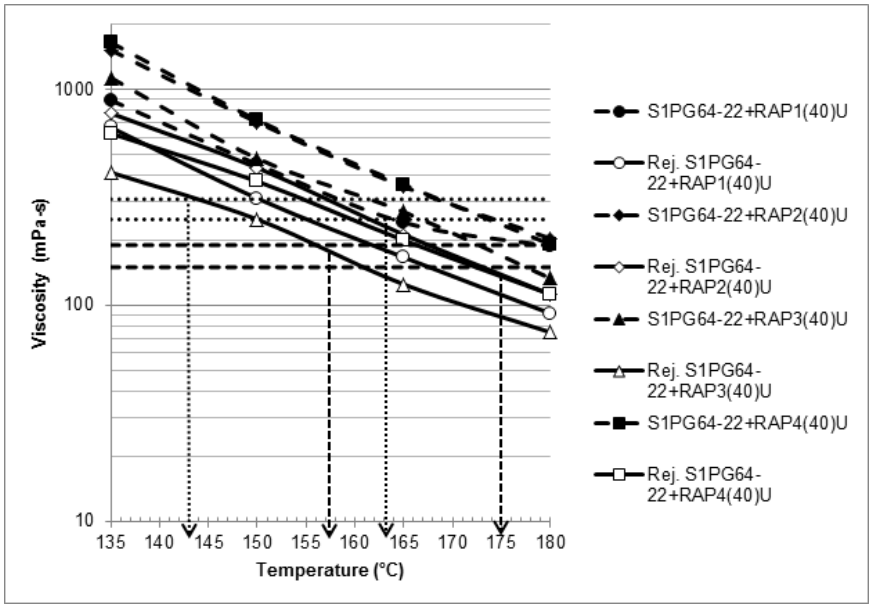

Figure 3.22. Compaction and Mixing Temperatures for Rejuvenated Blends

The rejuvenator affected the mechanistic properties like the viscosity and shear modulus values. The DSR test results on rejuvenated blend sets are presented in Figure 3.23. The effects of rejuvenator on the RAP blends were observed in the PG temperatures. The rejuvenated blends were softer than their base blends, hence failed earlier in high temperature DSR testing. All of the four RAP blends showed high PG temperature from 76 °C to 82 °C. The rejuvenated RAP blends failed at temperatures ranging from 63 °C to 73 °C. The high PG temperature of rejuvenated blends were in the same range of the base binder (PG 64-22) used in this study. As the rejuvenator acted like a binder softener

which has been seen in Figure 3.23, it is expected that the low PG temperature of these blends would also be lowered to some extent. From Tables 3.5 and 3.6, the influence of high RAP contents on base binder PG grade can be seen. The RAP binder increased the low temperature grade of the blends. The rejuvenator can be used to resolve this specific issue which would eliminate the requirement of using a softer base binder to achieve a target binder blend after the addition of the RAP binders.

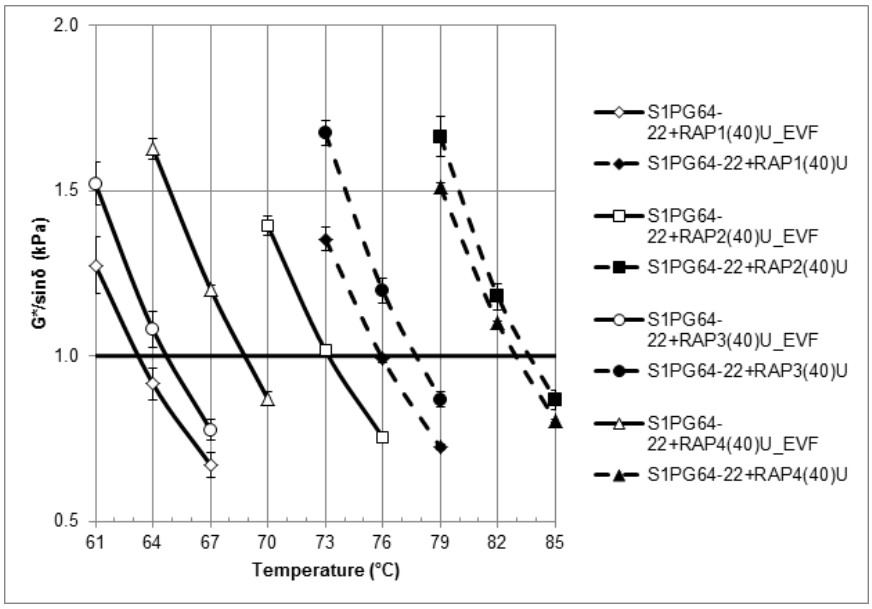

Figure 3.23. DSR Test Data of Rejuvenated RAP Blends

3.7 CONCLUSION

The Federal Highway Administration (FHWA) promotes using Reclaimed Asphalt Pavement (RAP) in new pavement construction. To achieve maximum use of RAP in the construction, the characterization of RAP blended asphalt binder is very important. One of the goals of this study was to investigate the differences in behavior of RAP binders from different origins. The findings of this study are summarized as follows:

3.7.1 Properties of RAP and Pavements

- The climatic data for the good performing and poor performing sections were similar. Hence, it can be said that construction weather had no effect on the field

performance of the pavements.

- The two poor sections (RAP2 and RAP4) showed high IRI values (up to 4.7 m km^{-1}) in their first three years of service lives, whereas the other two good performing sections showed low IRI values of 1.6 m km^{-1} or lower over their lifetimes. A high initial IRI value could have exacerbated the premature failure of the RAP2 and RAP4 pavement sections.
- The rut depths showed similar magnitudes and trends for all pavement (good and poor performing) sections over their lifetimes. Although higher rutting values were expected for poor performing sections, the ARAN data did not show such trend. The probable explanation could be that the field data collection system needed improved accuracy or that the rutting values were not associated with the poor performance of the sections RAP2 and RAP4.

3.7.2 Superpave Test Results

- The RV tests showed very high viscosity of RAP2 blends at all test temperatures compared to other blends. A high stiffness of the binder made it more susceptible to low temperature cracking, which was reflected in the field performance of the RAP2 pavement section.
- The DSR test on unaged and RTFO-aged binder blends showed increased high PG temperatures for all RAP blended binders. A higher amount of RAP binder increased the high PG temperature further. In the case of 60% RAP, the maximum PG temperatures of RAP1, RAP2, RAP3, and RAP4 blended binders were 85 °C, 91 °C, 82 °C, and 88 °C, respectively.
- The addition of RAP increased the low PG temperature similar to the way the high temperature grades increased. The BBR test revealed that all percentages of RAP binders failed around −20 °C, whereas the base binder's low critical temperature was −22 °C .
- The observation of DSR test results at intermediate temperatures and the BBR test results suggests that RAP binders can safely be applied up to 60% by weight of the mixture from the viewpoint of resistance to fatigue failure of the pavements. However, the ability of this parameter to accurately reflect fatigue cracking resistance itself has been questioned in the recent years. Moreover, the addition of RAP binders makes the blends susceptible to low temperature failure. The use of

a softer base binder or a rejuvenator with the RAP binder is suggested to maintain the design PG binder grade.

3.7.3 AFM Test Results

- The AFM tests revealed different phases and morphologies of the asphalt blends. Distinct dispersed, interstitial, and matrix phases could be identified. These phases were greatly changed due to the addition of RAP binder and the aging of the binder blends.
- The dispersed phase (bee structures) showed a tendency to disappear as the blends were aged or the amount of RAP binder was increased.

3.7.4 Influence of Rejuvenator

- The use of rejuvenator reduced the viscosity of the RAP blends, as expected.
- The amount of rejuvenator (12.5% of RAP binder) restored the original high PG temperature of 40% RAP1 and 40% RAP3 blends, but the PG high temperatures for the RAP2 and RAP4 blends were still higher than 64 °C .
- It can be said that the rejuvenator dosages were dependent on the RAP binder type and can be related to the viscosity values of the RAP binders.
- The use of a rejuvenator lowered the mixing and compaction temperature of high RAP content asphalt blends.
- The use of rejuvenator facilitates allowance of high RAP content in the asphalt mix. Rejuvenators also eliminate requirement of a softer grade base binder to maintain the design criteria of the final mix.

CHAPTER 4. SPECIMEN FABRICATION AND TEST METHOD

This chapter summarizes the devices and specimen fabrication methods that were employed in this study. Specifically the focus is on the methods used to measure the tensile strength of asphalt binders and mortars or FAM.

4.1 TEST DEVICES

Several testing devices were utilized to measure material properties to accomplish the goals of this study. In all cases, the tests were conducted using a beam specimen. Three testing devices used were used in this study: a Cannon Instrument Company TE-BBR (BBR), a Cannon Instrument Company TE-BBR Pro (BBR Pro), and an Instron E1000 (Instron). More specifically,

- standard creep tests were performed using the BBR and BBR Pro at low temperatures,
- monotonic load tests until failure were performed using the BBR Pro at low temperatures, and
- creep and monotonic load tests were performed using the Instron at intermediate temperatures.

4.1.1 Bending Beam Rheometer

The primary device that was used for testing in this study was the Cannon TE-BBR Pro Thermoelectric Bending Beam Rheometer (Figure 4.1). This device is similar to the Cannon TE-BBR specified in the AASHTO T 313 guide for determining the flexural creep stiffness of asphalt binder. Both devices use thermoelectrically cooled baths with a medium of methanol to achieve temperatures from 0 °C to −40 °C. This study will include the testing of asphalt binder specimens below a temperature of 0 °C therefore taking full advantage of the low temperature range of the BBR and BBR Pro. These devices were both designed as three point loading systems that use compressed air to control the air bearing and load shafts. Within this three point loading system the devices allow for variable span lengths of 100 mm, 120 mm, 140 mm, and 160 mm. For this study the 100 mm span length was chosen because that is the same span length used in the

AASHTO T 313 testing procedure.

Figure 4.1. TE-BBR Pro Thermoelectric Bending Beam Rheometer

Although the BBR and BBR Pro have a lot of similarities the main difference, and the reason why the BBR Pro was chosen, was because of the load capacity and programmable load patterns that are possible using the latter. The TE-BBR can only apply a single loading pattern consisting of a block loading of 0.98 N for a duration of four minutes, while the TE-BBR Pro can apply various loading patterns and has a maximum load of 44 N. Loading patterns such as block loading with multiple cycles or monotonic loading with different loading rates can all be programmed into the BBR Pro. These loading patterns can be programmed to apply various durations of block loads or number of loading cycles. Loads can also be applied in a linear monotonic fashion until the test specimen has reached failure. This increase in capacity and ability to program in various loading patterns was crucial for the goal of this study.

As stated before these testing devices were designed as three point loading systems. A three point loading system consists of two specimen supports and one point of load application at the midpoint, which can be observed in Figure 4.2. The loading contact is made of a hard durable plastic that applies a point load at the contact point. The load shaft applies the preset load at the midpoint between the two specimen supports; at this location the deflection is measured and using simple beam theory the beam stiffness, stress, and strain can be calculated using the force and deflection values at any given point in time. All of the binder tests were performed with this type of a load system.

Based on preliminary tests with the binder and mortars, it was observed that repeatability of the test could be improved using a four point loading system. This is particularly true for failure tests in which the beam is loaded until failure. This is unlike stiffness measurement where the beam is only subjected to small loads and deformation. In a three point loading system the maximum stress is at the center of the beam, which may or may not be the weakest point in a representative volume. The use of a four point beam configuration alleviates this concern and allows the failure to originate from any point within the middle third of the beam, thus accounting for the spatial heterogeneity in the specimen (particularly for mortar specimens).

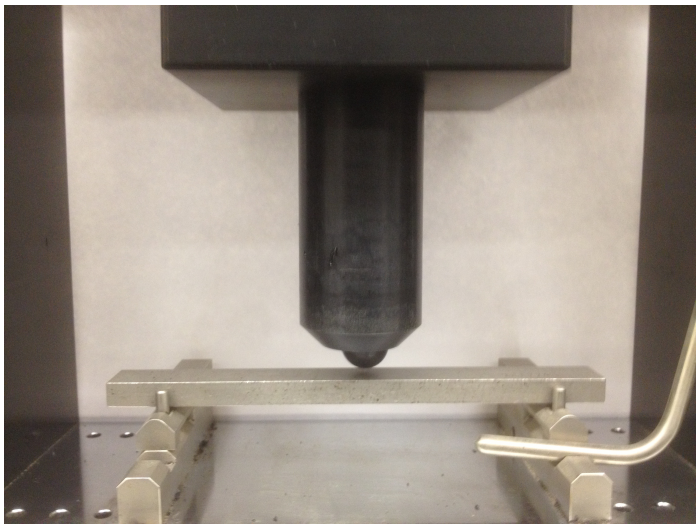

Figure 4.2. TE-BBR and TE-BBR Pro Three Point Loading System

Based on the aforementioned rationale, it was proposed that a four point loading system could possibly increase the repeatability and accuracy of the tests being run. The four point loading system that was designed and used in this study can be seen in Figure 4.3. The span length between the two load application points was 33 mm or 1/3 of the total span length. Due to the design of the machine the load is applied at these two points simultaneously through a single vertical axis while measuring the deflection of the vertical axis. The two load applicators are cylindrical in shape, span the entire width of the test specimen and are made of a solid piece of aluminum, unlike the load button in the three point system. The decision to make the load applicators cylindrical and span the entire width of the specimen came from similar geometries from ASTM polymer (ASTM D7264), plastics (ASTM 6272), and concrete (ASTM C78) standards. This load application beam

is connected to the load shaft via a swivel ball joint that allows the two load application bars to contact the beam as squarely as possible.

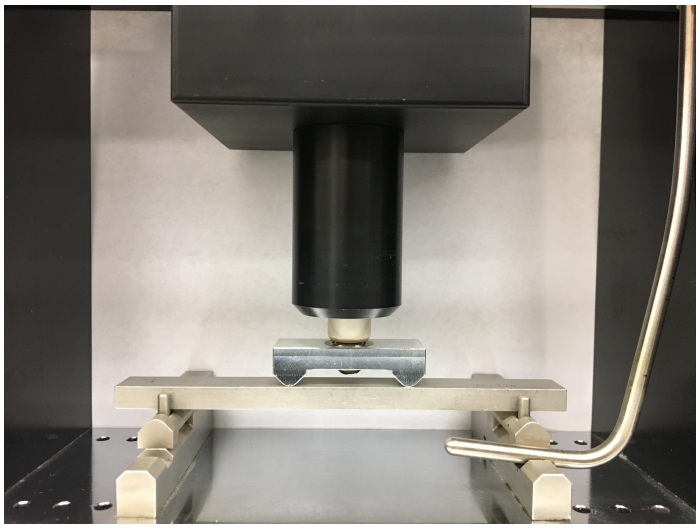

Figure 4.3. TE-BBR Pro Four Point Loading System

4.1.2 Instron E1000

A secondary device that was used to test fracture properties was the Instron E1000 universal testing machine. This device is similar to the TE-BBR Pro in that the load profiles can be customized and programmed into the machine for a specific test. The maximum capacity of this device is 1000 N which will provide more than enough force for the tests that will be conducted in this study. For this study the temperature of the beams being tested is important, so a plexiglass prismatic temperature chamber was constructed around the device's pneumatic grips. To keep the temperature from fluctuating drastically within the temperature chamber, insulation was added to the inside. A solid state air conditioner supplied an airflow through the plexiglass chamber to cool the test specimens as well as keep the temperature stable within the plexiglass temperature chamber. Therefore the cooling medium in this device was air as compared to methanol in the BBR devices.

Custom four point loading beam supports and load applicators were constructed to fit in the pneumatic grips of the Instron. The span length between the supports was chosen to be 100 mm to match the length chosen in the BBR devices. Similarly, the span length between the load applicators was set at 33 mm or 1/3 of the total span length. These supports were fabricated from various pieces of aluminum and similar to the BBR

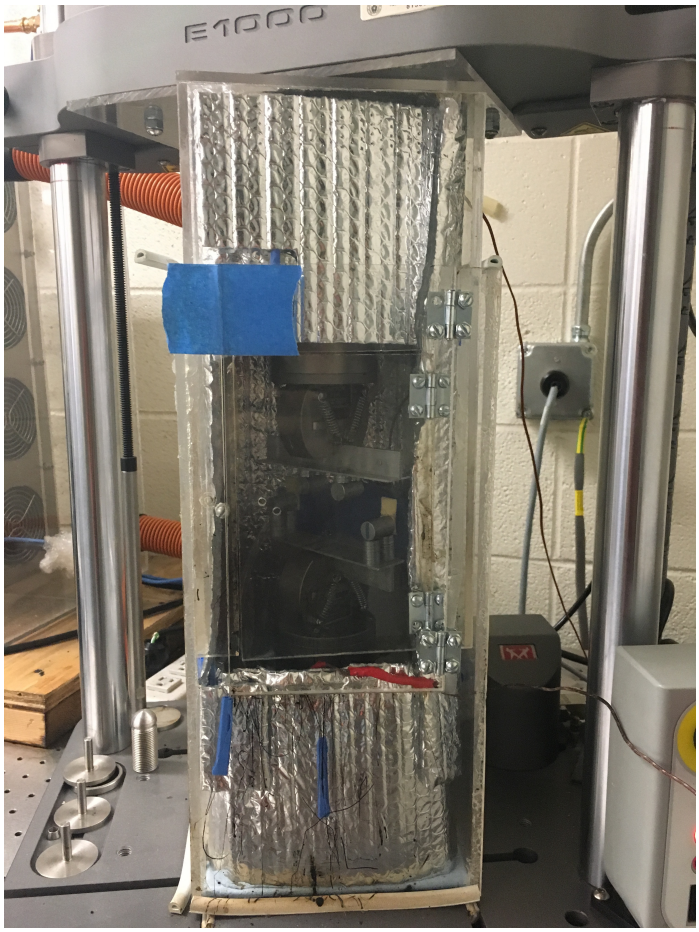

Figure 4.4. Instron E1000 Plexiglass temperature chamber with added insulation

load applicators, cylinders that spanned the entire width of the samples were used. The supports fabricated and used are pictured in Figure 4.5.

4.2 SPECIMEN FABRICATION

There were two different material types that were examined in this study asphalt binder and asphalt fine aggregate matrix (FAM). Fabrication of test specimens for these two materials is very different. The methods for preparing test specimens will be discussed further in the following sections.

Figure 4.5. Instron E1000 Supports Used for Mortar Testing

4.2.1 Specimen preparation for binders

Sample fabrication for asphalt binder is well outlined in the literature and easy to follow. For this study, the procedure in AASHTO T 313 was followed to fabricate binder specimens. The only addition to this procedure was a remolding process after the sample had been tested at a particular temperature. In order to conserve materials some of the binder specimens were remolded and tested at a different temperature. The remolding process consisted of placing the tested sample back into its mold and slowly heating it on a hot plate until observing a glassy surface and the fracture point close. Once both of the mentioned indicators had been observed, the mold containing the test specimen was removed from the hot plate and was allowed to cool to room temperature and then placed into a freezer to cool the sample for the standard demolding process. The remolding process was

only used when necessary, otherwise the standard AASHTO procedure was followed. In a separate side study the influence of aging on this process was found to be insignificant since the binder was heated to a very limited temperature for a very short duration of time.

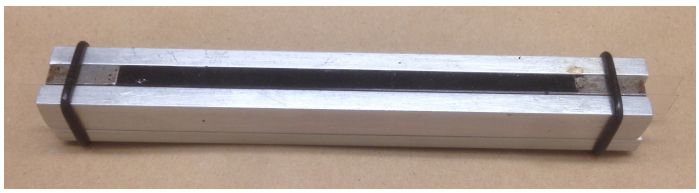

Figure 4.6. Asphalt Binder Beam in Standard Molds Described in AASHTO T 313

4.2.2 Specimen fabrication for mortars

Fabrication of FAM samples is not as standardized or well outlined as the binder process. For this reason, two different methods were used to fabricate FAM samples, one being a streamlined single sample direct compaction method, while the second was a more rigorous method that involved Superpave Gyratory Compaction and cutting samples out of a larger cylindrical sample. These two methods will be discussed in more detail in the following sections.

4.2.2.1 Direct compaction method

The use of direct compaction method to fabricate a single FAM specimen is a new process. There are several major reasons for implementing a specimen construction process as the one that will be described. High quality materials are essential for small scale lab testing and can be scarce for research purposes. Using these materials in the most efficient way possible is crucial in a research setting. The proposed process is efficient in terms of the materials, operator time, and laboratory space and capital equipment required to fabricate test specimens. The proposed process would not only economize material use, but it would also save the fabricator time.

The direct compaction method proposed and used in this study can be easily implemented on a benchtop workspace. This benchtop workspace could be deemed as a "mini compaction lab." For mixing purposes a small counter top mixer customarily used for

cooking applications was repurposed for the FAM mixtures. Compaction was performed via a mechanical hydraulic press and robust beam molds designed for this application. A small bulk specific gravity measuring setup was created for comparing densities between samples once compacted. For all the heating needs, a small oven was setup within close proximity of the benchtop setup. Figure 4.7 shows the mini compaction lab setup that was used for constructing these samples. As mentioned earlier, there are several major incentives for developing and implementing this procedure. The remainder of this section presents the method and reasoning behind some of the steps. The method is presented in as much detail as possible for the benefit of future researchers or engineers who may want to replicate this procedure. Also, the method as described is based on the outcome of several trials that were conducted before arriving at this procedure.

Figure 4.7. Benchtop Sample Fabrication Setup for FAM Specimens

FAM mixing was done in the small benchtop mixer shown in Figure 4.7. The process that was followed for mixing was similar to that described in TEX-205-F the Texas Department of Transportation Laboratory Method of Mixing Bituminous Mixtures. A FAM mix design was used as a guide for the FAM samples used in this method. This mix design called for the largest aggregate used to be retained on a # 30 (0.6 mm) sieve and the smallest aggregate to be used to pass a # 200 (0.075 mm) sieve (note that different studies have adopted slightly different maximum size). The gradation for this FAM mix can be observed in Table 4.1 A binder content of 9% was used for this mix design and all of the direct compaction method samples.

Table 4.1. Gradation Proportioning of Aggregate for FAM Mix

Sieve Size (mm)	1.18	0.6	0.3	0.15	0.075	0
Sieve Number	#16	#30	#50	#100	#200	-#200
Retained (%)	0.0	33.3	19.0	14.3	16.7	16.7

The separated aggregate was placed in the oven at the designated mixing temperature (150 °C) 24 hours before mixing to make ensure that the aggregates were devoid of moisture. The mixing bowl was also placed in the oven at least 30 minutes before the weighing process. All the aggregates were weighed out and added to the mixing bowl in the correct proportions. These aggregates were then dry mixed to ensure that segregation would not occur and then placed back into the oven to reach the proper mixing temperature. A PG 67-22 binder was chosen for the FAM samples which calls for a mixing temperature of 150 °C. The asphalt binder was placed in the oven two hours before mixing to reach the proper temperature. Once both the aggregate and asphalt binder had reached the proper mixing temperature, which was verified using a thermocouple, they were pulled out of the oven. The bowl was placed on a scale and a small depression was made in the center of the aggregates to receive the asphalt binder as recommended by TEX-205-F. Asphalt binder was then added in the proportion by weight and the bowl was placed under the mixer. The metal whisk used for mixing was pulled out of the oven attached to the device and the mixing was started. Two small heaters were turned on to supply heat to the bowl during the mixing process and reduce the rate at which the mix cooled as the asphalt binder coated the fine aggregates. Once all of the aggregates appeared to be fully coated by the asphalt binder, the mixing process was completed. The mixture was then spread out across a metal pan evenly and placed back in the oven to be short term aged for two hours at a temperature of 120 °C. After the short term aging process was completed the mixture was poured into a bowl and covered with aluminum foil to be stored at room temperature until the compaction process could begin.

For this direct compaction method, two compaction molds were designed and fabricated out of steel. Steel was used to help decrease heat loss during the compaction process and to minimize micro scratches that could damage the molds making sample extraction more difficult. These molds are put together using nine separate pieces and ten bolts, which can be seen in Figure 4.8. The bottom most plate is the thickest piece so that it can sustain high compaction loads and the sample side plates are easily removable

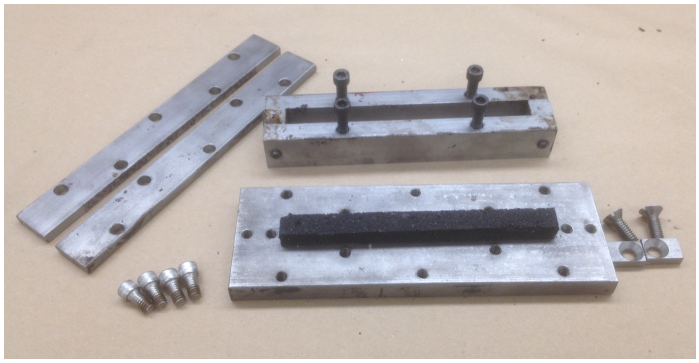

Figure 4.8. Compaction Mold Showing Separated Pieces and Sample Position

in order to simply remove the sample without damaging it. The setup was designed with a steel compaction plunger and a plunger guide to ensure square seating between the sample material and the compaction load (Figure 4.9). This mold worked well for the application it was designed for.

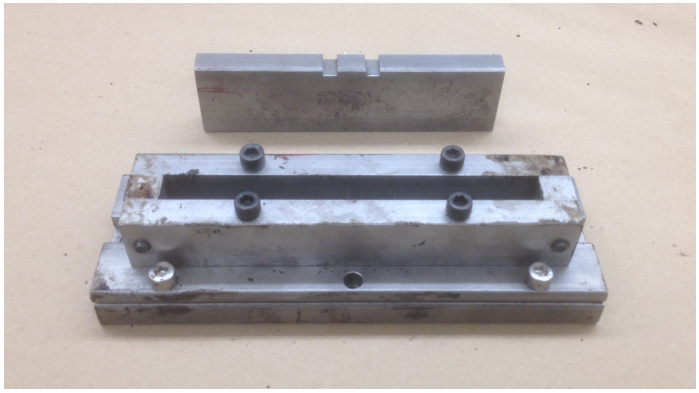

Figure 4.9. Constructed Compaction Mold with Compaction Plunger Used in Direction Compaction Method

This compaction process was started by assembling the clean mold and plunger and placing them in the oven that was set at the compaction temperature. The compaction temperature used for this method for this mix was 145 °C, the reasoning for the choice of this temperature will be discussed following this procedure. Using a warm spatula, 25 g of FAM mix was weighed out and placed into a small aluminum container. The mold and plunger were heated in the oven for at least one hour to ensure the uniform compaction temperature had been reached throughout the mold. The small aluminum cups containing the FAM mix were placed in the oven for 30 minutes to reach compaction temperature.

After both the mold and mix were thoroughly heated, they were taken out of the oven so the mix could be placed into the mold. FAM mix was then carefully scooped into the hot mold using a warm spatula ensuring minimal loss of mix during this process. The mix was placed into the mold as evenly as possible. Then a warm flat spatula was used to distribute any larger piles of mixture and was smoothed by inspection to achieve a level surface. Once a level surface was achieved the mold containing the mixture was placed back into the oven for 15 minutes to warm back up to compaction temperature. After 15 minutes had passed, the mold was removed from the oven and the hot plunger was placed into the guide making sure that it was square against the material. The mold was then placed under the ram of the press, ensuring that the center of the ram and the center of the plunger were squared against each other. A two metric ton load was then applied to the plunger and sample. This load would be applied for a duration of five minutes. Throughout this five minute loading time the FAM material would relax due to its viscoelastic nature causing the applied load to decrease. The load would be adjusted back up to two metric tons anytime the pressure gauge needle dipped down below the two metric ton line. Due to the capacity of the hydraulic press and the gauge there are no incremental lines between the one metric ton line and two metric ton lines, therefore the load couldn't be measured as it decreased. After the load had been applied for five minutes the load was released and the mold containing the material and plunger were placed back into the oven for 15 minutes. During these 15 minutes the plunger remained in the mold on top of the material and it was not removed during reheating. Subsequently the mold was taken out of the oven, placed back under the ram of the press and two metric tons was applied again for five minutes following the same reloading process described before. Once the five minutes had concluded the load was released and the mold was placed in front of a small fan to cool to room temperature.

After the mold had reached room temperature, the demolding process was begun. First the two side bolts holding the plunger guide together were loosened and the guide was lifted up off of the mold. Then using the back end of a screwdriver the plunger was tapped on either side until it was loosened from the sample and removed. Following the removal of the plunger the two end pieces were removed. Afterwards all four screws were removed from the two sample side plates and using a flat head screwdriver between the side plate and the base plate the side plates were lifted from the base. All that was remaining was the sample and base plate, but due to the high temperatures and compaction loads the sample adheres to the base plate. Taking one of the side plates and placing it square

against the sample then using the back of the screwdriver and tapping on the side plate produced enough force to break the sample free of the base plate without causing any damage.

The maximum specific gravity of the FAM was determined using a sample of the loose mix and a method very similar to that used for asphalt mixtures. In order to ensure that the direct compaction method samples had been compacted adequately, the bulk specific gravity of the direct compaction samples were measured and compared to the maximum specific gravity. The maximum specific gravity for this mix was 2.21, which would be the target value for the direct compaction method. The variables that would be altered were the compaction temperature, load applied, duration of load application, and number of load applications. Table 4.2 shows the changes that were made to the variables mentioned and the method that resulted in a bulk specific gravity within five percent of the target value.

Table 4.2. Compaction Methods Used to Achieve Bulk Specific Gravity Goal

Method	Temp. (°C)	Load Applied (t)	Load Duration (min)	Application Rounds	Bulk Sp. G.	Percent of Target
1	125	1	5	1	2.088	94.48
1	125	1	5	1	2.014	91.15
2	125	1	15	1	2.004	90.68
2	125	1	15	1	2.027	91.71
3	125	1	5	2	2.000	90.50
3	125	1	5	2	1.911	86.45
4	125	2	5	1	2.038	92.20
4	125	2	5	1	1.949	88.20
5	135	1	5	2	1.983	89.73
6	135	2	5	1	1.916	86.68
7	145	1.5	5	2	2.068	93.60
8	145	2	5	1	1.989	90.01
9	145	2	5	2	2.179	98.60
9	145	2	5	2	2.179	98.58

The goal of creating this compaction method was to try and minimize the amount of time it would take while also producing a test specimen that had been adequately compacted. To accomplish this, the load duration was kept reasonably low at five minutes

but in order to reach the proper compaction, multiple rounds were added to the process. It was also found that the compaction temperature was one of the most important variables in the process and this was increased throughout our experimentation from 125 °C to 145 °C until desired and consistent results were obtained. The warmer the material the more it flows therefore the compaction gets better as the temperature is increased. It was also observed that multiple rounds of loading with reheating in between the load application aided in meeting the goal bulk specific gravity. An increase in bulk specific gravity can be observed when reviewing the values starting at Method 3 and progressing to Method 7. This is also true when comparing Method 7 and Method 9, where the only difference between these two methods was the amount of load applied. Between Methods 7 and 9 a significant increase in bulk specific gravity can be observed from 2.068 to 2.179. Method 9 was within 98% of the bulk specific gravity goal. Once this method of compaction had been established the bulk specific gravity was tested for every sample making sure that it stayed above 95% of the goal (100% compaction). This method was developed to cut down on material use, fabrication time, as well as lab space and to have then entire fabrication process fit within a small benchtop area. Finally, it is important to highlight one additional factor. The maximum specific gravity calculated for FAM was not as repeatable as compared to the full asphalt mixes. This is because FAM comprises of a much higher percentage of finer aggregate particles. Therefore a bulk specific gravity of 97-99% could well be close to full compaction without any air voids.

4.2.2.2 Superpave gyratory compactor method

FAM specimens were also produced using a second method using the Superpave Gyratory Compactor (SGC). This method is utilized more often and has more of a standardized process such as the one used for fabricating the binder samples. The overall process is similar to that used in the direct compaction procedure in that there is a mixing component and compaction component, but one additional step is required in this process which involves cutting the sample.

The mixing process is similar to that used in the previous method. A main difference between the two methods being the amount of material being mixed. Since the mold for the SGC is much larger, it requires a significant increase in the amount of material. The standard AASHTO T 312 procedure was used as a guide for mixing. A gradation similar to that used in the previous method was used for these samples as well. The binder

content used for these samples was 8% by weight of the batch. Once all the materials had been properly mixed, the loose mix was placed in the SGC mold to be compacted. Also note that the SGC and the direct compaction methods were used for different parts of the study with very different objectives. This explains why the design of FAM was also so different between these two procedures.

After the mixing process was complete, the mix was placed into a 150 mm diameter cylindrical mold and placed into the SGC. Again the AASHTO T 312 procedure was used as the standard guide for compaction. A ram pressure, internal angle, and number of gyrations was input into the machine. The gyration at an angle induces a kneading action to compact the FAM mix inside of the mold. The compaction process is complete when the specified number of gyrations has been reached. Then the sample is allowed to cool for five to ten minutes and is extruded from the SGC mold.

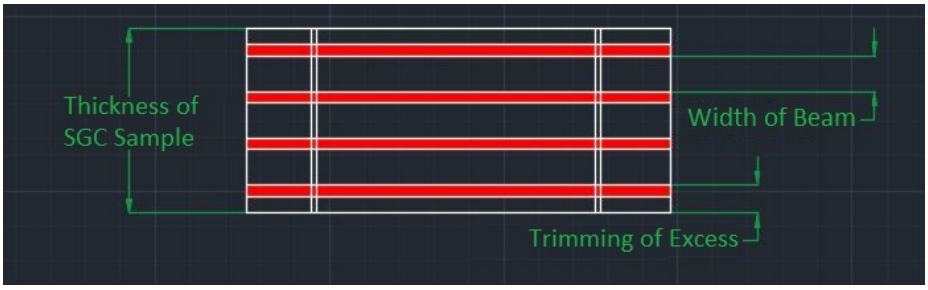

Figure 4.10. Side View of SGC sample showing the slicing locations

The final step in the SGC fabrication process is the cutting procedure. SGC yields a cylindrical asphalt sample that must be cut multiple times to produce beams that can be used in either the BBR Pro or the Instron four point loading systems. The first cuts made are thin slices on the top and bottom of the cylindrical specimen in order to exclude any material that may be susceptible to the boundary effect with non homogeneous air voids. Then the remaining cylindrical specimen was cut into thinner cylindrical slices with a thickness matching that of the desired width of the beams. The locations of the cuts described can be observed in Figure 4.10. Once these slices were cut to the width of the beam then the circular edges are cut off to produce a square prismatic sample. This square prismatic sample was then cut into individual beam samples by cutting vertically with each cut spanning the thickness of the beam samples. A top view showing the necessary cuts to fabricate the FAM beams can be seen in Figure 4.11. The red hatched areas in Figure 4.10 and Figure 4.11 deliniate the amount of material that would be lost

due to the thickness of the blade used in the cutting process. The amount of material being lost should be factored into the process when marking the location for the next cuts to be made. Marking and cutting the SGC sample is one of the most important parts of the SGC beam fabrication method.

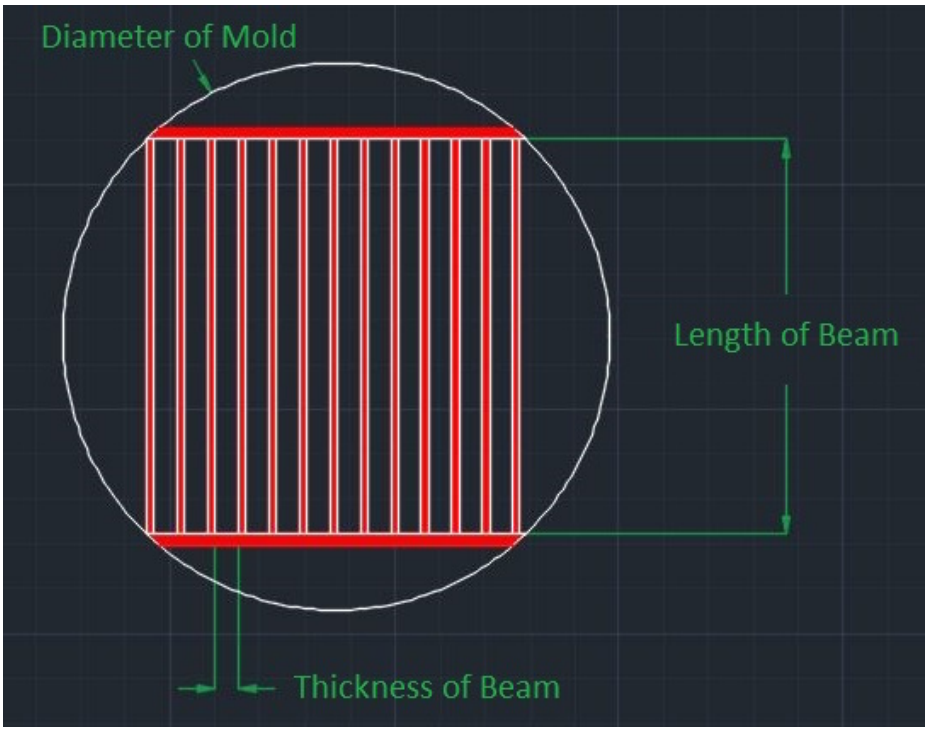

Figure 4.11. Top View of SGC sample showing the slicing locations

Although it may seem that the SGC method is more standardized, this method has its own intricacies as well. It should also be mentioned that even though an SGC standard exists it doesn't include details for FAM mixes or for cutting the samples. Therefore details regarding the mix and the cutting procedure are experiment or lab specific.

4.2.3 Mortar Beam Specimen Preparation

Samples fabricated using either method went through a strict process in order to prepare them for testing. This process was performed to help standardize each beam while also to help improve repeatability. The process included several steps that will be discussed in the following paragraphs.

As the first step in the specimen preparation process, each beam was sanded. The direct compaction method required less sanding than the SGC method. This is due to

the fact that the direct compaction method beams were level once the compaction and demolding process were completed. Since these specimens were level the only sections of the direct compaction mortar beam that were sanded were the points that would be in contact with the beam supports and load applicators. The sanding in these areas was light and was performed just to obtain a smooth surface on the beam.

The sanding process performed on the SGC asphalt beams was much more extensive. Due to the cutting procedure most of the beams were not level. In order to ensure that the load was applied evenly, the beams must be level. A large rotary sander was used to level each of the beams that were to be used in this study. Light and quick applications of pressure were used when sanding in order to ensure that heat did not accumulate within the beam due to the applied friction. Once the beams were leveled, all of the contact points were sanded to provide a smooth contact surface. The surface was smoothed to decrease the amount of friction between the beam and all of the testing devices metal contact points.

Finally, the sanded beams from either fabrication method were greased at all of the contact points. Standard vacuum grease was applied to all of the contact points in order to minimize the amount of friction experienced. This thin film of grease was applied using a cotton swab and any excess was removed by running a metal spatula across the top and bottom of the beams. Once this step was completed the preparation process was finalized. These measures were taken in order to standardize the amount of friction experienced between the beam and loading system. Minimizing this friction helped make the results between replicates more repeatable.

4.3 COMPARISON OF SIMPLE CREEP RESULTS FROM BBR TO BBR-PRO

A comparison between the BBR and BBR Pro was perfromed to ensure that the BBR Pro could produce accurate results that were similar to the standard BBR. This comparison was done while the BBR Pro still had its three point loading system installed. A total of four beams were fabricated using the direct compaction method. Two beams were tested in the standard BBR using the standard procedure, while the other two beams were tested in the BBR Pro using a similar procedure. Two replicates were used with each device to ensure that the repeatability between tests within a given machine was tolerable. All four beams were tested at 0 °C and with a block type loading pattern. As stated before the

BBR would apply the standard 0.98 N load and hold it for a duration of 240 seconds. The BBR Pro was programmed to perform a similar loading pattern in that a single cycle block load would be held for 240 seconds but instead the load would be 5 N. This load was chosen after a few trial and error tests on similar beams to ensure that the material was within its linear viscoelastic limit.

After testing was completed the output files containing the force and deflection experienced by the beams were used in conjunction with simple beam theory for calculations. Beam dimensions such as the width and thickness of the beam were measured three times in different locations over the length of the beam prior to testing. These three measured values were then averaged and used for the stress and strain calculations. As mentioned previously the span length for both machines was set at 100 mm and this was the value used in the beam theory calculations. The stress felt by the beam was calculated as shown in Equation 4.1 using the beam dimensions and the force applied by the machine over the prescribed time period. The strain could also be calculated based on the measured deflection of the beam throughout the duration of the test as shown in Equation 4.2. Stress and strain were calculated every half of a second for the full 240 second test in the standard BBR and every quarter of a second in the BBR Pro.

$$\sigma = \frac{3FL}{2bd^2} \tag{4.1}$$

$$\epsilon = \frac{6\delta d}{L^2} \tag{4.2}$$

Once all of the stress and strain values had been calculated for each sample the creep compliance values were obtained for each point in time using Equation 4.3. These values were then graphed with respect to time in order to make better comparisons between replicates and results from each machine.

$$D(t) = \frac{\epsilon(t)}{\sigma_0} \tag{4.3}$$

The results from the creep tests performed can be seen in Figure 4.12. It can be observed that the two replicates tested in the same machine show good repeatability. Comparing the results between both machines it can be seen that up to about 120 seconds the compliance for all four tests is similar. After 120 seconds the samples tested in the BBR Pro begin to diverge slightly from those tested in the standard BBR. A conclusion

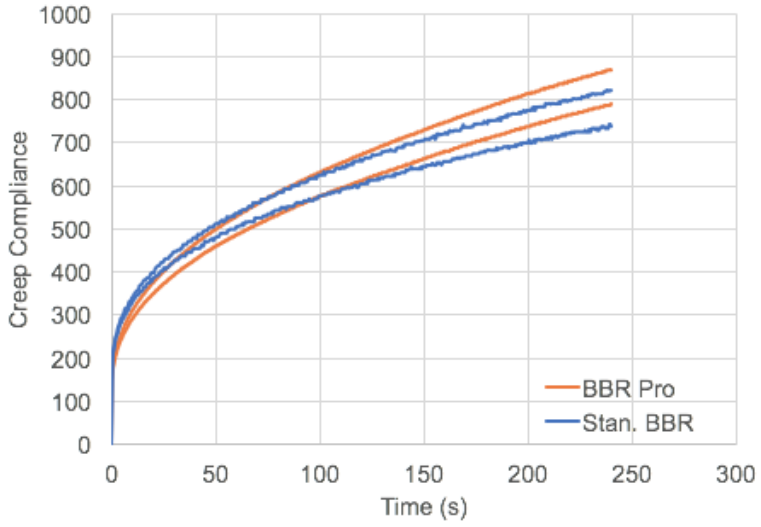

Figure 4.12. Results from Creep Test Performed in the Standard BBR and BBR Pro

can be made that both machines provide similar results given that the material being tested are similar in composition to one another. Similar results were obtained with other material specimens. The information obtained from this comparison will be important moving forward and when constructing a test method. The slight deviation (higher strain with BBR Pro) after 120 seconds could also be on account of some plastic deformation that was induced in the beam on account of the higher stress/loads with the BBR Pro.

4.4 SUMMARY

This chapter provided an overview of the testing devices and specimen fabrication methods. Three testing devices were described including the Cannon TE-BBR, Cannon TE-BBR Pro, and Instron E1000. Each device was used for a specific piece of this study and crucial in obtaining testing results. Descriptions for specific procedures used to fabricate both binder and mortar test specimens were provided in this chapter. Several of these procedures are standard procedures while others were more in a development stage. Lastly a comparison between both the BBR and BBR Pro was performed in order to ensure that similar results would be obtained between the two testing devices. The following chapter will describe the test methods and results obtained in this study.

CHAPTER 5. EVALUATION OF ASPHALT BINDERS AND MORTARS

5.1 OVERVIEW

Various systems have been developed to help characterize the performance and behavior of asphalt binder such as the penetration grading system or performance grading system. One of the main goals of this study was to evaluate not only the stiffness of asphalt materials but also their tensile strength, particularly in relation to their ability to resist thermal and other forms of cracking. More specifically, this goal was to be accomplished in the context of use of recycled asphalt and with two different types of materials; asphalt binders and mortars. The previous chapter reviewed the methods used to prepare test specimens for these two length scales. This chapter will present the specific matrix of materials that were evaluated along with the results for stiffness and strength.

The first half of this chapter explores the variation in tensile strength of asphalt binders with similar Performance Grade as well as the variation in tensile strength of the binders as a function of the amount of recycled binder added to the virgin binder. As stated previously, an increasing emphasis is being placed on understanding how additives influence the behavior or performance of asphalt binders and mixtures. In the context of recycled asphalt, rejuvenators have emerged as a class of additives that are intended to improve the properties of the mix. The second half of this chapter will focus on evaluating the influence of recycled asphalt and rejuvenators on the stiffness and strength of asphalt mortars or FAM mixes. Recall that the use of mortars or FAM was intended to serve as a fast and efficient evaluation tool that does not necessitate the extraction and recovery of binder from recycled materials. Simply put, fractionated fine recycled asphalt pavement (RAP) can be mixed with virgin aggregates, binders and additives to produce FAM specimens that can be used to evaluate the influence of factors such as RAP content and rejuvenator type on the overall performance of the FAM.

5.2 VARIATION IN TENSILE STRENGTH OF BINDERS WITH SIMILAR PG

5.2.1 Materials and Tests

The asphalt binders used in this part of the study were provided by multiple producers who supplied binders for TxDOT projects. Seven different grades of asphalt binder were included in this part of the study ranging from a PG 58-28 to a PG 76-28. Table 5.1 provides a better representation of all the materials used for this portion of the study.

Standard creep tests were first performed on these materials. These tests were performed in a three point loading system using a standard Cannon Instrument Company BBR testing device. Most of the asphalt binders were tested at multiple temperatures, these test temperatures were chosen based on assigned performance grade. The baseline test temperature for any given binder was 10 °C higher than its low temperature performance grade. This is based on the current practice. The other two test temperatures were 6 °C above and below this baseline temperature. Therefore, most binders were tested at three different temperatures. The standard conditioning procedure from AASHTO T 313 was used for temperature conditioning the test specimens. This procedure specifies 60 $\pm$5 minutes of conditioning in the methanol bath. All of the asphalt binders tested had been aged through both a rolling thin film oven (AASHTO T 240) and pressure aging vessel (AASHTO R 28) using the standard AASHTO methods. A block load was applied with a magnitude of 0.98 N for 240 seconds following the standard AASHTO T 313 procedure. The data collected from this testing device was then used to calculate the stress and strain experienced by each material tested, and subsequently the creep compliance of each material.

Once all of the standard creep tests were performed the next step was to evaluate the tensile strength of each material. A monotonic load at a rate of 5 N min^{-1} was applied in a three point loading system until failure occurred. This loading rate was chosen to keep the test short yet still achieve failure. Three test temperatures were selected as before and the same three point loading frame was used. These tests were performed using the Cannon Instrument Company BBR Pro because of its ability to program load patterns and higher load capacity.

Table 5.1. Summary of Asphalt Binders Tested for Strength with Similar PG

Binder #	High PG	Low PG	Age	Test Temperatures (°C)		
10265	58	-28	PAV 1	-18	-24	-12
10272	58	-28	PAV 1	-18	-24	-12
10279	58	-28	PAV 1	-24		
10287	58	-28	PAV 1	-18	-24	-12
10289	58	-28	PAV 1	-18	-24	
10269	64	-22	PAV 1	-12	-18	
10273	64	-22	PAV 1	-12	-18	-6
10274	64	-22	PAV 1	-12	-18	-6
10275	64	-22	PAV 1	-12	-18	-6
10278	64	-22	PAV 1	-12	-18	-6
10280	64	-22	PAV 1	-12	-18	
10293	64	-22	PAV 1	-12	-18	-6
10294	64	-22	PAV 1	-12	-18	-6
10297	64	-22	PAV 1	-12	-18	-6
10352	64	-22	PAV 1	-12	-9	
10270	64	-28	PAV 1	-18	-24	
10286	64	-28	PAV 1	-18	-24	-12
10267	70	-22	PAV 1	-12	-18	-6
10271	70	-22	PAV 1	-12		
10277	70	-22	PAV 1	-12	-18	
10281	70	-22	PAV 1	-12	-18	
10295	70	-22	PAV 1	-12	-18	
10298	70	-22	PAV 1	-12	-18	-6
10285	70	-28	PAV 1	-18	-24	
10288	76	-22	PAV 1	-12	-18	-6
10290	76	-22	PAV 1	-12	-18	-6
10296	76	-22	PAV 1	-12	-18	-6
10299	76	-22	PAV 1	-12	-18	-6
10282	76	-28	PAV 1	-18	-24	

5.2.2 Results and discussion

The stress and strain data over time were collected from each test and used to compute the creep compliance of the binder. The typical stress and strain results for these tests can be observed in Figure 5.1 and Figure 5.2. Figure 5.3 illustrates the typical creep compliance

over time computed using the stress-strain data. Creep compliance is important because it is a fundamental property. Therefore, these results were further studied and analyzed.

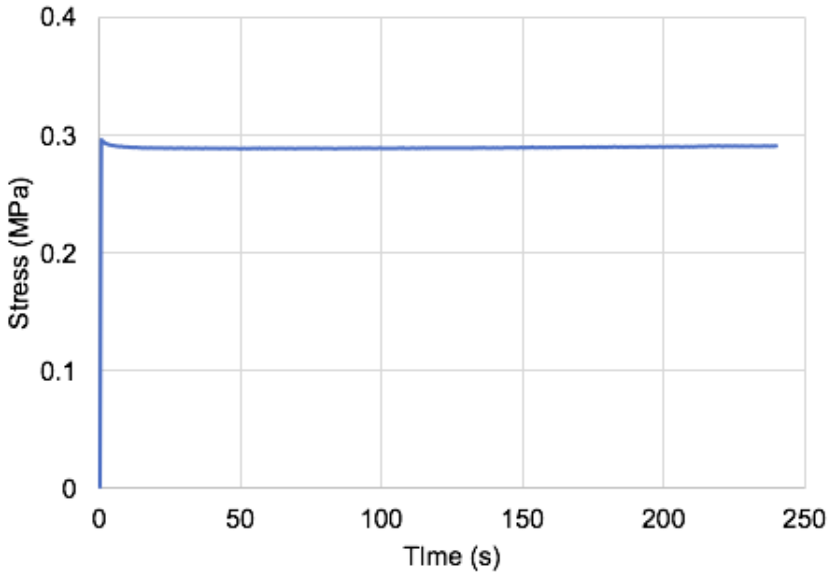

Figure 5.1. Typical Stress Results from Standard Creep Tests on Various PG Binders

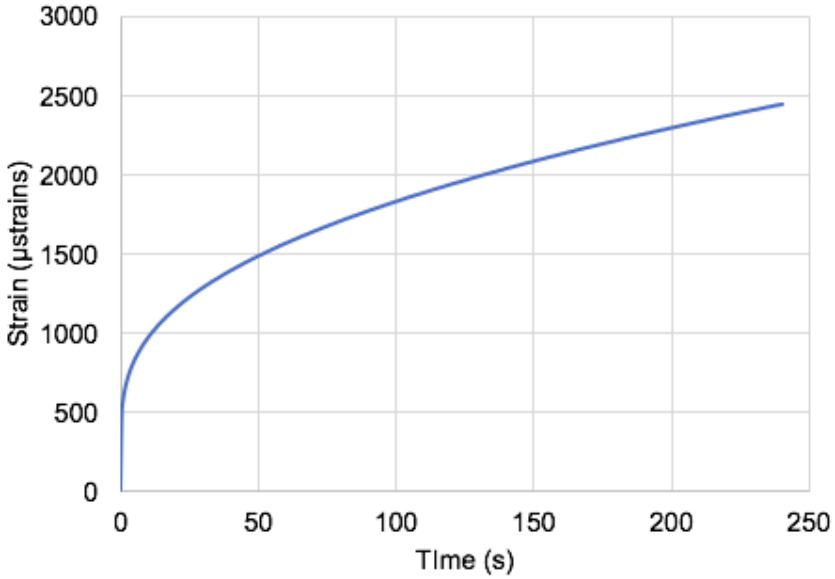

Figure 5.2. Typical Strain Results from Standard Creep Tests on Various PG Binders

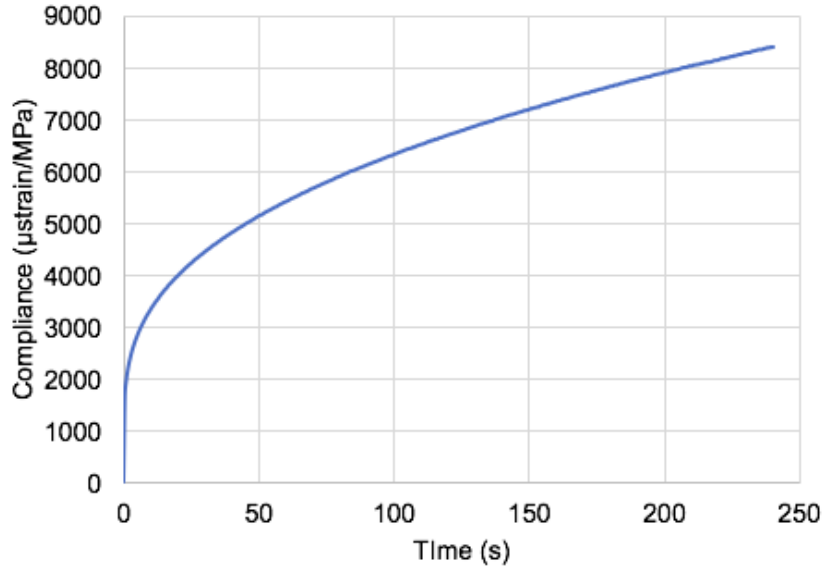

Figure 5.3. Typical Compliance Results from Standard Creep Tests on Various PG Binders

All of the compliance data collected from the standard creep tests were then separated according to the PG of the binder and examined further. Some observations made from

studying the creep compliance of the binders were:

- The range of compliance values at 60 seconds for binders within the same PG group at the same temperature was quite large (e.g. 4419 MPa^{-1} to 8138 MPa^{-1} for PG 64-22). Note that this range is not evident in conventional grading since all binders have to merely meet a maximum stiffness requirement at one temperature and just at one point in time.
- The m value or slope of these compliance curves was rather small but consistent within the same PG group at the same temperature.

These observations can be seen in Figure 5.4. Figure 5.4 shows the compliance curves for a group of PG 64-22 binders that were tested at $-12\,^{\circ}\text{C}$ and placed on a log-log scale. In the asphalt pavement community it is assumed that binders with the same grade have the same or at least similar behavior. This observation is important because it seems to go against the assumption made and followed within the asphalt pavement community. The observations made from Figure 5.4 and similar figures with varying PG binders could be due to the more empirically based guidelines for assigning a low temperature grade in the PG system. Since the PG system utilizes an empirically based maximum stiffness value or minimum m value (whichever is more conservative) as the cornerstones for grading the low temperature of a binder, the true material properties of these binders at low temperatures aren't being revealed. As a result, binders with significantly different material properties tend to be assigned the same grade.

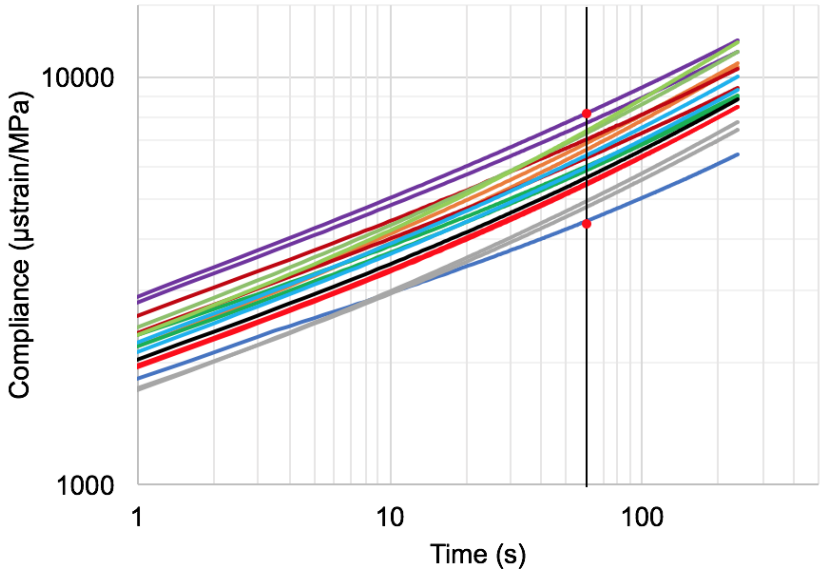

Note: The above curves illustrate a visual range of compliance curves for a PG 64-22 binder tested at −12 °C, this range is rather broad for a single grade of binder and the m value or slope is small.

Figure 5.4. Compliance Results for a PG 64-22 Binder Tested at −12 °C

The remainder of the section presents the results collected from the strength tests conducted by applying the 5 N min^{-1} monotonic loading pattern. Typical applied loads and resulting strains for these monotonic tests can be seen in Figures 5.5 and 5.6. From these results one can see that a linear trend was commanded and applied until the point of physical failure. The point of physical specimen failure was selected to define the maximum stress or strain experienced by the beam. These failure points were collected for all of the binders tested in Table 5.1. Once the failure points were collected the average between two replicates was found and used to compare the tensile strength of binders with similar PG. The results presented are separated by test temperature and low temperature grade. The columns represent the average tensile strength or strain, while the error bars indicate the maximum and minimum measured tensile strength and strain. Note that not all binders were evaluated at all these temperatures on account of the limited supply of the binder sample in some cases.

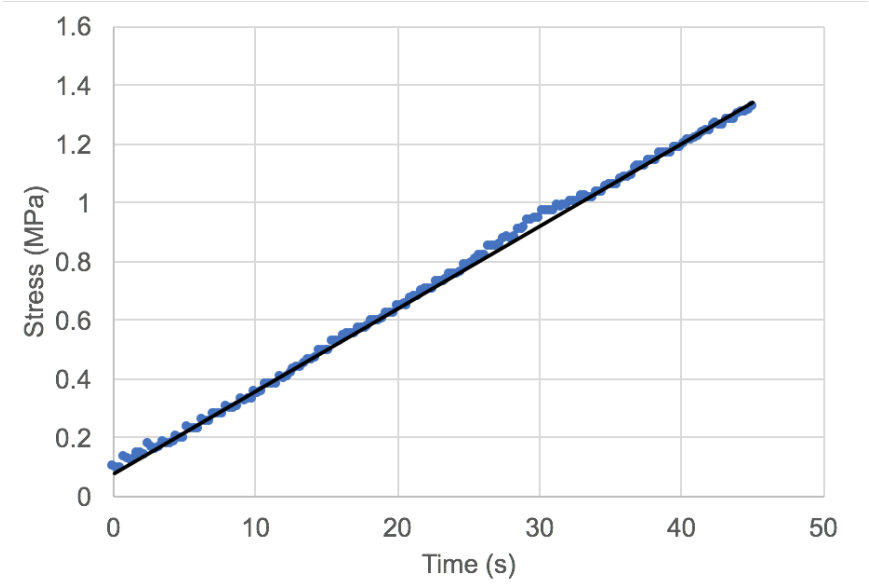

Note: Line shown only as a guide to the eye.

Figure 5.5. Typical Stress Results for Monotonic Load Test to Failure

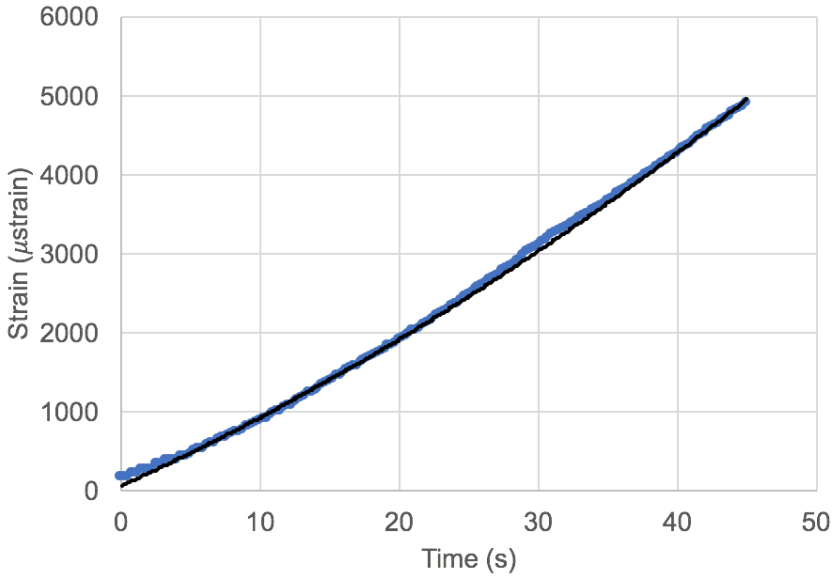

Note: Line shown only as a guide to the eye.

Figure 5.6. Typical Strain Results for Monotonic Load Test to Failure

The results presented in the remainder of this section either present tensile strength at failure or tensile strain at failure. Several different observations can be made from these results:

- Binder strength can vary significantly within the same assigned PG. For example, Figure 5.9 shows that one binder has a strength of 1.93 MPa while another binder has a strength of 0.86 MPa.
- Temperature has a subtle impact on tensile strength of binders with similar PG tested at various temperatures (compared to failure strain).
- Temperature has a more significant influence on the strain experienced at failure and it has a direct relationship i.e., as temperature increases the failure strain increases.

These observations were made after studying Figure 5.7 through Figure 5.18. The significance of these observations are discussed in seriatim.

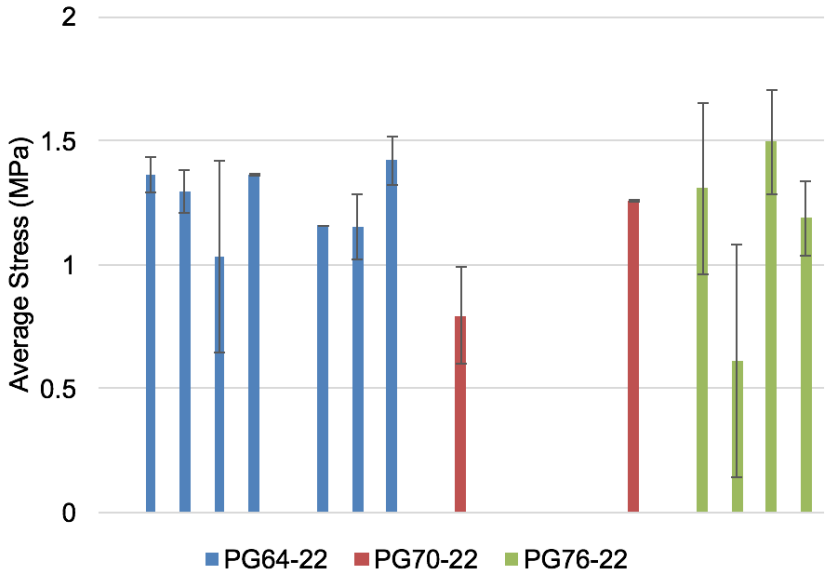

Figure 5.7. Average Tensile Strength for PG XX-22 Binders Tested at −6 °C

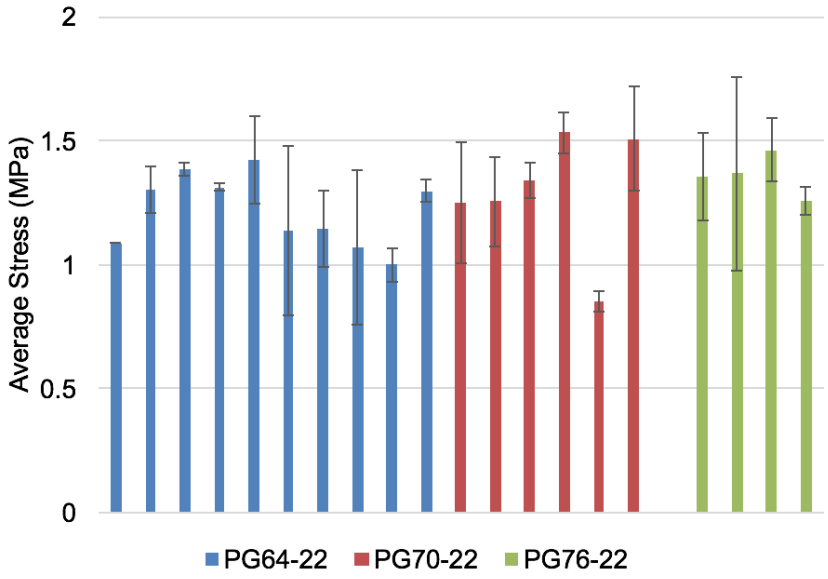

Figure 5.8. Average Tensile Strength for PG XX-22 Binders Tested at −12 °C

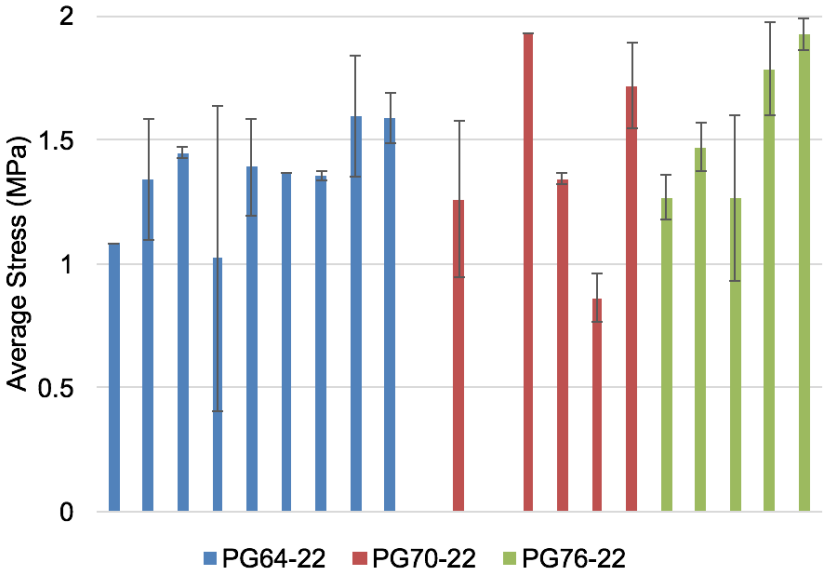

Figure 5.9. Average Tensile Strength for PG XX-22 Binders Tested at −18 °C

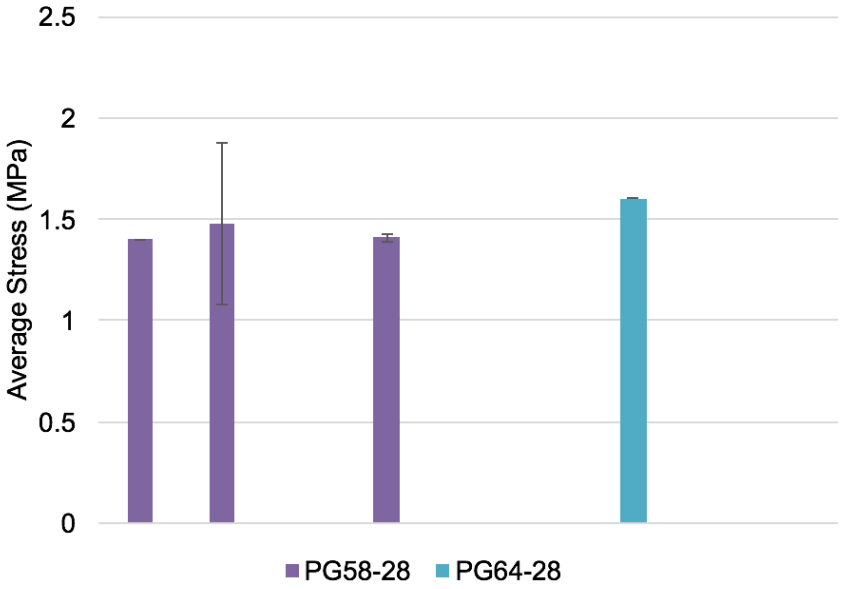

Figure 5.10. Average Tensile Strength for PG XX-28 Binders Tested at −12 °C

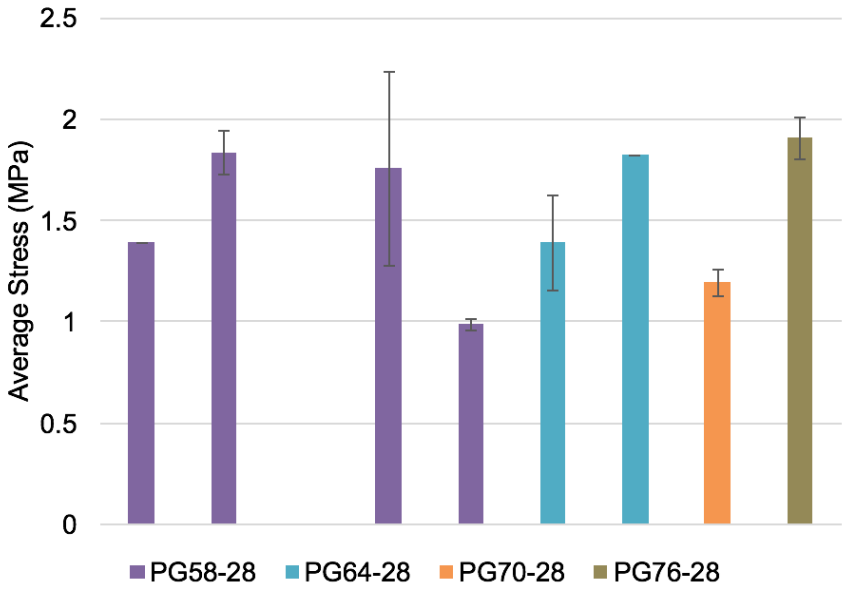

Figure 5.11. Average Tensile Strength for PG XX-28 Binders Tested at −18 °C

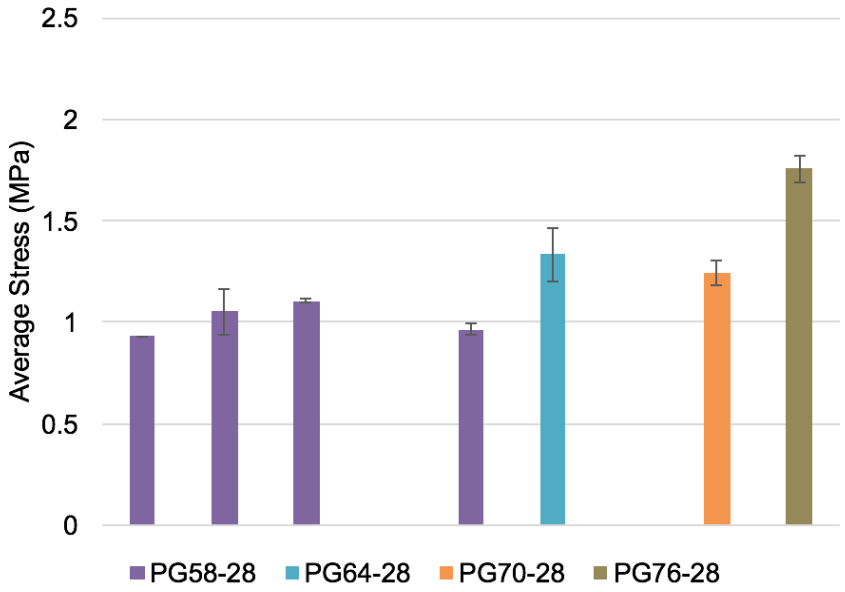

Figure 5.12. Average Tensile Strength for PG XX-28 Binders Tested at −24 °C

Tensile strength of binder is not a material characteristic that is currently being measured for grading. Strength of a material can provide insight into the future performance of the material once it is placed and loaded in the field. As of now, binders are graded based on their stiffness and m value, not taking into account the materials' strength. It can be clearly observed from Figure 5.9 that the tensile strength of a binder can vary between binders with the same PG. As discussed previously, the DTT is the only testing device that evaluates the binder until failure, but this device typically only measures the strain at failure not the stress. Furthermore, the DTT is currently not being used as a part of PG system since most binders are designed to meet the m value criterion at the low temperature grade. A strength test, as the one performed in this study, using the BBR Pro (Cannon Instrument Company) can provide more information for a given asphalt binder. The tensile strength of these materials is important for characterizing the material and predicting its performance when used in the field, therefore a consideration for including it into the grading process should be made.

After studying the results of tensile strength, as the temperature varied it can be observed that temperature has a relatively lesser impact on the magnitude of the strength or failure stress (compared to failure strain)> For the PG XX-22 binders most tensile strengths ranged from 1 MPa to 1.5 MPa when tested at −6 °C. When compared to the tensile strength of the same binders tested at −18 °C it can be observed that this range increases to 1.2 MPa to 1.7 MPa. For any given binder the tensile strength changes by a factor of 0.98 to 2.07 when the temperature is decreased from −6 °C to −18 °C. This is a fairly subtle difference in tensile strength, meaning temperature may not have much of an impact on the overall strength of the material at least within this temperature range. The fact that temperature may not effect the overall strength of the material may mean that strength may be a better property to use for characterizing the material than failure strain.

The tensile strain at failure was measured corresponding to the tensile strength discussed previously. From gathering and studying of these results the observation that temperature has a significant impact on the failure strain can be made. This phenomenon can be observed in Figure 5.13 through Figure 5.18. It can be observed that both -22 and -28 grades of asphalt binder experience a large change in failure strain with respect to a change in temperature. The failure strain and temperature are directly correlated in that as the temperature decreases the strain at failure decreases as well. The phenomenon being observed can be explained with simple knowledge of viscoelastic materials. As the

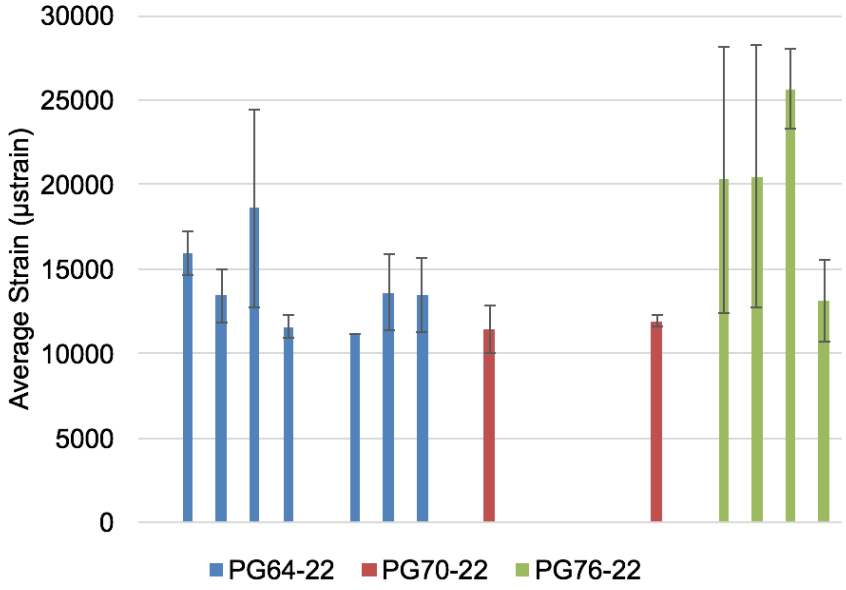

Note: Graph scale for Figures 5.13, 5.14, and 5.15 are kept the same to allow for direct visual comparison.

Figure 5.13. Average Tensile Strain for PG XX-22 Binders Tested at −6 °C

temperature decreases, the creep compliance of the material decreases, i.e., the material becomes stiffer therefore allowing the material to deform and relax less. This decreased deformation and ability to relax directly impacts the amount of strain that occurs before failure. Particularly, as discussed before, since the failure stress did not change significantly from one test temperature to another, it is evident that for a similar stress at reduced temperatures the failure strain will have to decrease on account of the reduced compliance of the material. The observation made regarding failure strain and temperature is important because it reaffirms some of the existing knowledge we have about asphalt binder while also helping us reconsider failure strain as a fundamental material property to characterize material strength or capacity. As a final note, a corollary from this observation is that failure strain is also very sensitive to rate of loading (at least within a certain range) whereas failure stress is less sensitive to rate of loading (again within a certain range).

Overall the tests conducted in this part of the study have provided insight on several important asphalt binder properties.

1. The compliance of binders within the same PG can have a wide range of values.

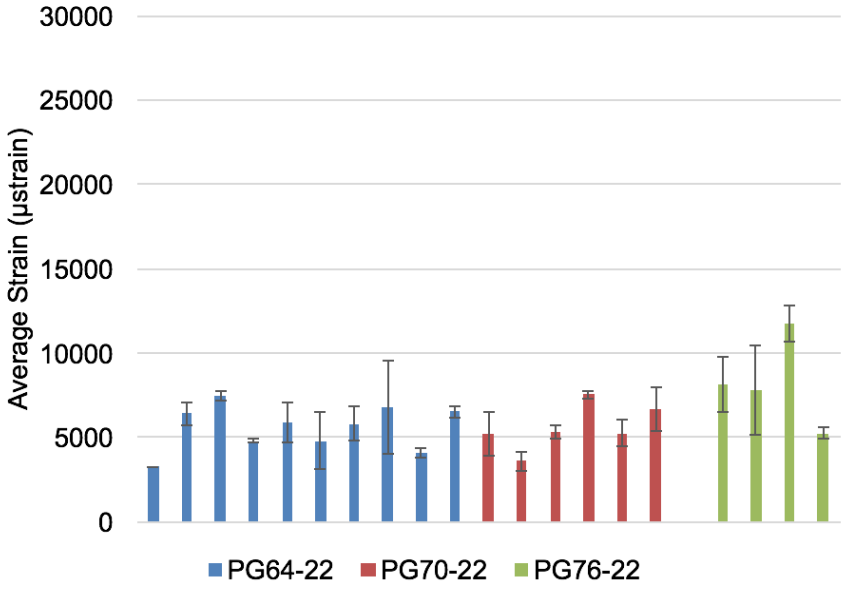

Note: Graph scale for Figures 5.13, 5.14, and 5.15 are kept the same to allow for direct visual comparison.

Figure 5.14. Average Tensile Strain for PG XX-22 Binders Tested at −12 °C

2. Tensile strength can vary between binders that have been assigned the same PG.
3. The tensile strength of asphalt binders are subtly effected by temperature.
4. Tensile strain at failure is substantially impacted by the temperature at which it is tested.

These observations provide useful information that can be applied to future work.

5.3 VARIATION IN TENSILE STRENGTH OF BINDERS WITH CHANGE IN RECYCLED BINDER CONTENT

5.3.1 Materials and Tests

This section will focus on the influence of recycled binder content on the properties of an asphalt binder. An asphalt binder with a PG of 64-22 was selected to be the base material or control to which various proportions and types of extracted recycled binder were added to. This binder was selected because it is common to the geographical area in which this study was taking place and was easily accessible to the lab in which the

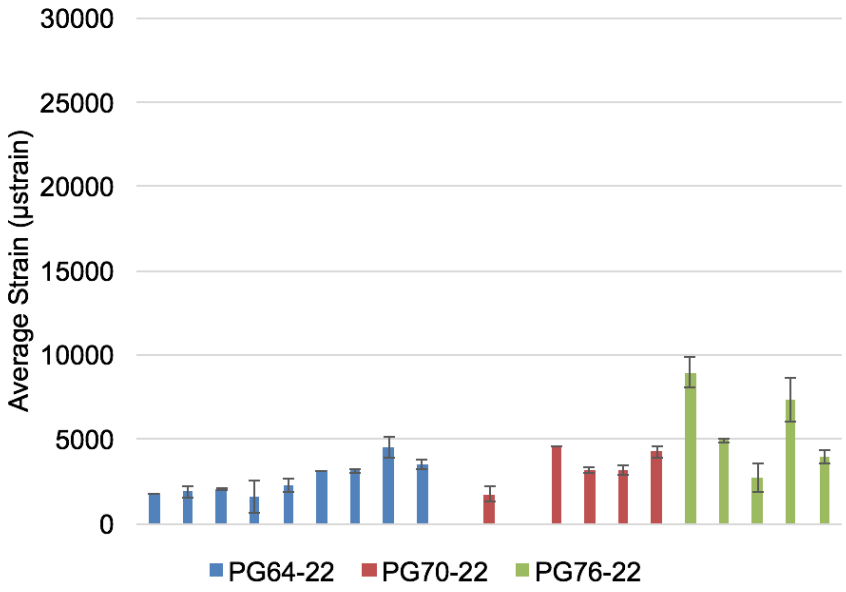

Note: Graph scale for Figures 5.13, 5.14, and 5.15 are kept the same to allow for direct visual comparison.

Figure 5.15. Average Tensile Strain for PG XX-22 Binders Tested at −18 °C

experiments took place. Field cores were taken from four specific locations in Arkansas; these field cores were then put through an extensive extraction process in order to reclaim the asphalt binder (as described in detail in Chapter 2 of this report). Therefore, four different recycled binders were collected from the field core samples. These binders were labeled as RAP 1, RAP 2, RAP 3, and RAP 4 to keep the future testing organized. Recycled binder was supplemented in proportions of 25%, 40%, and 60% by weight of the total binder. Once all mixing was complete each proportion of each binder was aged using the rolling thin film oven and pressure aging vessel using the standard AASHTO methods mentioned earlier. These mixtures were then prepared for further evaluation.

Similar to the binders of various PG discussed in the previous section, these mixtures were tested in both simple creep and monotonic scenarios. The simple creep tests were performed first in a standard Cannon Instrument Company BBR at three temperatures. These temperatures were selected by using the assigned low temperature grade of the control binder, which was −22 °C. The first test temperature was selected by adding 10 °C to the low temperature grade to get −12 °C. The other two test temperatures were obtained by offsetting this temperature by 3 °C on either side to get −9 °C and −6 °C. Not

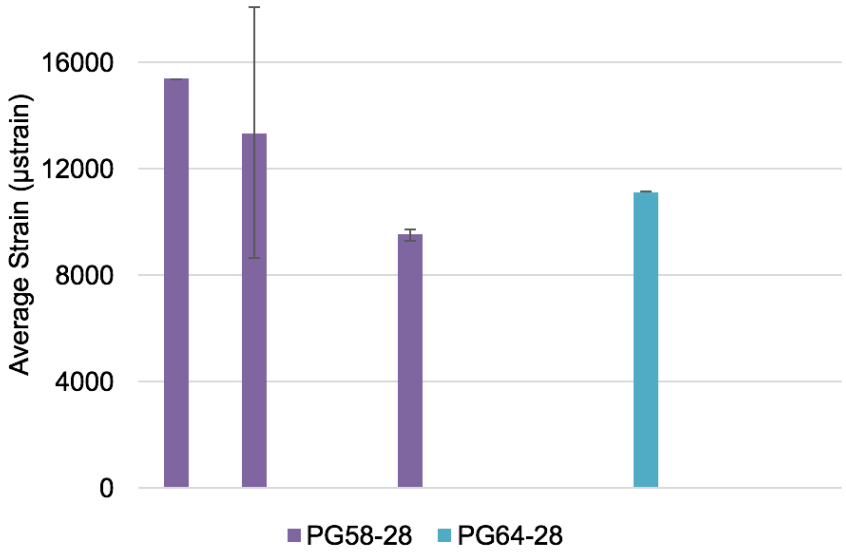

Note: Graph scale for Figures 5.16, 5.17, and 5.18 are kept the same to allow for direct visual comparison.

Figure 5.16. Average Tensile Strain for PG XX-28 Binders Tested at −12 °C

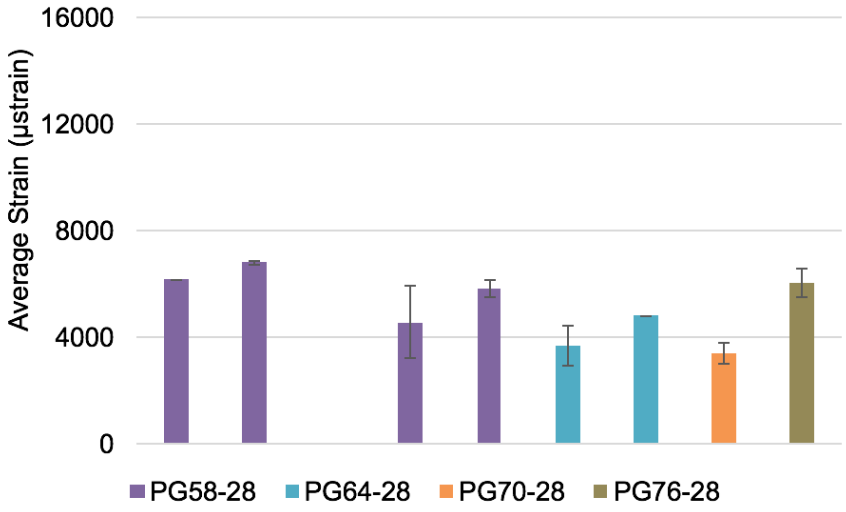

Note: Graph scale for Figures 5.16, 5.17, and 5.18 are kept the same to allow for direct visual comparison.

Figure 5.17. Average Tensile Strain for PG XX-28 Binders Tested at −18 °C

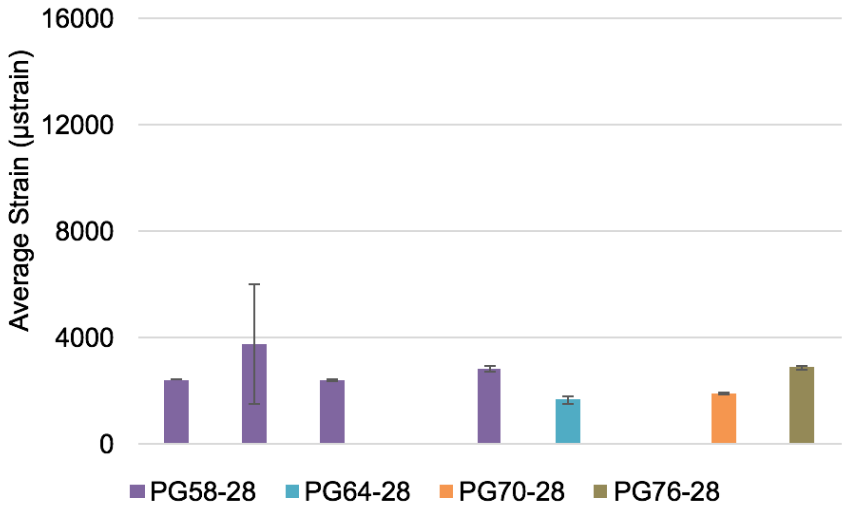

Note: Graph scale for Figures 5.16, 5.17, and 5.18 are kept the same to allow for direct visual comparison.

Figure 5.18. Average Tensile Strain for PG XX-28 Binders Tested at −24 °C

all of the mixtures were tested at all three temperatures. Table 5.2 shows the breakdown of tests performed for this portion of the study. As before the standard creep tests were performed with a block loading of 0.98 N for a total of 240 seconds. These tests yielded force and deflection data from a three point loading system that was then used to calculate stress, strain, and compliance. An additional step was taken to analyze the compliance data further which will be discussed in the following section.

After the standard creep tests were completed, strength tests were performed on two of the four recycled binders. Both RAP 1 and RAP 2 binder specimens of each proportion were tested in the Cannon Instrument Company BBR Pro under a monotonic loading pattern. The same 5 N per minute loading rate that was used in the previous section was implemented in this study and applied until failure. These tests were performed in the original three point loading system. Once all the tests had been performed, the recorded stress and strain at failure were amassed and used to compare differing RAP sources as well as proportions.

Table 5.2. Test Matrix for Simple Creep Tests Performed on Recycled Binder Specimens

Material	Test Temperatures (°C)		
	-12	-9	-6
Control PG64-22	T	T	
+25% RAP 1	T	T	
+40% RAP 1	T	T	T
+60% RAP 1	T	T	T
+25% RAP 2	T	T	
+40% RAP 2	T	T	T
+60% RAP 2	T	T	T
+25% RAP 3	T	T	
+40% RAP 3		T	T
+60% RAP 3		T	T
+25% RAP 4	T	T	
+40% RAP 4		T	T
+60% RAP 4		T	T

NOTE: T indicates the combination was tested

5.3.2 Results and discussion

Procedurally, the standard creep tests were performed the exact same way they were executed in the previous section. Hence, these tests produced similar stress, strain, and compliance results. The typical results for these tests were identical to those shown in Figure 5.1 through 5.3. However, these results were further analyzed to better understand the influence of RAP type and content on the binder properties

The stress and strain over time from a each test were used to compute the creep compliance of the material. To reiterate, creep compliance is the ratio of strain to stress as a function of time. The computed creep compliance over time was then used with the curve fitting toolbox from MATLAB. Using this curve fitting application in MATLAB, a user can fit a specific function to data by solving for unknown variables within the fitted function. For this study a power law model was fit to the creep compliance versus time data. The power law model is commonly used in the asphalt industry to represent the

compliance of a viscoelastic material. The function can be identified by Equation 5.1.

$$D(t) = D_0 + D_1 t^m \tag{5.1}$$

The MATLAB curve fitting application then solved for the D_0, D_1, and m while fitting the power law function to the computed creep compliance data. The values of D_0, D_1, and m were found for every test specimen in Table 5.2. After these values were obtained, they were used to model the relationship between RAP content and binder properties as shown in Figure 5.19 through Figure 5.24. It must be emphasized that the m value shown in these figures is slightly different from the m value computed using local data at sixty seconds from BBR testing and used in the PG specification but it is based on the overall slope of the response. This relationship at the temperature of −6 °C was excluded because little information could be gained since tests were not run on the control at this temperature due to limited sample size. After organizing and studying these relationships several observations were made.

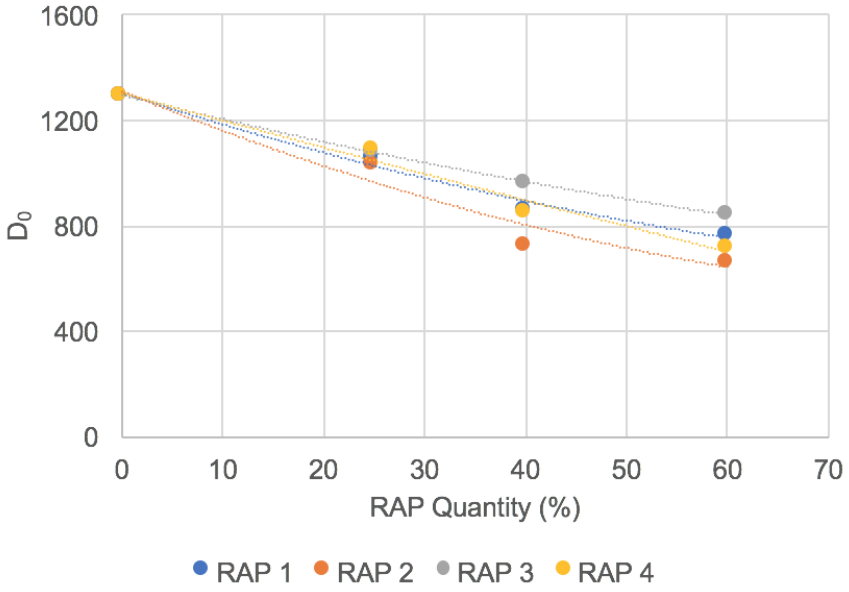

Note: Line shown only as a guide to the eye.

Figure 5.19. Average D_0-values With Respect to Increasing RAP Binder Content at −9 °C

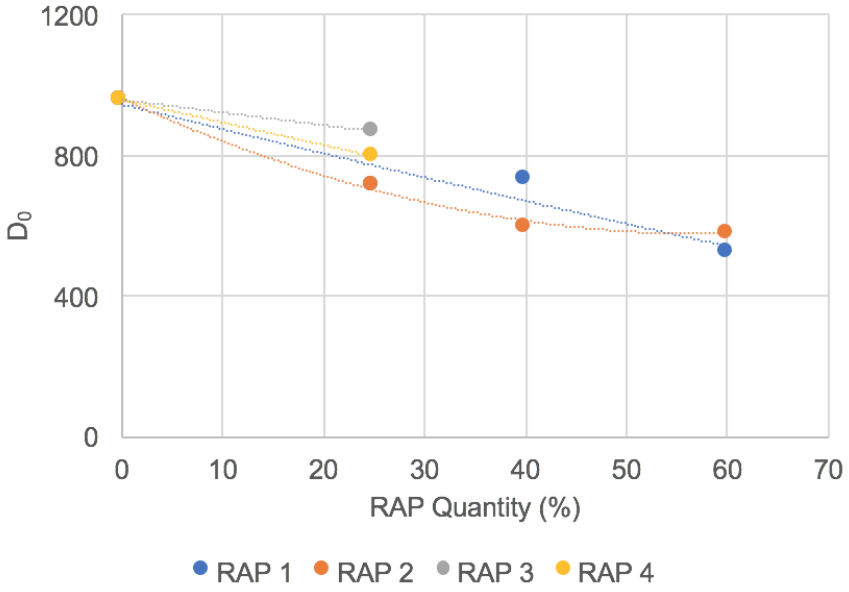

Note: Line shown only as a guide to the eye.

Figure 5.20. Average D_0-values With Respect to Increasing RAP Binder Content at −12 °C

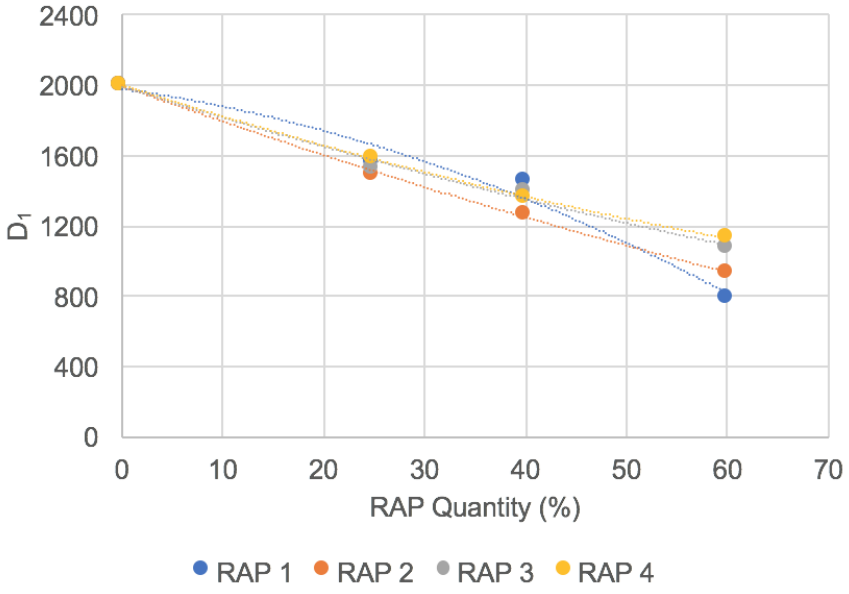

Note: Line shown only as a guide to the eye.

Figure 5.21. Average D_1-values With Respect to Increasing RAP Binder Content at −9 °C

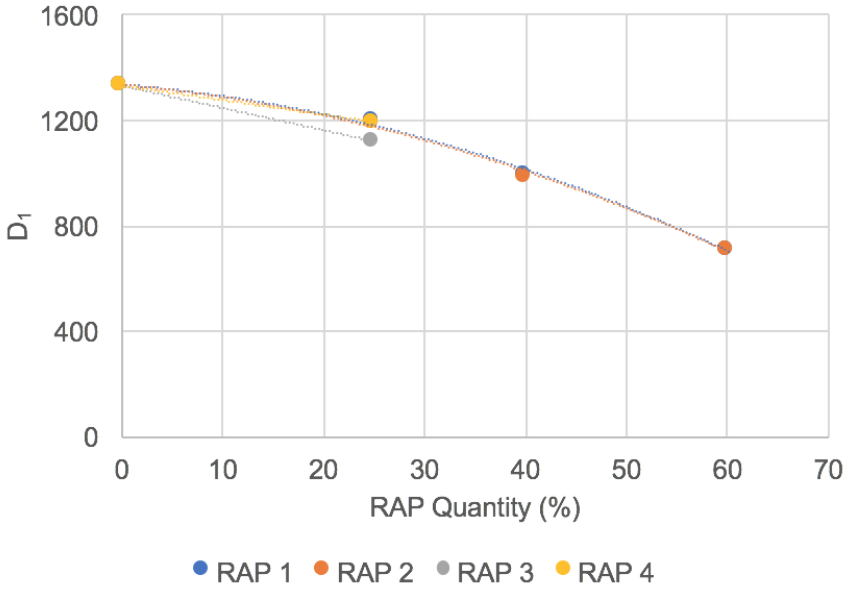

Note: Line shown only as a guide to the eye.

Figure 5.22. Average D_1-values With Respect to Increasing RAP Binder Content at −12 °C

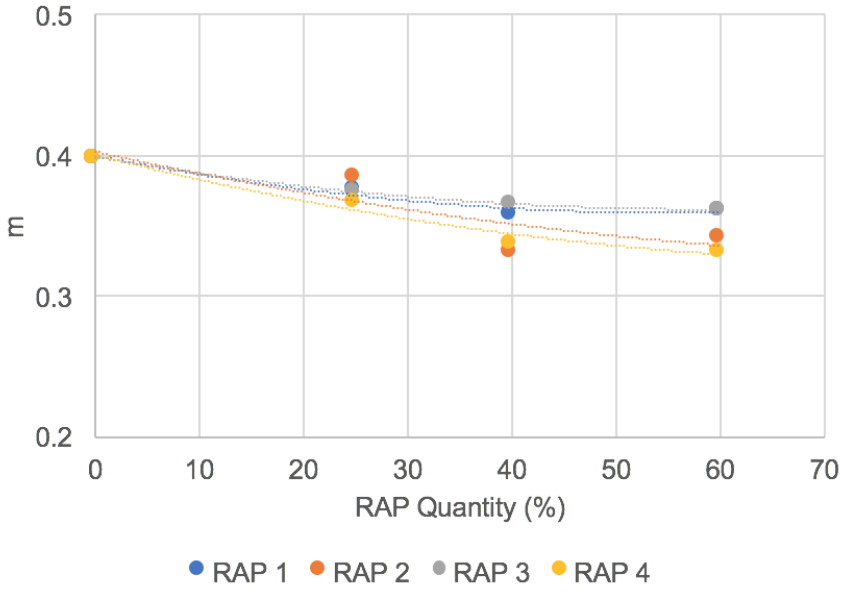

Note: Line shown only as a guide to the eye.

Figure 5.23. Average m-values With Respect to Increasing RAP Binder Content at −9 °C

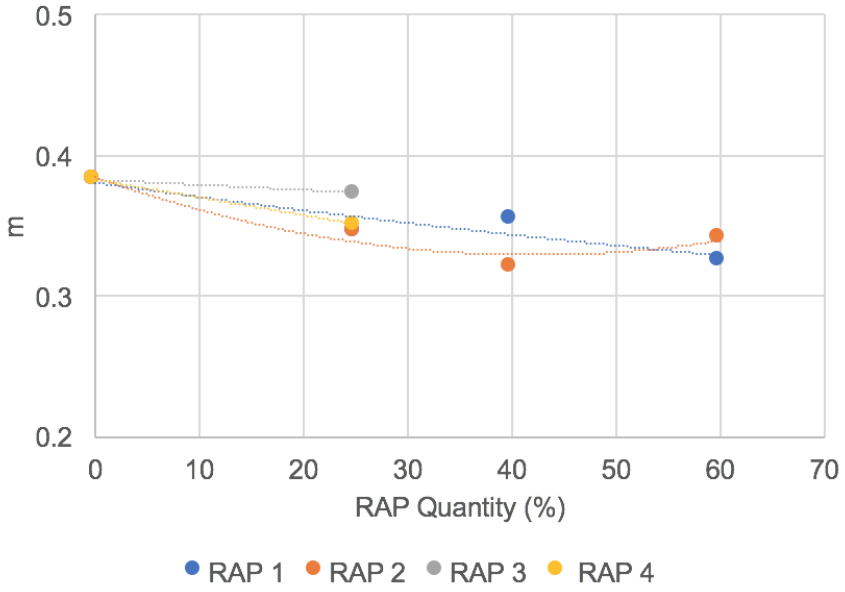

Note: Line shown only as a guide to the eye.

Figure 5.24. Average m-values With Respect to Increasing RAP Binder Content at −12 °C

A few observations that were made when studying these graphs were as follows:

- Temperature does have an effect on the power law fitting parameters. This is expected for a thermo-visco-elastic material such as asphalt binder.
- The three power law fitting parameters were sensitive to the RAP content.
- There is a plateau in fitting parameters after the RAP binder content reaches a certain value. This is particularly true for m rather than the stiffness parameters D_0 and D_1.

These observations may provide some insight as to the effects that temperature and RAP additives may have on asphalt binders and their behaviors. A discussion regarding these observations in seriatim follows.

The first and most evident observation made after studying the power law parameters was the influence of temperature on these parameters. This phenomenon can be seen when comparing Figures 5.19, 5.21, and 5.23, to Figures 5.20, 5.22, and 5.24. Values of D_0, D_1, and m are noticeably lower at $-12\,^{\circ}$C than they are at $-9\,^{\circ}$C. This is expected because viscoelastic materials such as asphalt binder demonstrate a lower rate of relaxation at reduced temperature and at increased stiffness (or reduced compliance). It is noted that both the elastic component (D_0) and the dependent parameter (D_1) reduced with a reduction in the temperature.

Also, as the content of RAP binder increases the values for all three material constants (D_0, D_1, and m) decreases. This was expected because, extracted RAP binder due to its age has been oxidized over time causing it to be stiffer than the control binder with which it was mixed. One of the most interesting observations from these data is that at 25% RAP content, the influence of RAP on the material properties as represented by D_0, D_1, and m was very similar. In other words the source of RAP did not matter at this limit (of course given the constraint that all RAP samples were from the same state). It is only at high RAP concentrations that some differences in values for parameters such as D_1 can be seen for one RAP source to another. Note that the small changes in the parameter m (when comparing different RAP sources) are within the typical errors of measurement.

The final observation is that the change in m parameter reaches an asymptote after a certain amount of RAP. However, it must also be noted that this change is small and possibly not substantial. The change in D_0 and D_1 parameters on the other hand was almost linear with an increase in the concentration of RAP. Given that these measurements were made after PAV aging the virgin and RAP binder blend, it appears that the stiffness parameters are more sensitive to aging and RAP content compared to the relaxation

parameter.

While the aforementioned discussion relates to the change in stiffness and relaxation rates with RAP type and content, the remainder of this section evaluates the influence of these factors on the tensile strength of the binder. Recall from the earlier discussion that both strength and stiffness dictate ultimate failure.

Monotonic tests performed on these specimens provided stress and strain values recorded at failure. The values obtained from each replicate were averaged and the averages are shown in Figures 5.25 through 5.28. As before the error bars represent the maximum and minimum values used in calculating the average.

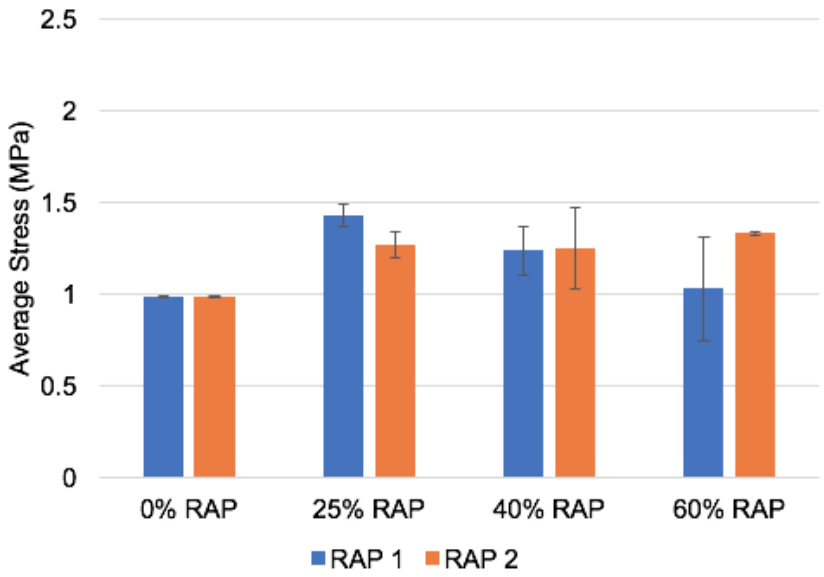

Figure 5.25. Average Tensile Strength for RAP Blended Binders of Varying Content at −9 °C

A couple of key observations from the strength tests are as follows:

- The proportion of RAP did in fact influence the failure strength and strain at failure.
- Temperature seems to have a subtle impact on the measured properties of the binder-RAP blend (particularly tensile strength or stress at failure).

These observations will be discussed in further detail in the following paragraphs.

In both Figures 5.25 and 5.26 one can see that the strength increases slightly with the increasing RAP binder content. This observation is more evident in Figure 5.26 and can be discerned fairly easily. This is a very important observation, given that most current specifications and performance indicators for asphalt binders focus on measurement of

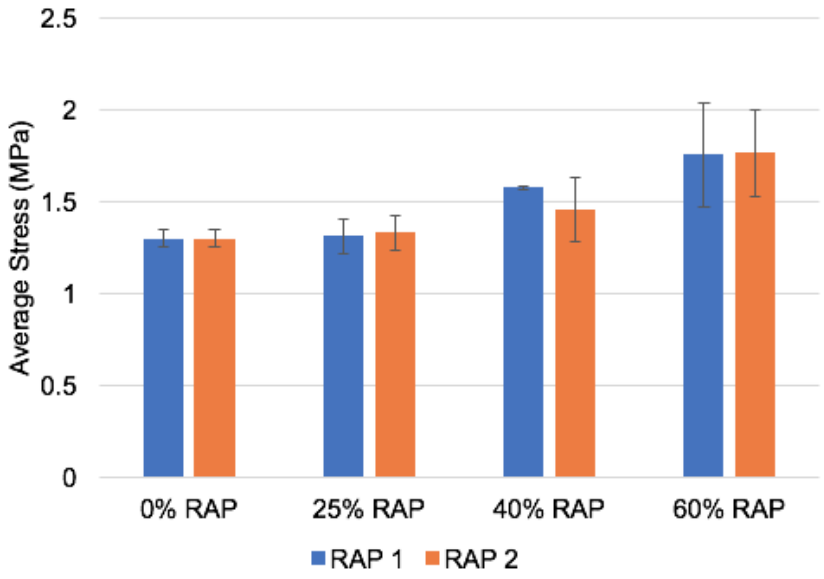

Figure 5.26. Average Tensile Strength for RAP Blended Binders of Varying Content at −12 °C

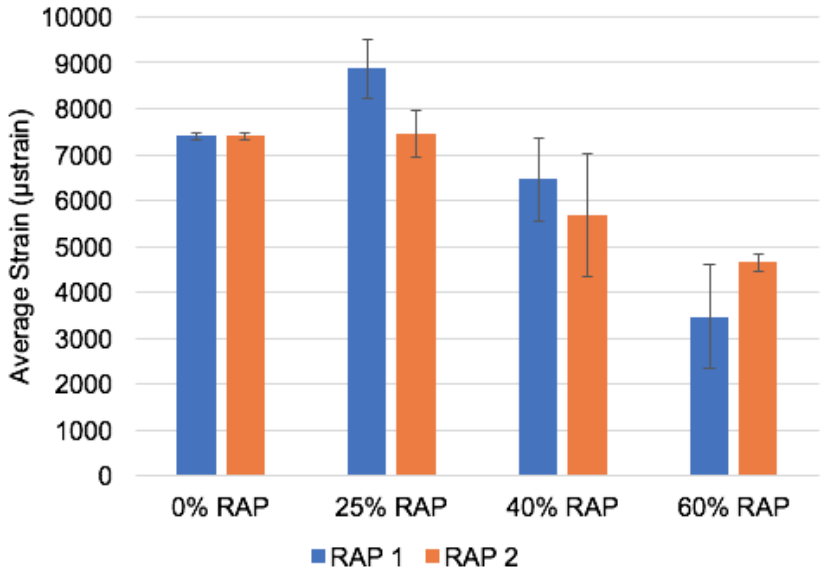

Figure 5.27. Average Tensile Strain for RAP Blended Binders of Varying Content at −9 °C

stiffness and not on strength. A possible mechanism for this increase in strength is as follows. RAP binder is highly oxidized and consequently has relatively higher polar

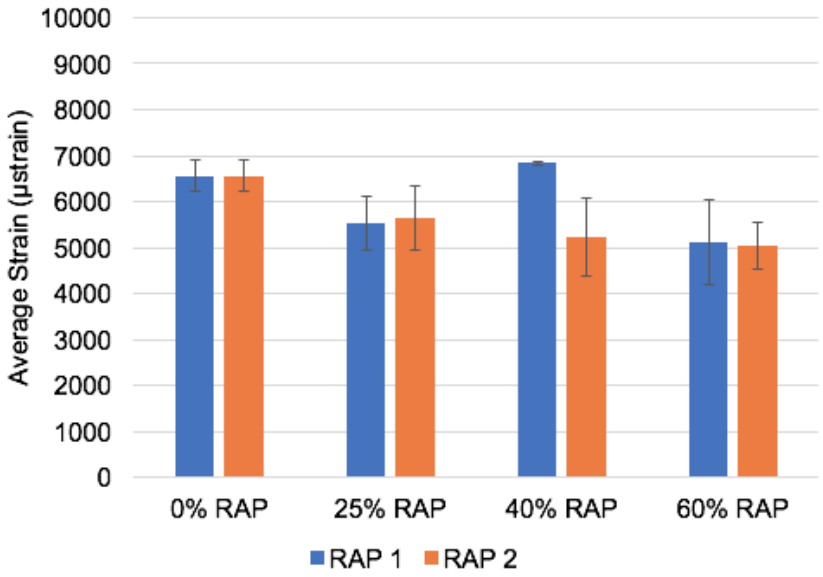

Figure 5.28. Average Tensile Strain for RAP Blended Binders of Varying Content at −12 °C

fractions in terms of its molecular composition. These polar fractions contribute to the reduced rate of relaxation and increased stiffness, which is well established in the literature and also demonstrated in the previous results. By extension, one can also expect that these polar fractions increase the inter-molecular cohesive forces and therefore increase the tensile strength of the material. This is evident from the results presented here. An increase in stiffness (or decrease in compliance) and decrease in rate of relaxation due to aging or addition of RAP can cause thermal stresses to build up faster and higher in magnitude. However, this does not necessarily mean that the material is now more susceptible to thermal cracking. This is because the failure stress has also increased to some extent. In summary, aging and/or addition of RAP results in two competing effects: increase in stiffness with reduced rate of relaxation and increase in tensile strength of the material. It is the combined influence of these two effects that dictates the susceptibility of the material to cracking. This is contrary to the common belief that addition of RAP or aged binder simply make the material more susceptible to thermal cracking.

Regarding the strain at failure, it must be noted that strain is simply the product of compliance and stress (via a convolution integral). With aging and/or addition of RAP, the compliance decreases and as discussed previously stress at failure increases. Therefore, the strain at failure will increase or decrease depending on the relative change in these two

parameters. This effect is clearly seen in Figures 5.27 and 5.28. For example at 25% RAP content the strain at failure slightly increased at $-9\,^{\circ}C$ and slightly decreased at $-12\,^{\circ}C$.

The final observation made based on these results is related to the impact of temperature on the various virgin-RAP binder blends. The tensile stress at failure or tensile strength of the binder was not substantially influenced by the temperature. On the other hand, since the compliance of the binder changes significantly with temperature, the failure strain also significantly changes (at least within the range of temperatures used in this study). This response was consistent with the observations made for the regular asphalt binders in the previous section. In fact, one can argue that a virgin-RAP binder blend is just another type of binder.

In conclusion, this portion of the study evaluated the influence of temperature, type, and proportion of RAP binder on the RAP-virgin binder blend. The effects of these three variables were visible in both the stiffness and rate of relaxation of the binder and more importantly in the tensile strength. Observations and relationships stemming from these experiments provide insight for work related to RAP additives in the asphalt industry.

5.4 EVALUATION OF INFLUENCE OF RECYCLING AGENTS AND RECYCLED BINDER ON PROPERTIES OF ASPHALT MORTARS

5.4.1 Materials and Tests

This final section is intended to develop and demonstrate a simplified test procedure using asphalt mortars to evaluate the efficacy of different asphalt rejuvenators without the need for binder extraction. The materials used in this portion of the study were supplied by the São Carlos Engineering School at the University of São Paulo Brazil under the supervision of Prof. Adalberto Faxina. These materials are a part of a larger study and provide a unique opportunity to obtain a much larger body of performance data for the same materials. A total of ten FAM mixes were constructed using the SGC method as well as the cutting method mentioned earlier. These mixes include differing proportions of a control binder of PG 64-16, RAP, and various rejuvenators. Table 5.3 displays all ten mixes and their compositions. All of the mixes used a binder content of 8%, and varied the percent of RAP, control binder, and rejuvenators. From Table 5.3 it can recognized that both FAM 5 and 6 have two different variations. For these mixes similar proportions were used but the difference between the mix labeled with an N and the one labeled with

an X was the type of rejuvenator that was used. These mixes were setup this way to test whether different rejuvenators result in different performance. In summary, FAM1 represents a 100% RAP mix as is. FAM2 represents a mix with a virgin soft binder. Most realistic cases will fall between these two extremes. FAM3 and FAM4 are also almost close to 100% RAP mixes. A small amount of virgin binder (0.9%) for different grades was added simply to achieve a 8% binder content for comparison with other cases. FAM5 and FAM6 evaluate the influence of two different rejuvenators in two different concentrations (compared to FAM4 as the baseline). Finally, FAM7 and FAM8 are more realistic RAP mixes with 17.75% and 35.5% RAP binder to total binder ratio but without any rejuvenators.

Table 5.3. Composition of the Mortar Mixes Used in This Study

Mix Label	RAP (%)	Asphalt Binder (%)		Rejuvenator (%)	
		PG 58-16	PG 64-16	NPA	XISTO
FAM1	7.1	0	0	0	0
FAM2	0	8	0	0	0
FAM3	7.1	0	0.9	0	0
FAM4	7.1	0.9	0	0	0
FAM5_N	7.1	0	0.45	0.45	0
FAM5_X	7.1	0	0.45	0	0.45
FAM6_N	7.1	0	0	0.9	0
FAM6_X	7.1	0	0	0	0.9
FAM7	1.42	0	6.58	0	0
FAM8	2.84	0	5.16	0	0

Two main test methods were used to evaluate the behavior and properties of these materials: the creep test and the monotonic load until failure. These tests were conducted in a similar fashion as the methods used in the previous sections. Changes were made to the creep test in order to acquire more repeatable results from the much stiffer mortar samples. For the creep method used on the mortar samples the load was increased to 20 N and the duration of the load was shortened to two minutes. The increased magnitude of load was implemented to achieve a higher deformation on the beam in order to get better sensitivity in strain measurements and consequently a better estimate for compliance. As for the shortened loading time, the rationale was to have a fast test that could produce accurate results while also not damaging the beam that would need to be retested later for strength using a monotonically increasing load.

In this study the influence of rate of loading was also studied. Therefore three different loading rates were chosen for the monotonic tests, which consisted of $24.96\,\mathrm{N\,min^{-1}}$, $12.48\,\mathrm{N\,min^{-1}}$, and $6.24\,\mathrm{N\,min^{-1}}$. The basis for these rates came from a study performed by **?** in which the rates used for testing full asphalt mixes were extensively studied. In that study rates of $16.64\,\mathrm{N\,min^{-1}}$ and $4.16\,\mathrm{N\,min^{-1}}$ were used with a three point loading system. Since the testing in this study would be performed with a four point loading system the rates were adjusted by a factor of 3/2 in order to achieve the same stress rate with the four point loading system. As in the case of previous sections of this study the loading patterns were applied until failure occurred in the material.

The temperature at which these tests were conducted was important as well. A similar ideology to the binder tests was implemented to acquire the test temperatures for these specimens. This began by using the assigned low temperature grade of $-16\,^{\circ}\mathrm{C}$ and adding $10\,^{\circ}\mathrm{C}$ to get a test temperature of $-6\,^{\circ}\mathrm{C}$. From this point on, the test temperature was increased in $6\,^{\circ}\mathrm{C}$ increments to ge $0\,^{\circ}\mathrm{C}$ and $6\,^{\circ}\mathrm{C}$ as the other two test temperatures. This method of obtaining the test temperatures is slightly modified from the first method in order to achieve better results by using warmer temperatures that would cause a slight increase in deformation. The rationale for targeting an increased deformation will be discussed later in this section. Test temperatures for the Instron were chosen based on the limits of the temperature chamber. The lowest temperature that could be held consistently within the chamber was $15\,^{\circ}\mathrm{C}$ so this temperature was chosen as the first test temperature. For the second test temperature $22\,^{\circ}\mathrm{C}$ or room temperature was used because it provided a good range between the two temperatures and could be held constant. The tolerance for these test temperatures was $\pm 0.2\,^{\circ}\mathrm{C}$.

Although the loading patterns and test temperatures were different from the binder tests, the standard one hour of conditioning was used when testing with the BBR Pro. As for the conditioning in the Instron testing device, a custom procedure was used based on a small study conducted using a mortar beam with a thermocouple inserted into its center. Conditioning began by placing the mortar beam inside of the Instron temperature chamber for one hour. After the beam had been in the chamber for an hour it was moved up to the supports where it was conditioned for an additional 20 minutes before testing commenced. This procedure was used for all beams tested in the Instron. These procedures were important for conducting the tests at the same temperature for every replicate.

Table 5.4 shows how each of the ten mixes was tested in this study. The CR abbre-

viation stands for the standard creep test, while ML stands for the monotonic load test. The number as a suffix to ML indicates a different loading rate, where 1=24.96 N min^{-1}, 2=12.48 N min^{-1}, and 3=6.24 N min^{-1}. The number appended after the dash of the testing abbreviations represents the number of replicates that were tested at that specific temperature with that specific loading pattern. This testing scheme was used for every mortar mix in this study.

Table 5.4. Mortar Mix Testing Regimen

Equipment	Temperature (°C)	Loading Pattern		
		1	2	3
BBR-Pro	-6	CR-2		
	0	CR-2		
	6	CR-2		
Instron E1000	15	ML1-2	ML2-2	ML3-2
	22	ML1-2	ML2-2	ML3-2

Note: CR = Creep Recovery Test, ML = Monotonic Load Test, ML1 = 24.96N/min., ML2 = 12.48N/min., ML3 = 6.24N/min., and -2 = 2 replicates

A four point loading system was chosen for this study in order to minimize variability and increase the repeatability between replicates. After running a collection of preliminary tests it was noticed that the variability between replicates using the original three point loading system was larger than expected. In an attempt to reduce the variability between replicates a four point system was designed and installed in the Cannon Instrument Company BBR Pro. The reasoning for switching to a four point loading system was that a consistent tensile strain could be achieved over a larger volume of the mortar beam. This volume would consist of the span of beam between the two load noses. Spreading out this load would allow for a more even stress distribution over the beam leading to more consistent failure patterns. After the four point system had been installed and the testing device had been calibrated an improvement in repeatability between replicates was observed.

5.4.2 Results and discussion

Of the two loading patterns discussed earlier, creep tests were performed first. These tests were performed on all ten of the mortar mixes at the various temperatures shown in Table

5.4. The simplest form of results produced by these tests were values of time, load, and deflection. Using simple beam theory, these output values were used to calculate corresponding stress and strain values, which were eventually used to compute the compliance of the material. Since these tests were performed in a four point loading system, the equations to calculate stress and strain were modified accordingly as Equation 5.2 and 5.3 show.

$$\sigma = \frac{FL}{bd^2} \tag{5.2}$$

$$\epsilon = \frac{81\delta d}{21L^2} \tag{5.3}$$

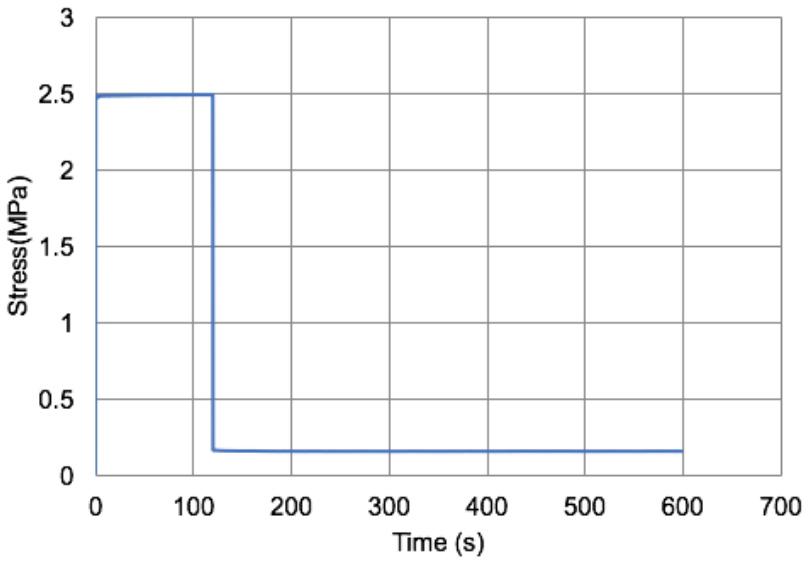

Figure 5.29. Typical Stress Results from Standard Creep Tests on Mortar Beams

The stress, strain, and compliance values were computed and examined as a function of time. Figure 5.29, 5.30, and 5.31 are examples of typical results acquired from the standard creep test. The compliance graphs were then used in a separate power law analysis that was conducted in MATLAB and is similar to the one described in the RAP binder section. This analysis involved fitting a power law model to the compliance using the curve fitting toolbox in MATLAB. After the power law analysis had been completed, values for D_0, D_1, and m were collected and tabulated. Reviewing Figure 5.32 helps

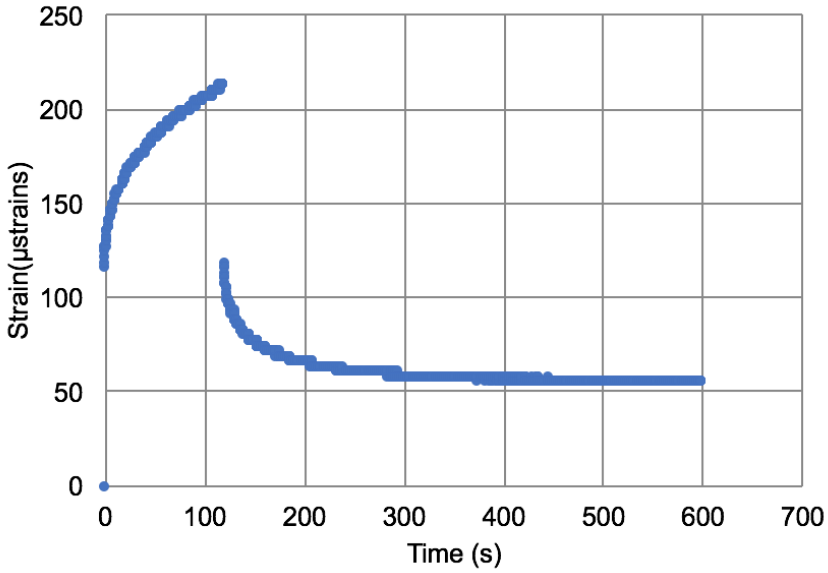

Figure 5.30. Typical Strain Results from Standard Creep Tests on Mortar Beams

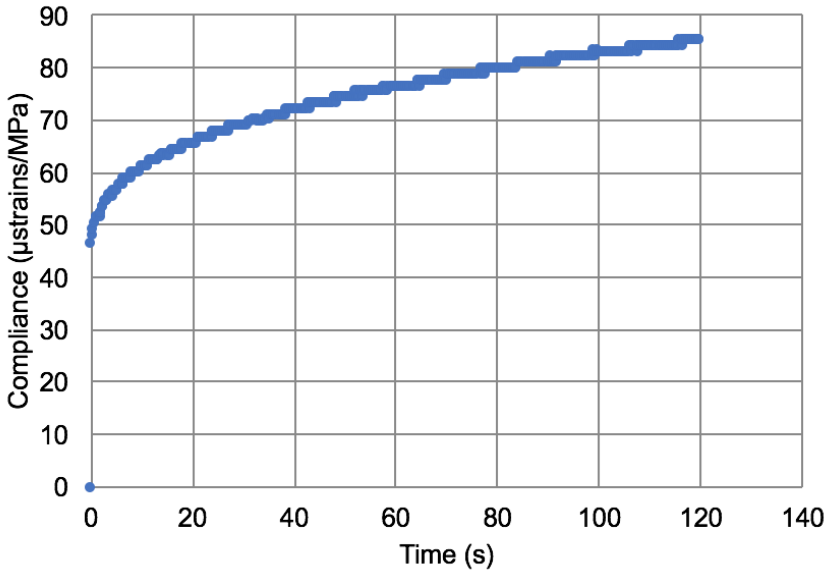

Figure 5.31. Typical Compliance Results from Standard Creep Tests on Mortar Beams

illustrate each step in the standard creep test analysis process.

An observation made during this process, that was alluded to earlier, was that warmer

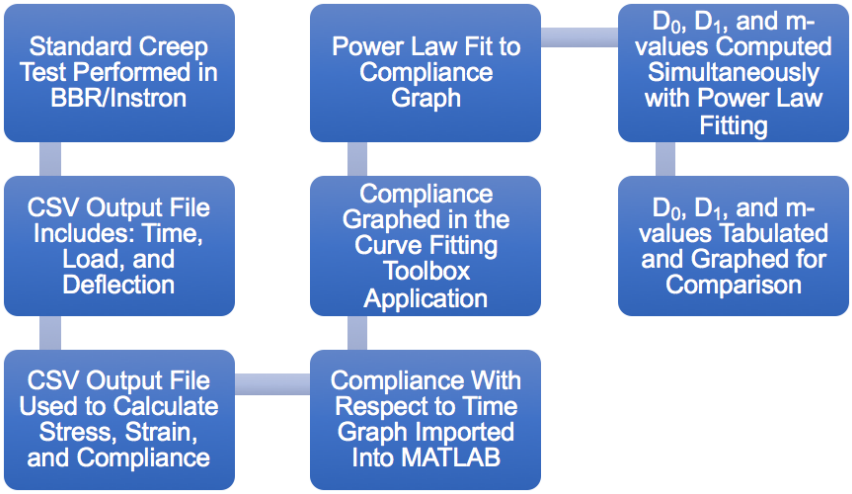

Figure 5.32. Flow Chart Illustrating the Standard Creep Analysis Process

temperatures helped produce better results. This was because mortar is substantially stiffer compared to binder and an increase in temperature (for the same load) results in higher deformation or strain during testing, which in turn resulted in a better (higher) signal to noise ratio. Evidence of this observation can be seen by comparing Figure 5.31 with Figure 5.33. These tests were run on the same beam at two different temperatures. Figure 5.31 was run at 0 °C, while Figure 5.33 was run at 6 °C. The test run at 6 °C produced a smoother compliance graph due to a slight increase in deformation during testing.

The first set of results are based on the creep power law parameters with respect to temperature. The results are organized by each parameter versus temperature for the ten mixes. Both the D_0 and D_1 parameters are represented using a log-linear scale to help better display the data. After reviewing these results several observations can be made.

Based on Table 5.3 it is clear that the two most extreme scenarios are FAM1 and FAM2. Strictly speaking, since there is a difference in the binder content between these two mixes (7.1% vs. 8%), the two extremes would be FAM2 and FAM3, where FAM3 is the same as FAM1 except the deficient binder content has been bumped up using a PG64-16 to get to 8%. An examination of D_0 reveals that the difference between the FAM mixes is not very significant until we get to higher temperatures. However, an examination of D_1 and m reveals that FAM1 and FAM2 are indeed the two boundaries for these parameters for all the mixes that were considered with FAM1 showing the lowest m and D_1 values as expected and FAM2 showing the highest m and D_1 values as expected.

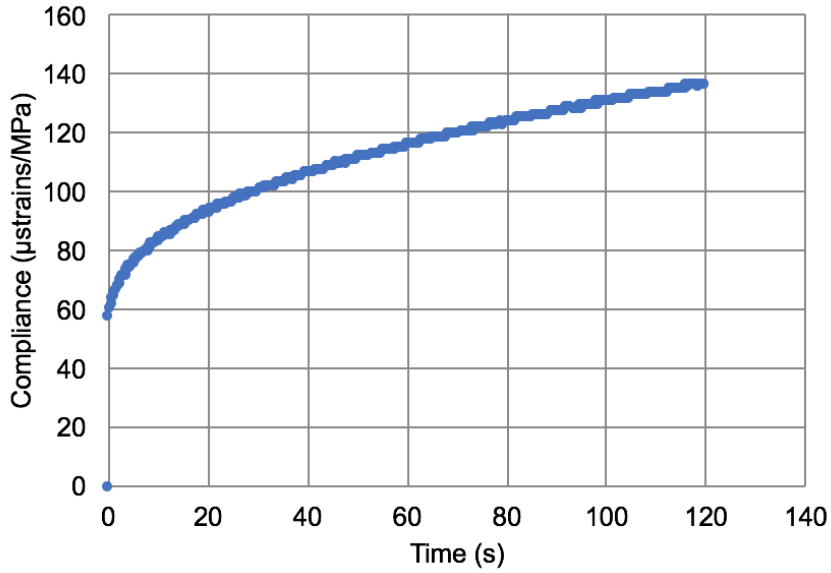

Figure 5.33. Compliance Results from a Standard Creep Test Performed on a Mortar Beam at 6 °C

Moreover, FAM3, closely follows FAM1 (with a small percentage of 64-16 added to it) with slightly higher compliance and m, as expected.

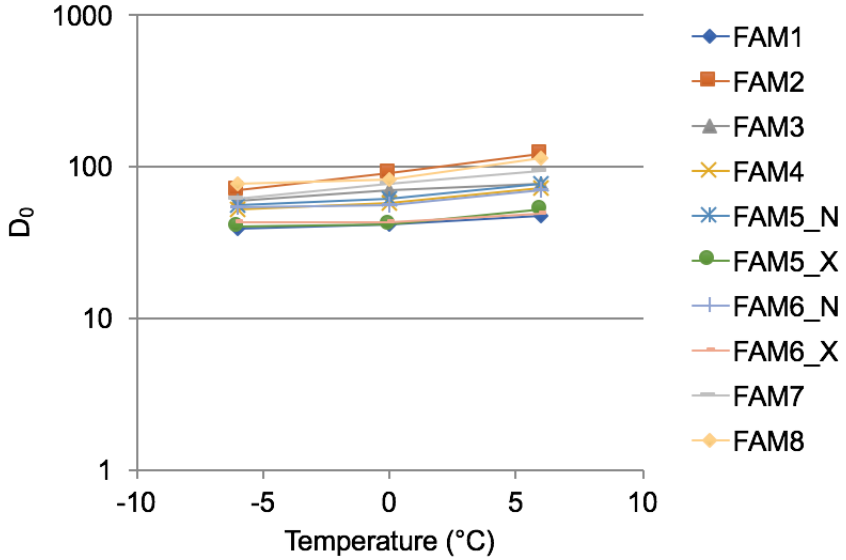

Figure 5.34. Average D_0-values With Respect to Temperature on Mortar Beams

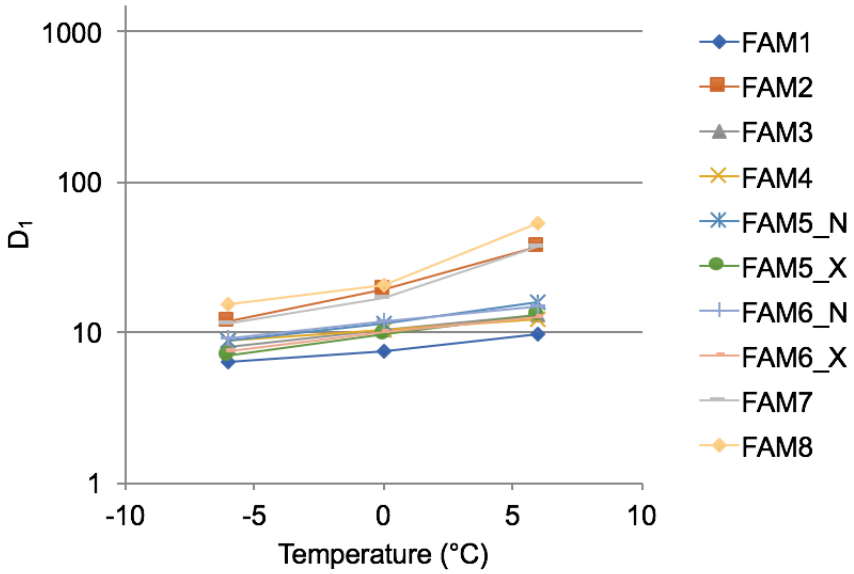

Figure 5.35. Average D_1-values With Respect to Temperature on Mortar Beams

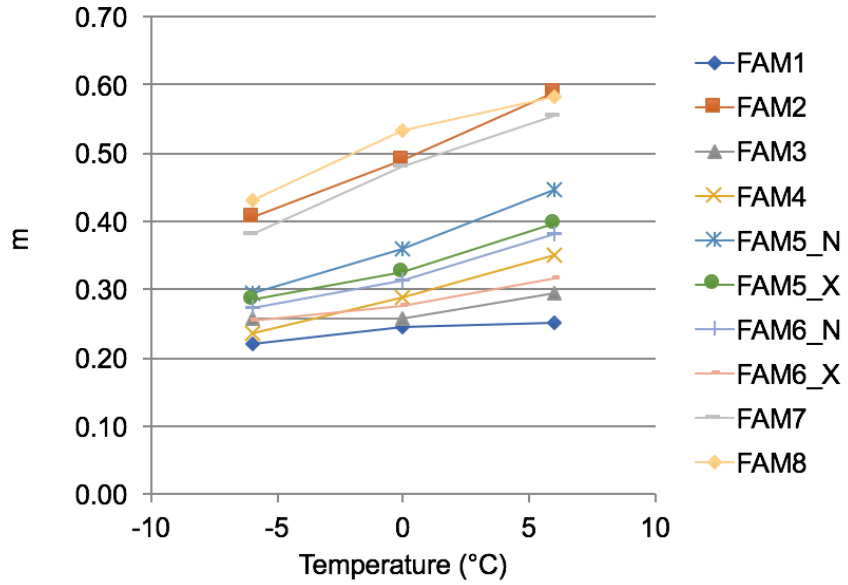

Figure 5.36. Average m With Respect to Temperature on Mortar Beams

Moving on to the tensile strength measurements, as before the output files for these tests contained the time, load, and deflection. Using simple beam theory and Equations 5.2 and 5.3 the stress and strain were computed. After the stress and strain had been

calculated a method for determining the failure point needed to be established.

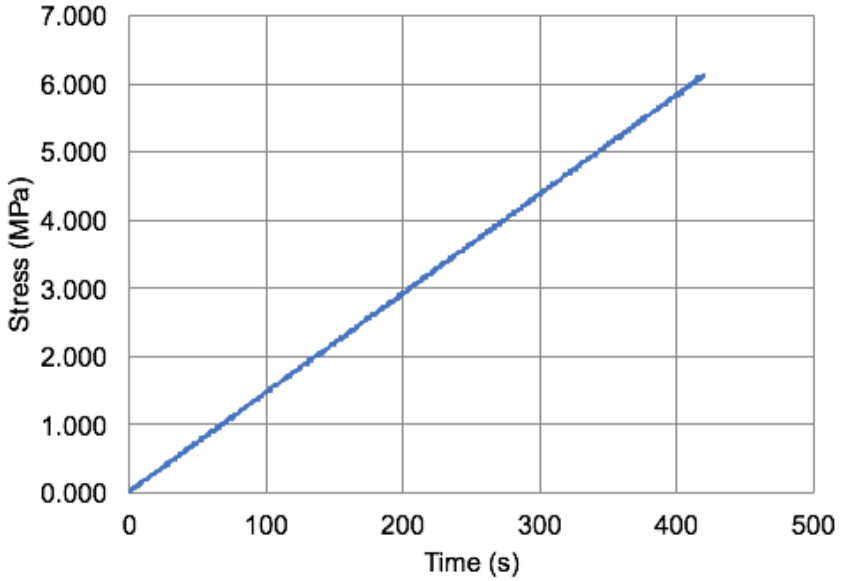

Figure 5.37. Typical Stress Results from Monotonic Load Tests on Mortar Beams

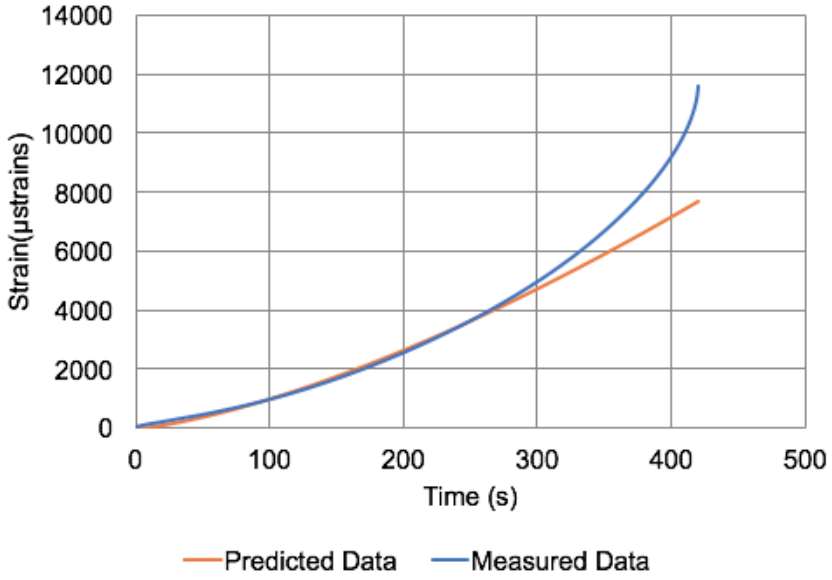

Figure 5.38. Typical Strain Results from Monotonic Load Tests on Mortar Beams

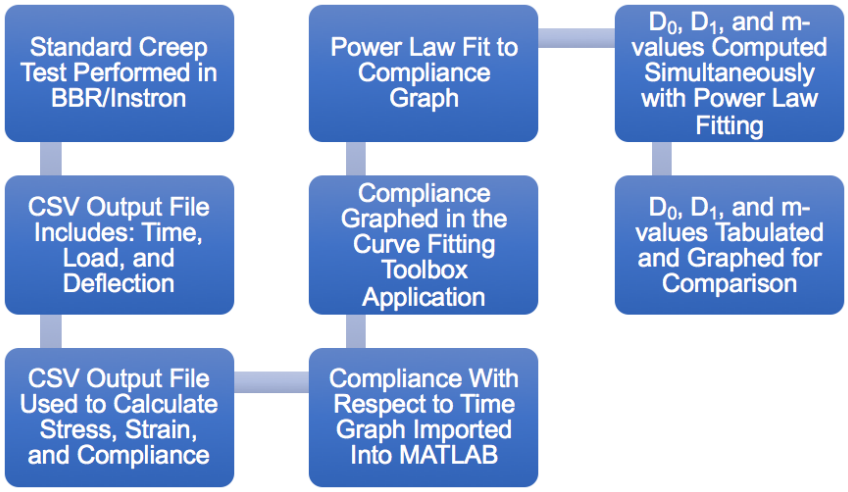

Figure 5.39. Flow Chart Illustrating the Monotonic Load Analysis Process

Since the strain response from these tests wasn't linear, a different method from the one used on the binder tests was developed. Figure 5.39 helps to illustrate the steps taken to identify a point of failure. While using the power law parameters, average values of the replicates tested at a specific temperature were used. Note that not all beams tested monotonically were tested with the creep recovery first, which will be important and discussed later (although other beam specimens for the same material were tested). Stress rate, as the one described in the flow chart, was obtained from the slope of the stress versus time graph for the specimen being analyzed. Note that the stress rate was slightly different from the commanded loading rate on account of slight differences in the actual applied loading rate and the geometry of the specific test specimen. The convolution integral is mentioned in this process and is an important piece of this analysis. Strain is predicted using the formula derived from the integration of the power law model used previously, which can be reviewed in Equation 5.7. The rupture value described in Figure 5.39 is the maximum strain value attained by the specimen before breaking. In order to find the point at which the measured strain data and predicted strain data diverge from each other, the difference between these two data sets was computed. As shown in the flow chart 5% of this rupture value was used as the target value for the difference or divergence point between the two graphs. Once this target value was located, the corresponding stress and strain values were collected and labeled as the values at failure. This analysis process is what was used in order to determine the stress and strains at failure that will be shown in the next few graphs.

$$D(t) = D_0 + D_1 t^m \tag{5.4}$$

$$\epsilon(t) = \int (D_0 + D_1 \tau^m) \alpha d\tau \tag{5.5}$$

$$= \alpha \int_0^t (D_0 + D_1 \tau^m) d\tau \tag{5.6}$$

$$= \alpha D_0 t + \alpha D_1 \frac{t^{m+1}}{m+1} \tag{5.7}$$

An observation made during this analysis process was that the density of the beams played a role in how well the power law parameters could predict the strain. Since not every beam was tested for creep compliance preceding the strength test, the creep compliance parameters for the material from other replicates had to be used. If these parameters were computed using beams with a higher bulk specific gravity (or more dense beams) the predictions for beams with a lower bulk specific gravity weren't as accurate. This could also be true if it was the reverse and the parameters were calculated using beams with a lower bulk specific gravity and were used to predict the behavior of beams with a higher bulk specific gravity; although this was not verified in this study. These differences in density could be due to the location from which the beams were cut from the SGC sample. The center most portion of the sample is going to be the most dense while the outer most portion is the least dense. One remedy that could have lessened this effect would have been using the direct compaction method instead of the SGC method for compacting the samples. Using the direct compaction method would have helped keep the density of each beam more consistent. Another remedy would be to use only beams from the middle portion of the SGC specimen.

Once all of the stresses and strains at failure had been determined the values were examined based on the material type and temperature. Each of the three graphs that show the tensile strength of each mix are separated by loading rate. After reviewing the results presented in Figures 5.40, 5.41, and 5.42 several observations can be made including:

- Both temperature and loading rate have an impact on the failure strength of the material.
- Rejuvenators did effect the failure strength of the material.

These observations are important for understanding the behavior of the material and will be discussed in further detail.

The first observation sheds light upon the impact of both temperature and loading

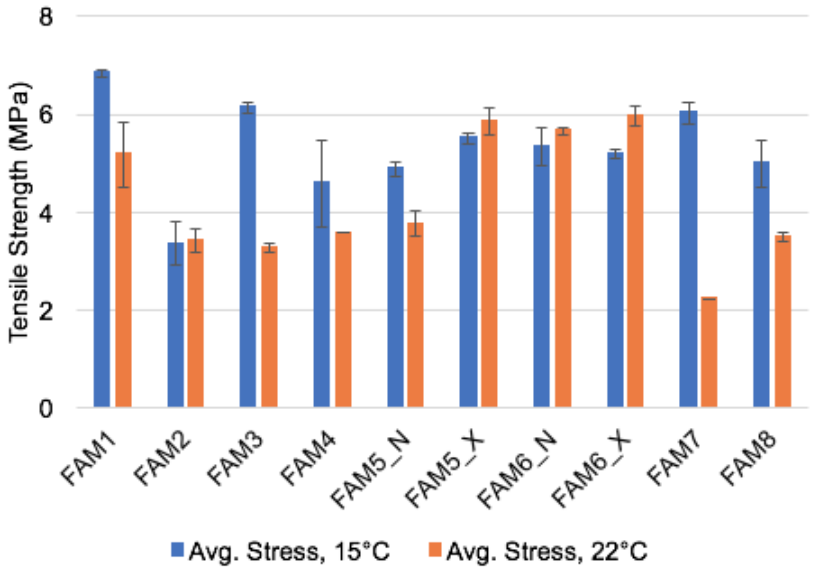

Figure 5.40. Average Tensile Strength for Mortar Mixes with a 24.96 N min^{-1} Loading Rate

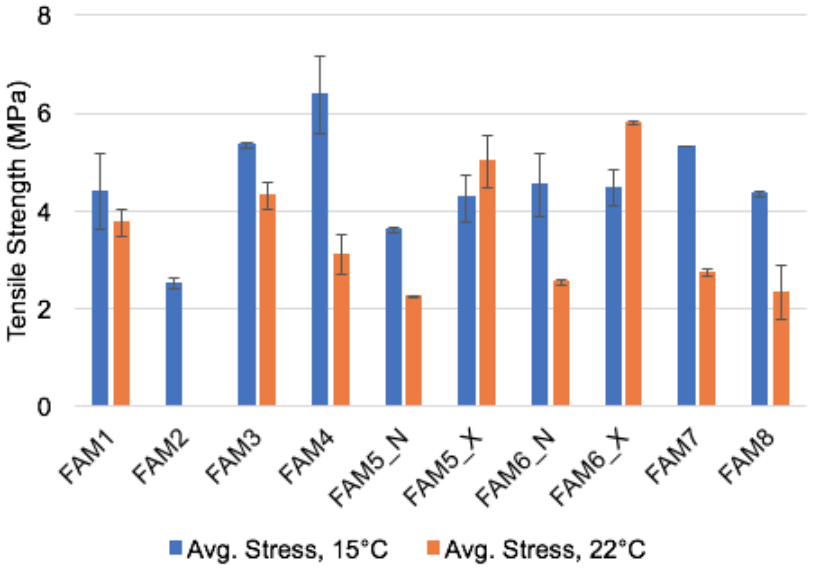

Figure 5.41. Average Tensile Strength for Mortar Mixes with a 12.48 N min^{-1} Loading Rate

rate on the tensile strength of the material. For most of the materials the tensile strength was higher at the lower temperature. It was also noticed that the faster loading rate

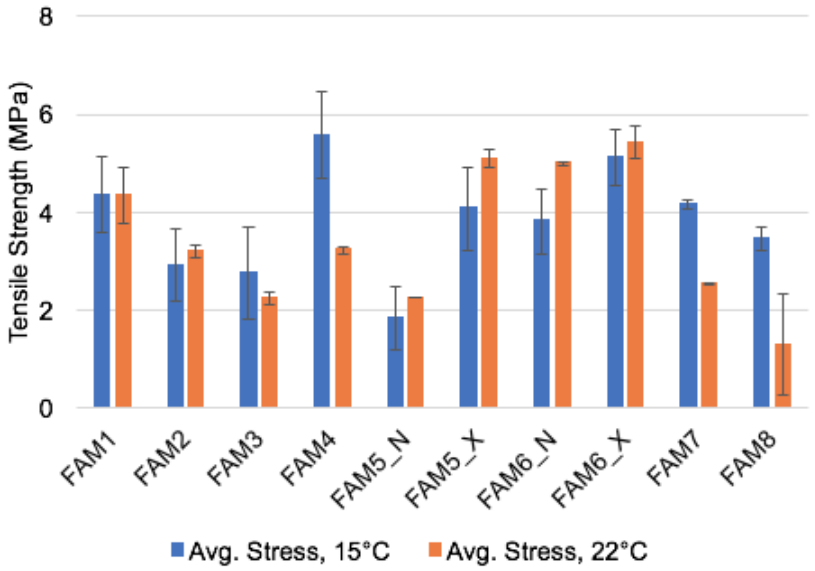

Figure 5.42. Average Tensile Strength for Mortar Mixes with a 6.24 N min^{-1} Loading Rate

seemed to have higher tensile strengths as well, which is consistent with the influence of lower temperature.

It was also noticed that the rejuvenators influenced the tensile strength of the material. FAM5 and 6 had comparable strengths to FAM1 (100% RAP) and much higher strengths than FAM2 (100% New Binder) at the fastest loading rate. Again FAM5 and 6 had comparable to slightly greater strengths at the slowest loading rate as well. A higher strength value is a desirable quality in a mix because it generally demonstrates a higher resistance to cracking (all other factors being the same). Another interesting observation is that all of the mixes that contained rejuvenators showed slightly higher strengths at the warmer of the two temperatures. Compare this to mixes without rejuvenators that had higher strengths at the cooler of the temperatures. This is an interesting phenomenon that was observed during this study.

The last set of results are the strain at failure for all ten mortar mixes. After reviewing these results several observations were made which include:

- Temperature appears to have a noticeable effect on the strain at failure of the mortar mixes.
- Failure strain does seem to be substsantially influenced by the addition of rejuvenators into the mortar mix.

The observations made will be discussed in depth next.

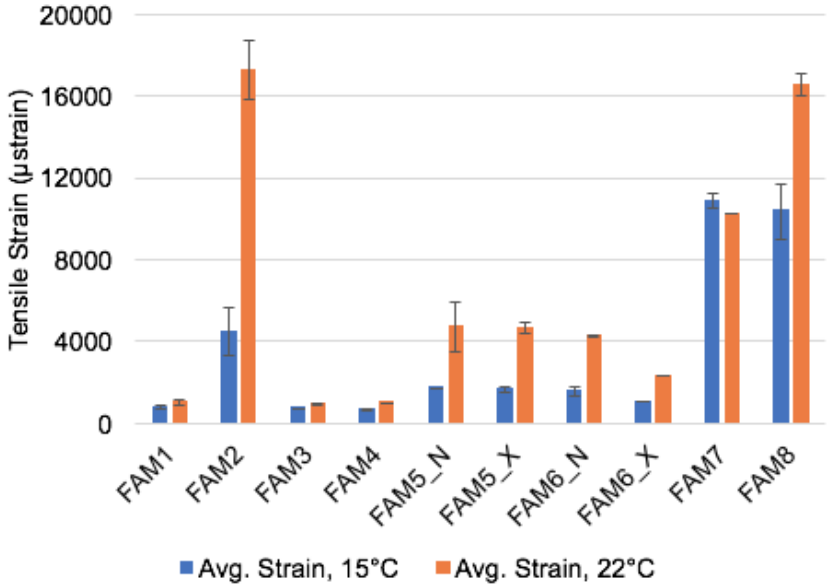

Figure 5.43. Average Tensile Strain for Mortar Mixes with a 24.96N/min. Loading Rate

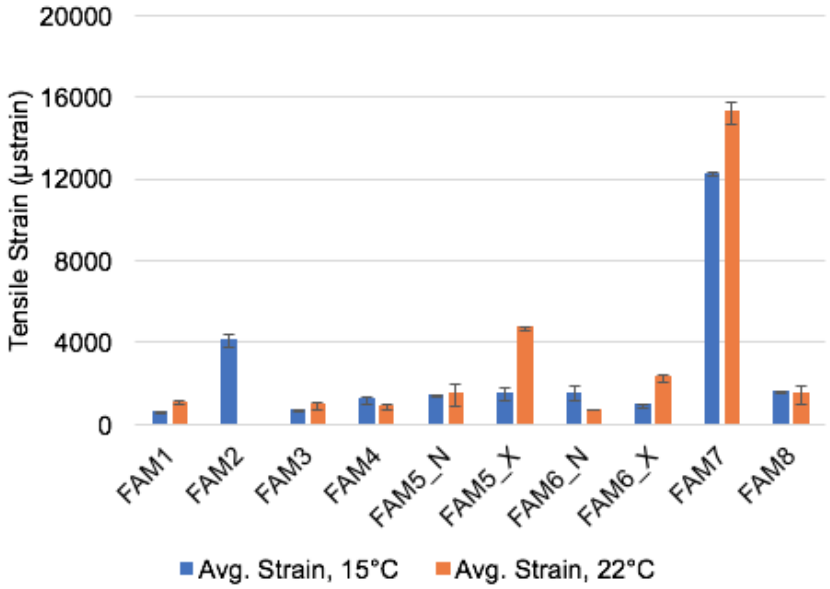

Figure 5.44. Average Tensile Strain for Mortar Mixes with a 12.48N/min. Loading Rate

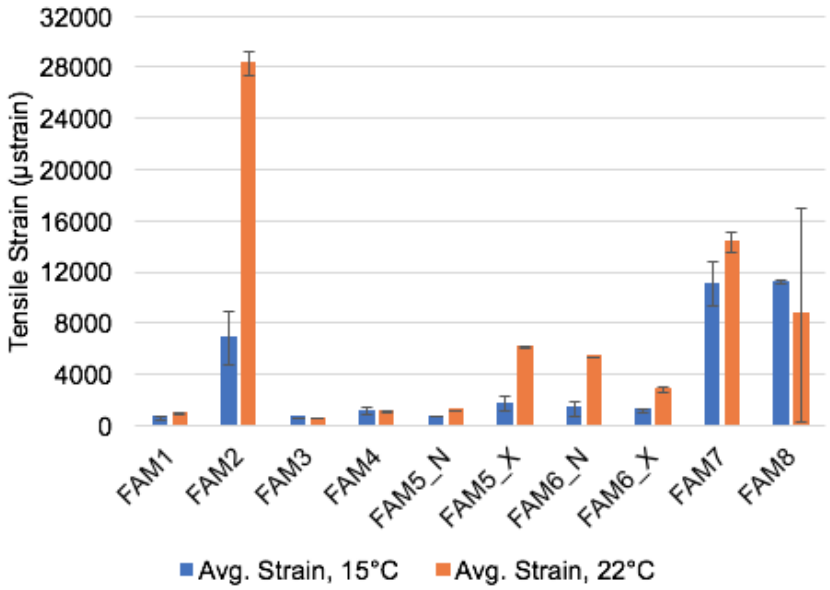

Figure 5.45. Average Tensile Strain for Mortar Mixes with a 6.24N/min. Loading Rate

The first observation highlights the impact that temperature has on the failure strain. As expected, on account of the relatively smaller changes in tensile strength and substantial changes in the compliance of the material with a change in temperature, the warmer temperature (22 °C) resulted in substantially higher failure strains. Second, it was noticed that the failure strain was also influenced by the use of rejuvenators. Typically the mixes that had some quantity of rejuvenator in them also had higher failure strain than the control mix made of 100% RAP material (FAM1). This shows that the mixes with rejuvenator experienced more deformation before failure meaning the rejuvenator must have had a softening effect. The type of rejuvenator used within the mix also made a difference. When comparing within a mix such as FAM5 one of the rejuvenators resulted in noticeably higher failure strain compared to the other. Differing quantities of rejuvenator were used when comparing FAM5 and FAM6 but the influence of the quantity was harder to discern due to the fact that the failure strains were comparable in magnitude. Overall, rejuvenators did have a recognizable impact on the failure strain of the mixture.

5.5 CONCLUDING REMARKS

In summary, the results from these tests show that binders with similar PG have a significantly broad range of stiffness values at low temperatures. In addition, these binders also show a range of different tensile strengths. In the context of using RAP with binders, it was interesting to note that in some cases addition of recycled binder increased the stiffness and tensile strength of the composite (virgin + RAP binder) while decreasing the rate of relaxation. Although the changes in stiffness and rate of relaxation are well documented and expected, the changes in tensile strength are important because they reveal that incorporation of RAP does not necessarily imply poor thermal performance. Finally, the use mortars showed the differences in stiffness, rate of relaxation and tensile strength as a function of RAP content and rejuvenator.

Perhaps the most important conclusion here is not that rejuvenators aid in improving the properties of a mix with RAP and that different rejuvenators respond differently; rather the most important conclusion here is that the mortar can be used as an effective screening tool to compare different material combinations without the use of any extraction.

CHAPTER 6. CONCLUSIONS AND SUMMARY

This study covered several different specimen fabrication processes and tested various materials. Conclusions can be drawn from the many topics discussed in this study.

6.1 FABRICATION OF MORTAR SPECIMENS

1. The direct compaction method used to fabricate mortar specimens can help economize the use of materials, time, and laboratory space. Consistency of the density of each specimen can be more easily controlled as well. As shown in the results in later part of this study, the creep compliance is sensitive to small changes in the density of the test specimen.
2. Sanding and greasing the beams before testing can help minimize friction between the beam and the testing device contact points. Less friction helps increase repeatability between replicates during testing.
3. An important feature of the mortar or FAM fabrication procedure was that it used sieved RAP of a certain size fraction that was directly incorporated in the mix. This avoids the extraction and recovery of binder, which in turn not only saves time but also helps avoid artifacts due to differences between blending versus composite response.

6.2 INVESTIGATION OF BINDERS WITH SIMILAR PG

1. Binders of the same PG tested at the same temperature show a large range of compliance values. Even though binders are assigned the same grade, their stiffness can be significantly different from each other depending on the source of the binder. The rate of relaxation or m value was more consistent among different binders of the same grade at their grade temperature. This discrepancy has been recently recognized by several different researchers. In fact, a parameter referred to as ΔT_c, which reflects the gap between the true grade based on the stiffness and m value has recently been introduced as a surrogate for resistance to fatigue and thermal cracking.
2. The tensile strength of binders with the same assigned PG can vary significantly. This property is currently not measured in evaluating binders, whereas strength is

the most critical property to model failure susceptibility of any given material.

6.3 INFLUENCE OF RECYCLING AGENTS AND RECYCLED BINDER ON PROPERTIES OF ASPHALT MORTARS

1. The four point loading system can help increase repeatability between replicates. This is due to the creation of a uniform stress zone over a larger portion of the beam.
2. Since mortar or FAM is much stiffer than binder better results were achieved by testing at warmer temperatures. This allowed for greater deflection in the beam thus leading to better fits and predictions.
3. Mixes that had virgin binders and mixes with RAP were easily identifiable by studying the D_1 and m value graphs. The mixes with virgin binder had much higher D_1 and m values.
4. Both temperature and loading rate had an impact on the strength measured at failure. As before temperature has an inverse relationship with strength. While loading rate had a direct relationship to strength.
5. Temperature also substantially influenced the failure strain experienced by the material. The warmer the temperature the higher the strain measured at failure.
6. Rejuvenators impacted both the strength and strain at failure. The strengths of mixes with rejuvenators were comparable if not slightly higher than the mix with 100% RAP. The presence of rejuvenator also seemed to increase the deformation or strain when comparing it to the 100% RAP control mix. This means some softening may have occurred compared to a 100% RAP control.
7. Perhaps the most important conclusion here is not that rejuvenators aid in improving the properties of a mix with RAP and that different rejuvenators respond differently; rather the most important conclusion here is that the mortar can be used as an effective screening tool to compare different material combinations without the use of any extraction.

REFERENCES

Abbas, A. R., Mannan, U. A., and Dessouky, S. 2013. Effect of recycled asphalt shingles on physical and chemical properties of virgin asphalt binders. *Construction and Building Materials*, 45:162–172.

Anderson, M. R., King, G. N., Hanson, D. I., and Blankenship, P. B. 2011. Evaluation of the Relationship between Asphalt Binder Properties and Non-Load Related Cracking. *Asphalt Paving Technology*, 80:615–663.

Arega Z.Z., A. Bhasin, and Kesel, T. D. 2013. Influence of extended aging on the properties of asphalt composites produced using hot and warm mix methods. *Construction and Building Materials*, 44:168–174.

Bahia, H., Wen, H., and Johnson, C. M. 2010. Developments in intermediate temperature binder fatigue specifications. *Development in Asphalt*, page 25.

Behnia, B. and Dave, E. 2011. Effects of recycled asphalt pavement amounts on low-temperature cracking performance of asphalt mixtures using acoustic emissions. *Transportation Research Record: Journal of the Transportation Research Board*.

Bouldin, M., Dongré, R., and D'Angelo, J. 2001. Proposed refinement of superpave high-temperature specification parameter for performance-graded binders. *Transportation Research Record: Journal of the Transportation Research Board*, (1766):40–47.

Boyer, R. E. and Engineer, P. S. D. 2000. Asphalt rejuvenators "fact, or fable". *Transportation systems*, 58:l.

Brownridge, J. 2010. The role of an asphalt rejuvenator in pavement preservation: use and need for asphalt rejuvenation. In *Compendium of papers from the first international conference on pavement preservation*, pages 351–364.

Chowdhury, N., Hossain, Z., Yang, S., and Braham, A. 2015. A framework for premature pavement distress evaluation. In *IFCEE 2015*, pages 2492–2501.

Chowdhury, N. H. 2015. *Root causes of premature pavement failures of Arkansas interstate system*. Arkansas State University.

De Moraes, M., Pereira, R., Simão, R., and Leite, L. 2010. High temperature afm study of cap 30/45 pen grade bitumen. *Journal of Microscopy*, 239(1):46–53.

Dourado, E., Simao, R., and Leite, L. 2012. Mechanical properties of asphalt binders evaluated by atomic force microscopy. *Journal of microscopy*, 245(2):119–128.

Falchetto, A. C., Marasteanu, M. O., Balmurugan, S., and Negulescu, I. I. 2014. Investigation of asphalt mixture strength at low temperatures with the bending beam rheometer. *Road Materials and Pavement Design*, 15(S1):28–44.

García, Á., Schlangen, E., van de Ven, M., and Sierra-Beltrán, G. 2010. Preparation of capsules containing rejuvenators for their use in asphalt concrete. *Journal of hazardous materials*, 184(1):603–611.

Henderson, K. G. and Muller, R. A. 1997. Extreme temperature days in the south-central United States. *Climate Research*, 8(2):151–162.

Hesp, S. A. M., Soleimani, A., Subramani, S., Phillips, T., Smith, D., Marks, P., and Tam, K. K. 2009. Asphalt pavement cracking: analysis of extraordinary life cycle variability in eastern and northeastern Ontario. *International Journal of Pavement Engineering*, 10(3):209–227.

Hossain, Z., Lewis, S., Zaman, M., Buddhala, A., and O'Rear, E. 2012. Evaluation for warm-mix additive-modified asphalt binders using spectroscopy techniques. *Journal of Materials in Civil Engineering*, 25(2):149–159.

Hossain, Z., Rashid, F., Mahmud, I., and Rahaman, M. Z. 2016. Morphological and nanomechanical characterization of industrial and agricultural waste–modified asphalt binders. *International Journal of Geomechanics*, 17(3):04016084.

Jäger, A., Lackner, R., Eisenmenger-Sittner, C., and Blab, R. 2004. Identification of microstructural components of bitumen by means of atomic force microscopy (afm). *Pamm*, 4(1):400–401.

Karl, T. R., Kukla, G., Razuvayev, V. N., Changery, M. J., Quayle, R. G., Heim, R. R., Easterling, D. R., and Fu, C. B. 1991. Global warming: Evidence for asymmetric diurnal temperature change. *Geophysical Research Letters*, 18(12):2253–2256.

Karlsson, R. and Isacsson, U. 2006. Material-related aspects of asphalt recycling, state-of-the-art. *Journal of Materials in Civil Engineering*, 18(1):81–92.

Kennedy, T. W., Huber, G. A., Harrigan, E. T., Cominsky, R. J., Hughes, C. S., Quintus, H. V., and Moulthrop, J. S. 1994. Superior Performing Asphalt Pavements: The Product of the SHRP Asphalt Research Program. Technical report, Strategic Highway Research Program, Washington, DC.

Kodrat, I., Sohn, D., and Hesp, S. 2007. Comparison of Polyphosphoric Acid-Modified Asphalt Binders with Straight and Polymer-Modified Materials. *Transportation Research Record: Journal of the Transportation Research Board*, 1998(-1):47–55.

Leathers, D., Palecki, M., Robinson, D., and Dewey, K. 1998. Climatology of the daily temperature range annual cycle in the United States. *Climate Research*, 9(1984):197–211.

Lin, J.-D., Yau, J.-T., and Hsiao, L.-H. 2003. Correlation analysis between international roughness index (iri) and pavement distress by neural network. In *Paper Publication at the 82th Annual Meeting of the Transportation Research Board, Washington, DC*.

Ma, T., Mahmoud, E., and Bahia, H. 2010. Estimation of reclaimed asphalt pavement binder low-temperature properties without extraction: Development of testing procedure. *Transportation Research Record: Journal of the Transportation Research Board*, (2179):58–65.

Mannan, U. A., Islam, M. R., and Tarefder, R. A. 2015. Fatigue behavior of asphalt containing reclaimed asphalt pavement. In *Transportation Research Board 94th Annual Meeting*, number 15-5828.

Marasteanu, M., Zofka, A., Turos, M., Li, X., Velasquez, R., Li, X., Buttlar, W., Paulino, G., Braham, A., Dave, E., Ojo, J., Bahia, H., Williams, C., Bausano, J., Gallistel, A., and McGraw, J. 2007. Investigation of Low Temperature Cracking in Asphalt Pavements National Pooled Fund Study 776. Technical report.

Masad, E., Huang, C.-W., Airey, G., and Muliana, A. 2008. Nonlinear viscoelastic analysis of unaged and aged asphalt binders. *Construction and Building Materials*, 22(11):2170–2179.

Masson, J.-F., Leblond, V., and Margeson, J. 2006. Bitumen morphologies by phase-detection atomic force microscopy. *Journal of Microscopy*, 221(1):17–29.

National Asphalt Paving Association. National Asphalt Paving Association.

Rada, G. R. 2013. *Guide for Conducting Forensic Investigations of Highway Pavements (with supplemental material on CD-ROM)*, volume 747. Transportation Research Board.

Ramm, A., Sakib, N., Bhasin, A., and Downer, M. 2016. Optical characterization of temperature-and composition-dependent microstructure in asphalt binders. *Journal of microscopy*, 262(3):216–225.

Rashid, A. F. 2016. *Multiscale mechanistic characterization of reclaimed asphalt pavements*. PhD thesis, Arkansas State University.

Rashid, A. F. and Hossain, Z. 2016. Morphological and nanomechanical analyses of ground tire rubber-modified asphalts. *Innovative Infrastructure Solutions*, 1(1):36.

Roberts, F. L., Kandhal, P. S., Brown, E. R., Lee, D. Y., and Kennedy, T. W. 1996. *Hot Mix Asphalt Materials, Mixture, Desgin, and Construction*. National Asphalt Pavement Association Research and Education Foundation, Lanham, Maryland.

Roy, S. and Hesp, S. 2001. Low-Temperature Binder Specification Development: Thermal Stress Restrained Specimen Testing of Asphalt Binders and Mixtures. *Transportation Research Record*, 1766(1):7–14.

Sabouri, M. 2014. *Development of a unified fatigue failure criterion for asphalt mixtures and its applications to reclaimed asphalt pavement (RAP) mixtures*. North Carolina State University.

Sayers, M. W. 1986. The international road roughness experiment: establishing correlation and a calibration standard for measurements.

Shen, J., Amirkhanian, S., and Aune Miller, J. 2007a. Effects of rejuvenating agents on superpave mixtures containing reclaimed asphalt pavement. *Journal of Materials in Civil Engineering*, 19(5):376–384.

Shen, J., Amirkhanian, S., and Tang, B. 2007b. Effects of rejuvenator on performance-based properties of rejuvenated asphalt binder and mixtures. *Construction and Building Materials*, 21(5):958–964.

Shen, J. and Ohne, Y. 2002. Determining rejuvenator content for recycling reclaimed asphalt pavement by shrp binder specifications. *International Journal of Pavement Engineering*, 3(4):261–268.

Sultana, S., Bhasin, A., and Liechti, K. M. 2014. Rate and confinement effects on the tensile strength of asphalt binder. *Construction and Building Materials*, 53:604–611.

Tarefder, R., Zaman, M., and Hobson, K. 2003. A laboratory and statistical evaluation of factors affecting rutting. *International Journal of Pavement Engineering*, 4(1):59–68.

Tarefder, R. A. and Zaman, A. M. 2009. Nanoscale evaluation of moisture damage in polymer modified asphalts. *Journal of Materials in Civil Engineering*, 22(7):714–725.

Valdés, G., Pérez-Jiménez, F., Miró, R., Martínez, A., and Botella, R. 2011. Experimental study of recycled asphalt mixtures with high percentages of reclaimed asphalt pavement (rap). *Construction and Building Materials*, 25(3):1289–1297.

Vasconcelos, K. L., Bhasin, A., and Little, D. N. 2010. Influence of reduced production temperatures on the adhesive properties of aggregates and laboratory performance of fine aggregate-asphalt mixtures. *Road Materials and Pavement Design*, 11(1):47–64.

Velásquez, R. a., Labuz, J. F., Marasteanu, M. O., and Zofka, A. M. 2009. Revising Thermal Stresses in the TSRST for Low-Temperature Cracking Prediction. *Journal of Materials in Civil Engineering*, 21(11):680–687.

Wang, D., Linbing, W., Christian, D., and Zhou, G. 2012. Fatigue properties of asphalt materials at low in-service temperatures. *Journal of Materials in Civil Engineering*, 25(9):1220–1227.

Yang, S., Braham, A., Chowdhury, N., and Hossain, Z. 2015. Linking the field and lab performance of interstate pavements. In *Innovative Materials and Design for Sustainable Transportation Infrastructure*, pages 19–27.

Yildirim, Y., Ideker, J., and Hazlett, D. 2006. Evaluation of viscosity values for mixing and compaction temperatures. *Journal of materials in civil engineering*, 18(4):545–553.

Zollinger, C. 2005. *Application of Surface Energy Measurements to Evaluate Moisture Susceptibility of Asphalt and Aggregates*. PhD thesis.

APPENDIX A. WEATHER AND IN-SERVICE DATA

Table A.1. Calculation of Rutting and Roughness Data for RAP1

		IRI (in/mile)				Rut	
Year	Month	L.M. 223	L.M. 223.2	L.M. 223.4	Avg IRI	L.M. 223	L.M. 223.2
2013-10	October	23.76	52.275	33.9	36.65	0.039	0.039
2013-02	February	30.41	45.3	31.045	35.59	0.059	0.079
2012-03	March	51.64	34.53	34.85	40.34	0.079	0.118
2011-04	April	21.225	34.85	26.61	27.56	0.079	0.0985
2010-03	March	28.83	51.635	62.725	47.73	0.059	0.0985
2009-04	April	23.13	68.745	79.52	57.13	0.137	0.177
2008-06	June	57.655	40.87	68.43	55.65	0.197	0.2165
2007-11	November	29.145	38.015	55.12	40.76	0.177	0.1375
2006		28.51	38.015	50.055	38.86	0.157	0.118
2005-04	April	35.48	66.215	58.605	53.43	0.256	0.2165
2005-11	November	32.395	59.245	48.155	46.6	0.157	0.177
2004-08	August	33.58	35.165	59.69	42.81	0.216	0.1965
2004-01	January	70.33	81.735	48.155	66.74	0.177	0.177
2003-04	April	41.185	41.815	58.925	47.31	0	0
2003-01	January	33.895	57.025	62.09	51	0.098	0.0985
2002-06	June	57.97	49.41	61.455	56.28	0.098	0.1375
2002-03	March	78.565	79.835	79.83	79.41	0.177	0.157
2001		85.22	130.205	165.59	127.01	0.256	0.197

Table A.2. Calculation of Rutting and Roughness Data for RAP2

		IRI (in/mile)			Rut (in/mile)		
Year	Month	L.M. 14.80	L.M. 15.0	Avg IRI	L.M. 14.80	L.M. 15	Avg Rut
2013-10	October	50.055	52.275	51.165	0.24	0.236	0.236
2013-2	February	41.5	77.935	59.7175	0.28	0.315	0.2955
2012-3	March	30.095	52.59	41.3425	0.35	0.2955	0.32475
2011-4	April	49.105	52.905	51.005	0.32	0.2955	0.30525
2010-3	March	45.62	22.81	34.215	0.32	0.276	0.2955
2009-4	April	47.84	48.47	48.155	0.43	0.394	0.4135
2008-6	June	54.805	62.725	58.765	0.32	0.3545	0.33475
2007-11	November	67.795	62.405	65.1	0.37	0.315	0.3445
2006C		43.72	29.145	36.4325	0.24	0.2165	0.22625
2005-4	April	54.49	50.69	52.59	0.39	0.315	0.3545
2005-11	November	58.925	63.04	60.9825	0.26	0.236	0.246
2004-8	August	53.855	44.665	49.26	0	0	0
2004-1	January	58.29	71.28	64.785	0.28	0.315	0.2955
2003-4	April	58.29	57.975	58.1325	0.12	0.1575	0.13775
2003-1	January	202.435	87.44	144.9375	0.18	0.2165	0.19675
2002-6	June	139.39	136.54	137.965	0.16	0.1575	0.15725
2002-3	March	169.485	197.05	183.2675	0.16	0.157	0.15725
2001		432.115	194.515	313.315	0.22	0.1375	0.177

Table A.3. Calculation of Rutting and Roughness Data for RAP3

		IRI (in/mile)				Rut (inch)		
Year	**Month**	**L.M 75.6**	**L.M 75.8**	**L.M 76.0**	**Avg IRI**	**L.M 75.6**	**L.M 75.8**	**L.M 7**
2013-10	October	126.09	69.7	106.44	100.74	0.1575	0.0785	0.1
2013-2	February	106.44	62.26	114.05	94.25	0.1965	0.1185	0.1
2012-3	March	124.19	48.79	133.06	102.01	0.1575	0.0785	0.1
2011-4	April	148.9	31.68	63.36	81.31	0.0585	0.0785	0.1
2010-3	March	90.6	36.12	101.38	76.03	0.2755	0.0985	0.0
2009-4	April	86.17	62.09	126.72	91.66	0.1575	0.138	0.1
2008-6	June	89.97	96.94	91.24	92.72	0.551	0.512	0.
2007-11	November	93.14	99.48	93.77	95.46	0.394	0.3545	0.
2006C		99.48	48.79	104.54	84.27	0.453	0.315	0.2
2005-4	April	75.35	107.71	85.54	89.53	0.1965	0.1575	0.1
2005-11	November	96.31	83	89.97	89.76	0.315	0.3345	0.2
2004-8	August	91.87	136.86	72.23	100.32	0	0	
2004-1	January	102.64	89.34	100.11	97.36	0.3935	0.3735	0.3
2003-4	April	84.9	83.64	91.87	86.8	0	0	
2003-1	January	90.6	93.77	100.74	95.04	0.1965	0.2755	0.2
2002-6	June	87.44	70.33	84.9	80.89	0.1965	0.1575	0.
2002-3	March	79.83	98.21	102.01	93.35	0.3145	0.3145	0.2
2001		72.23	70.96	87.44	76.88	0.1575	0.1575	0.2

Table A.4. Calculation of Rutting and Roughness Data for RAP4

		IRI (in/mile)				Rut (inch)		
Year	Month	L.M. 68.9	L.M. 70	L.M 71.5	Avg IRI	L.M. 68.9	L.M. 70	L.M 71
2013-10	October	199.9	319.3	196.1	238.45	0.157	0.1575	0.09
2013-2	February	79.835	139.3	260.095	159.78	0.118	0.2165	0.1
2012-3	March	133.69	152.7	114.365	133.59	0.157	0.1575	0.17
2011-4	April	129.57	95.67	96.625	107.29	0.098	0.0785	0.0
2010-3	March	78.565	76.98	143.195	99.58	0.079	0.079	0.0
2009-4	April	52.905	56.07	92.68	67.22	0.177	0.118	0.17
2008-6	June	70.33	69.06	75.715	71.7	0.236	0.5705	0.29
2007-11	November	58.295	64.94	64.33	62.52	0.196	0.256	0.13
2006C		38.65	48.78	55.12	47.52	0.118	0.118	0.1
2005-4	April	61.775	57.97	63.36	61.04	0.118	0.118	0.09
2005-11	November	58.605	65.58	59.24	61.14	0.196	0.236	0.21
2004-8	August	56.39	62.09	59.875	59.45	0	0.177	
2004-1	January	65.895	68.43	65.58	66.64	0	0	
2003-4	April	178.675	212.8	326.305	239.29	0.236	0.1375	0.2
2003-1	January	125.135	211.6	261.995	199.59	0.196	0.453	0.25
2002-6	June	166.005	204	107.395	159.14	0.177	0.256	0.0
2002-3	March	162.205	197.6	204.02	187.97	0.196	0.236	0.21
2001		134.325	201.4	377.945	237.92	0.177	0.2165	0.15

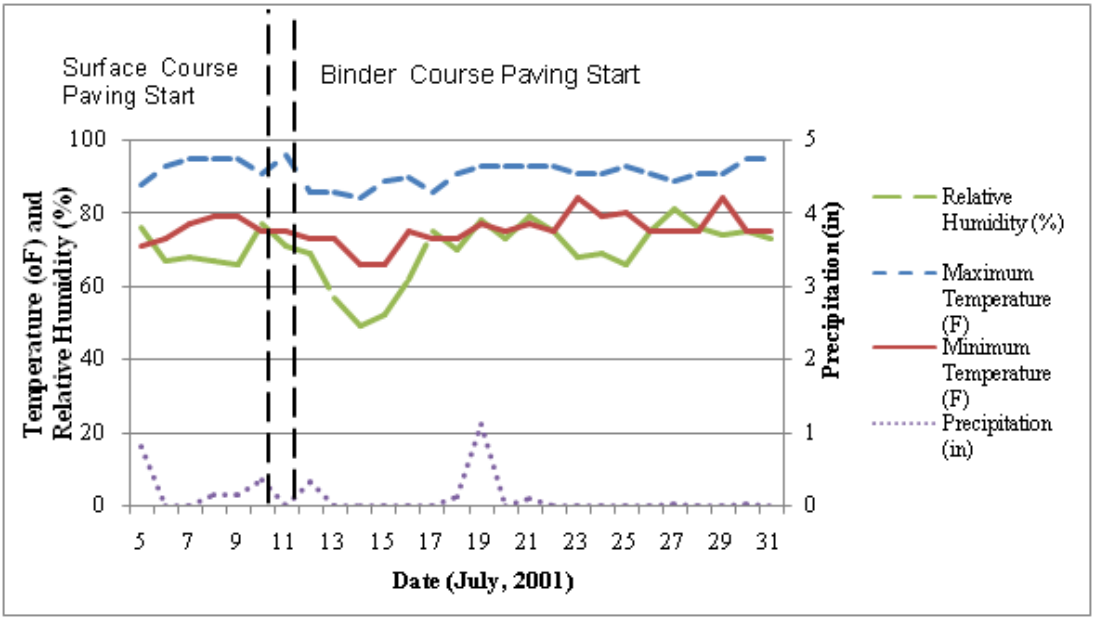

Figure A.1. Weather Data for RAP1 (July, 2001).

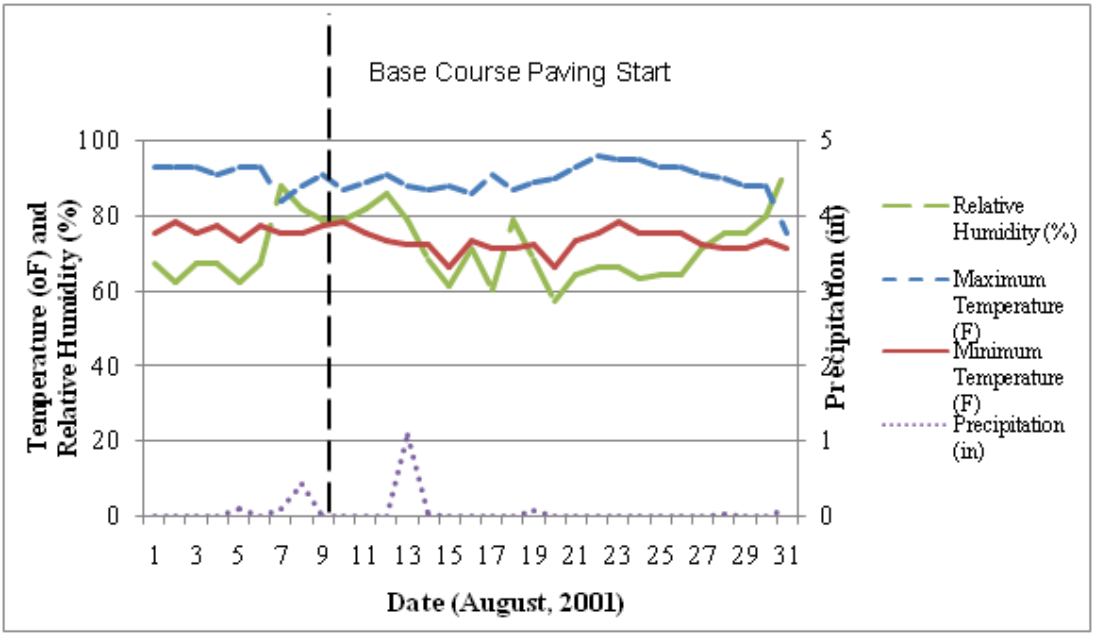

Figure A.2. Weather Data for RAP1 (August, 2001).

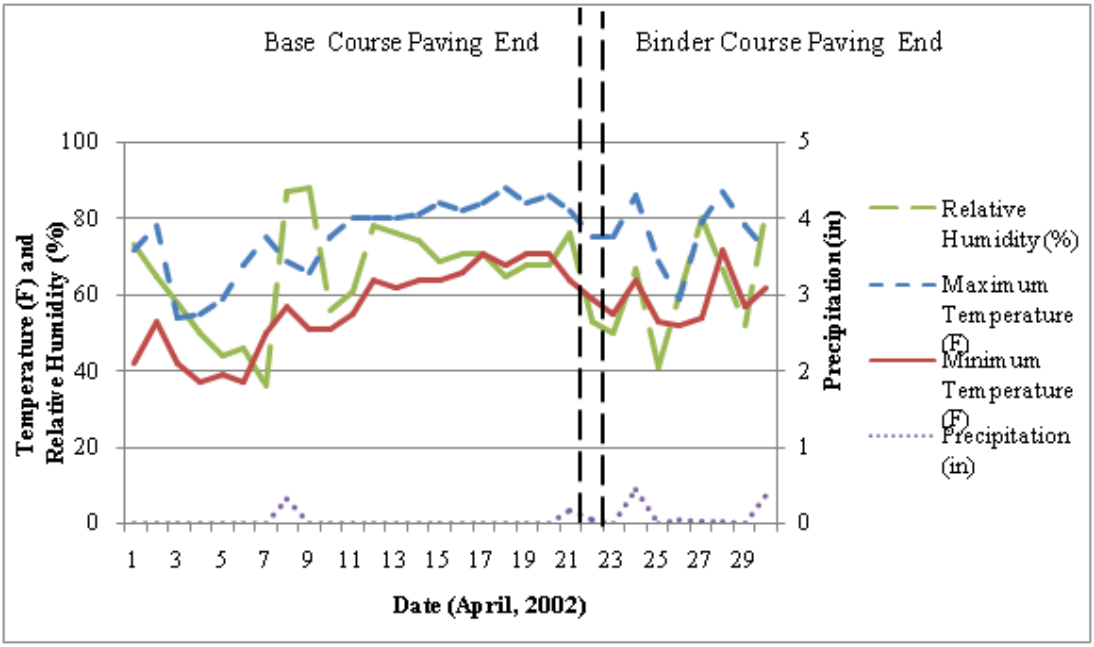

Figure A.3. Weather Data for RAP1 (April, 2002).

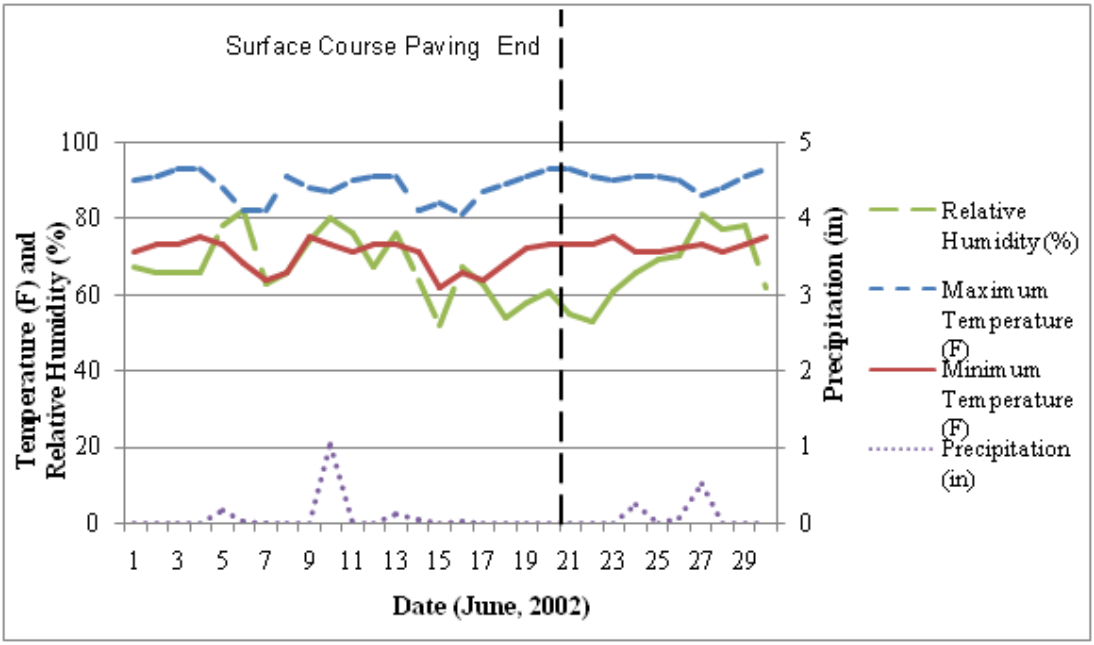

Figure A.4. Weather Data for RAP1 (June, 2002).

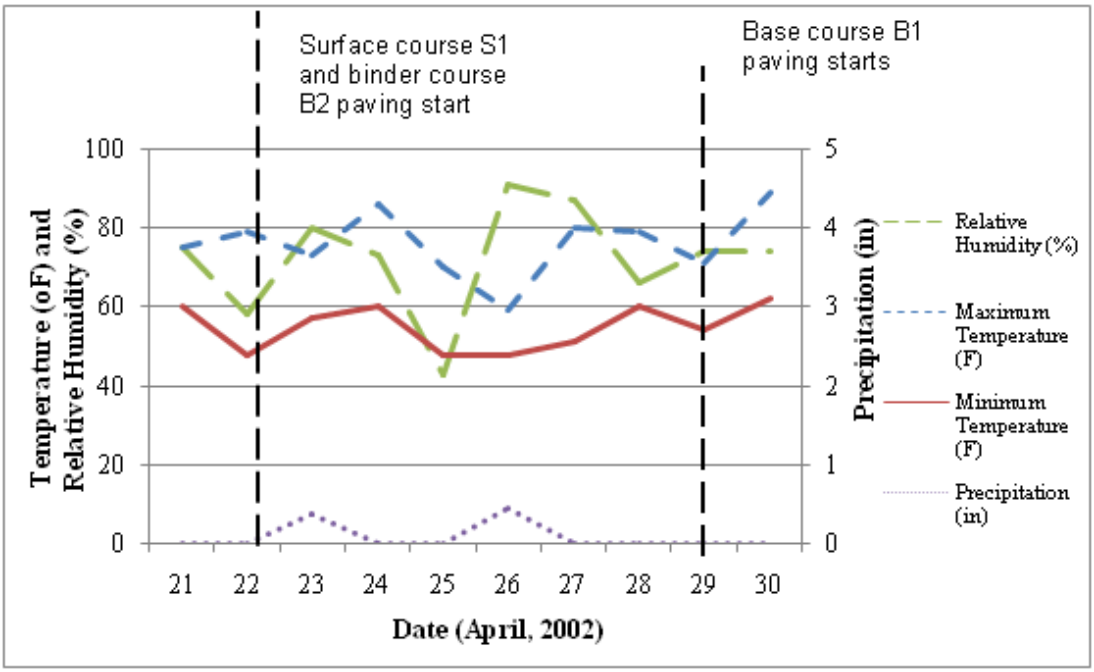

Figure A.5. Weather Data for RAP2 (April, 2002).

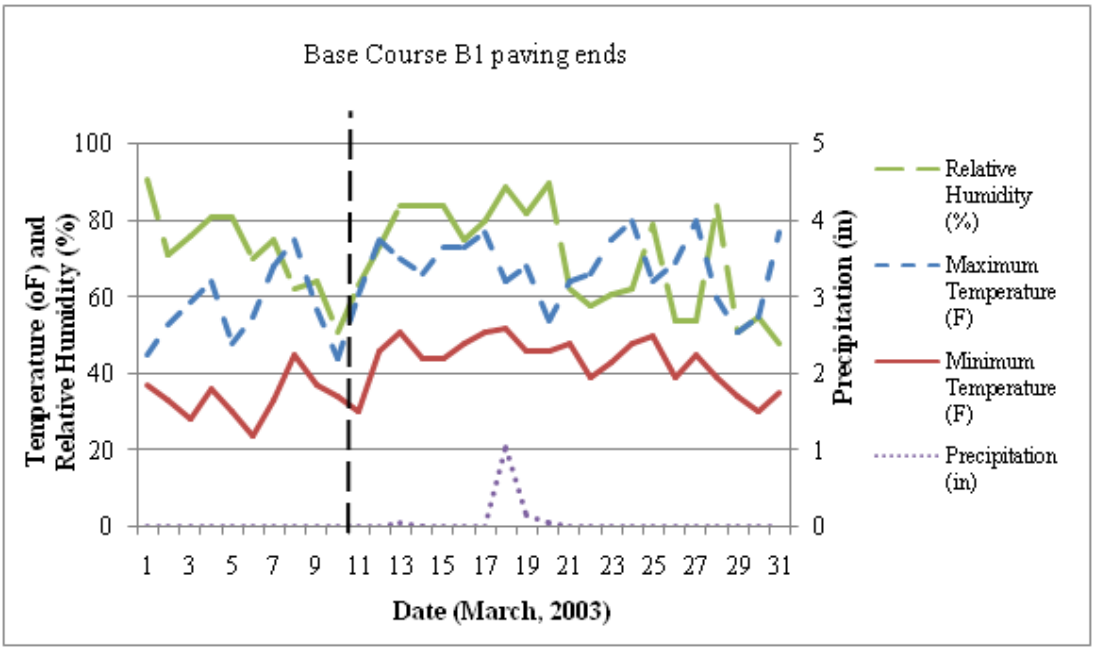

Figure A.6. Weather Data for RAP2 (March, 2003).

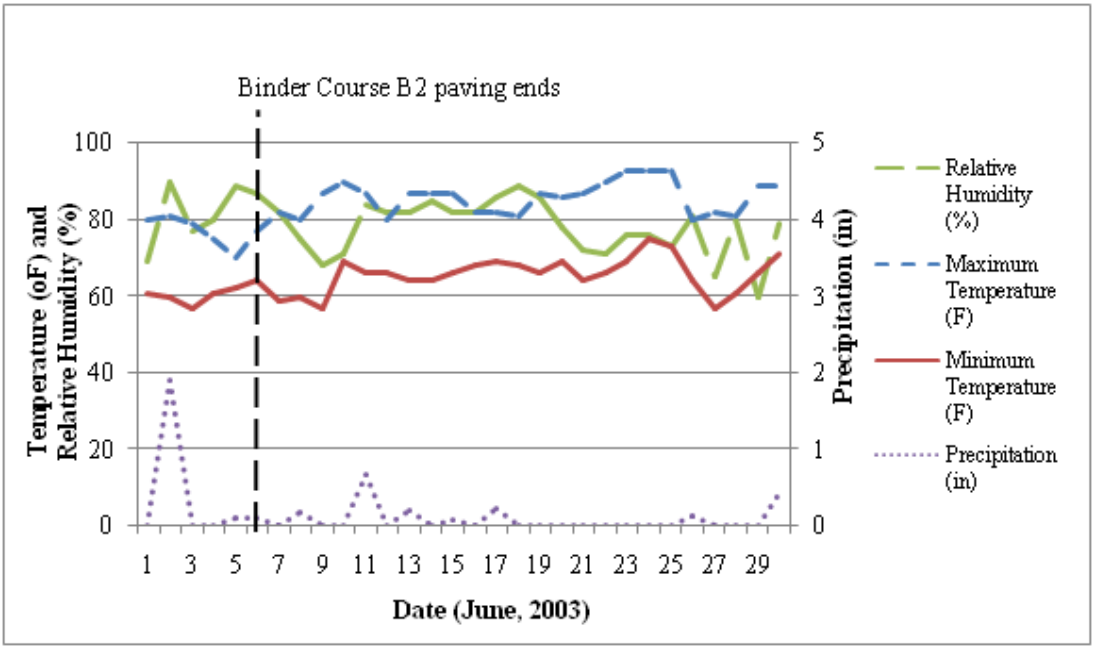

Figure A.7. Weather Data for RAP2 (June, 2003).

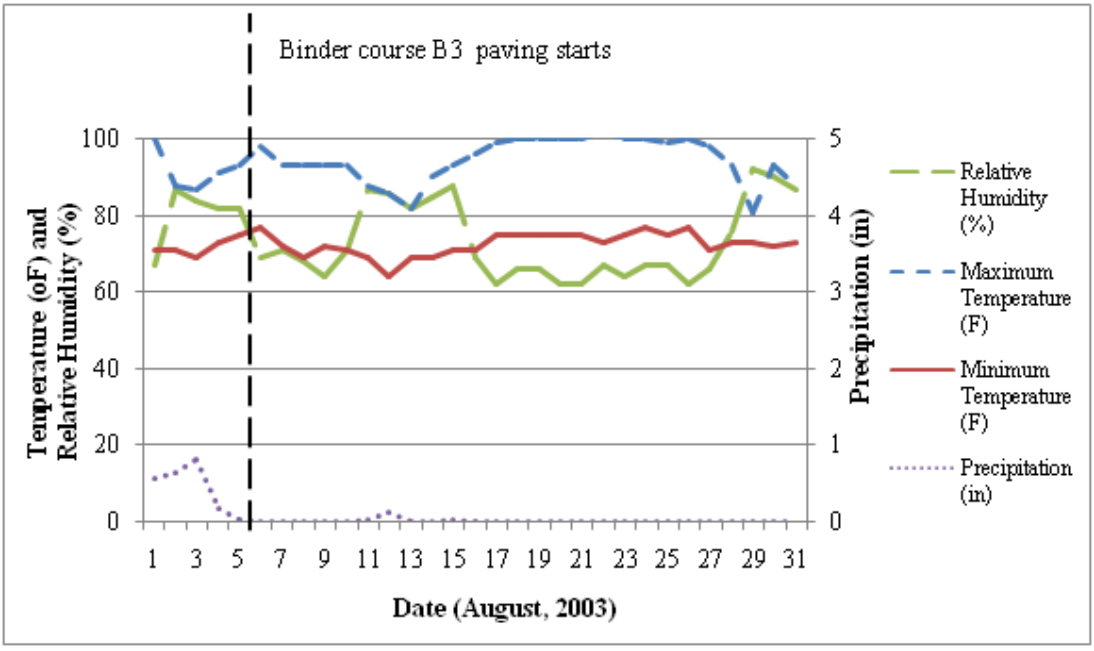

Figure A.8. Weather Data for RAP2 (August, 2003).

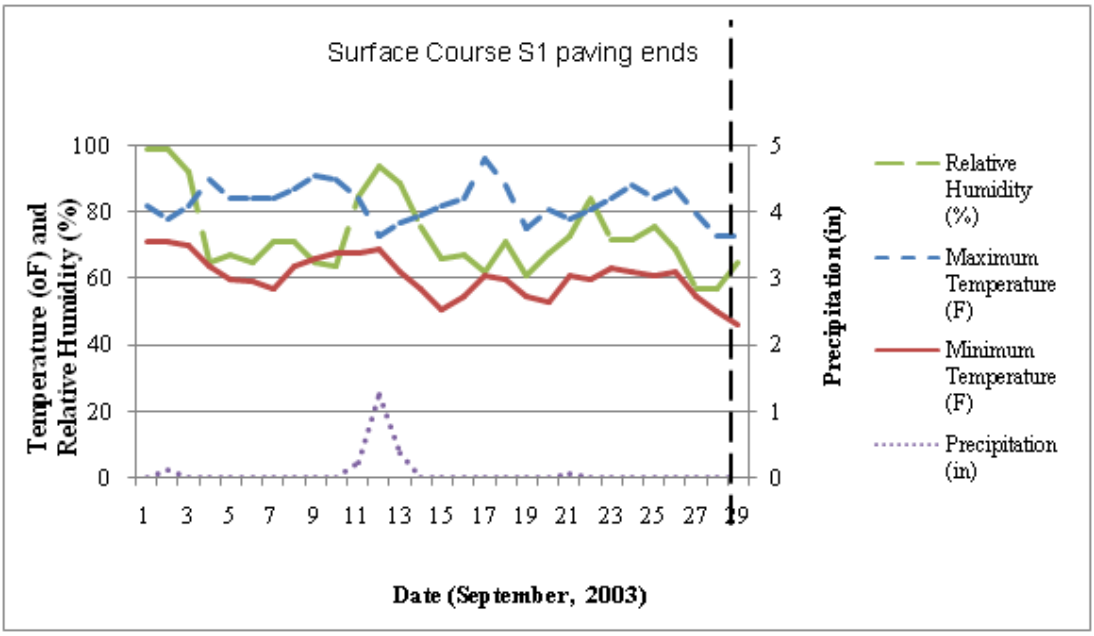

Figure A.9. Weather Data for RAP2 (September, 2003).

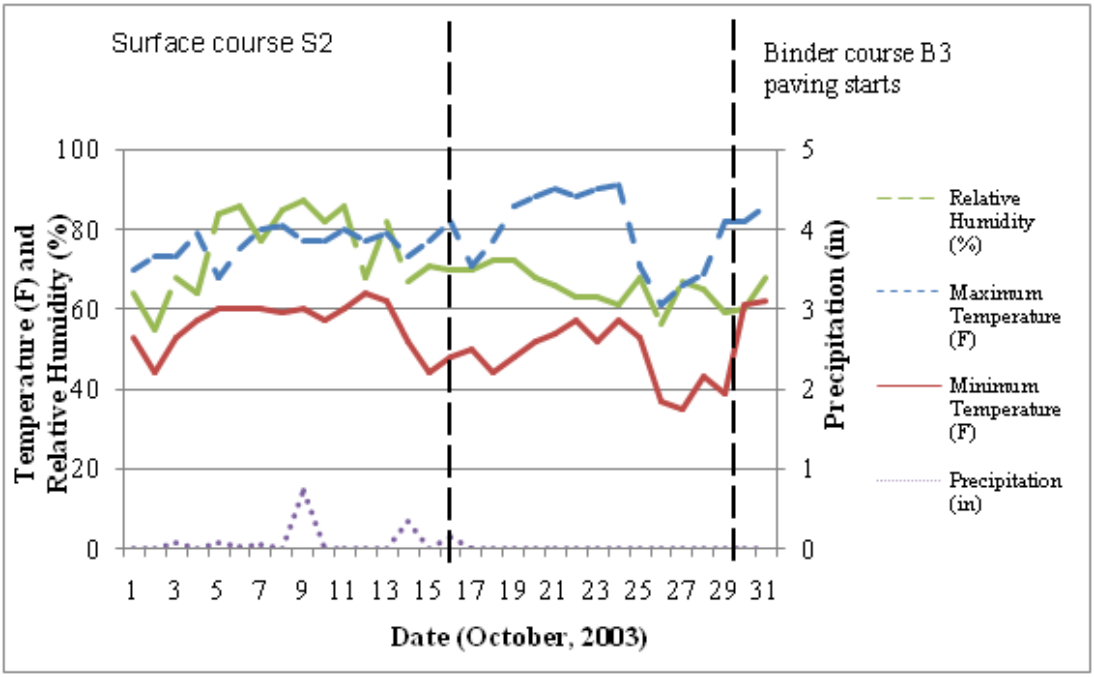

Figure A.10. Weather Data for RAP2 (October, 2003).

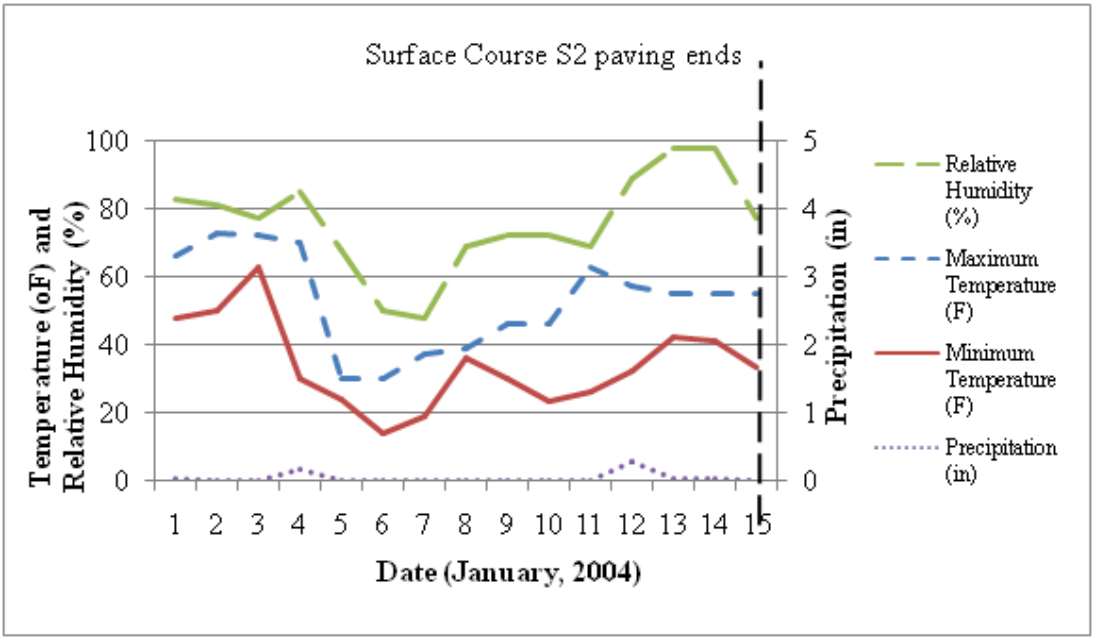

Figure A.11. Weather Data for RAP2 (January, 2004).

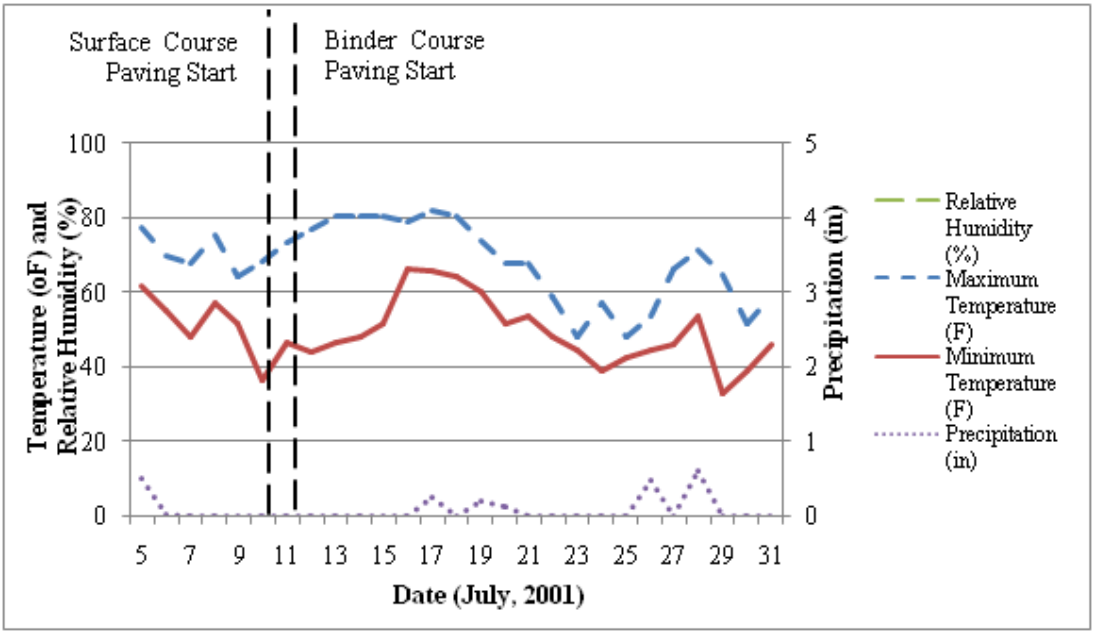

Figure A.12. Weather Data for RAP3 (July, 2001).

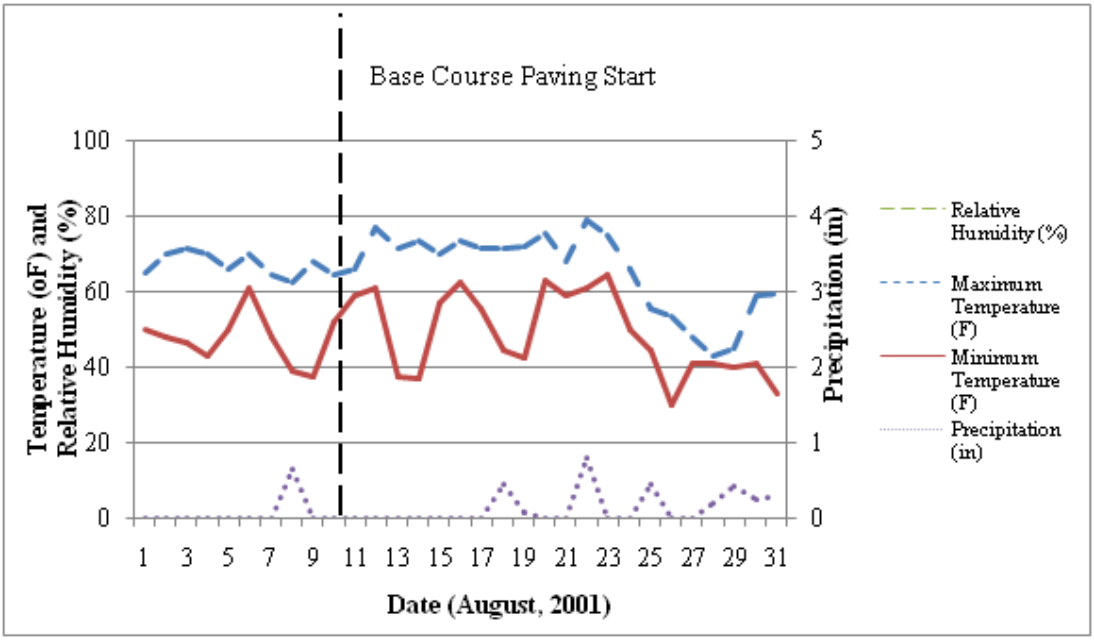

Figure A.13. Weather Data for RAP3 (August, 2001).

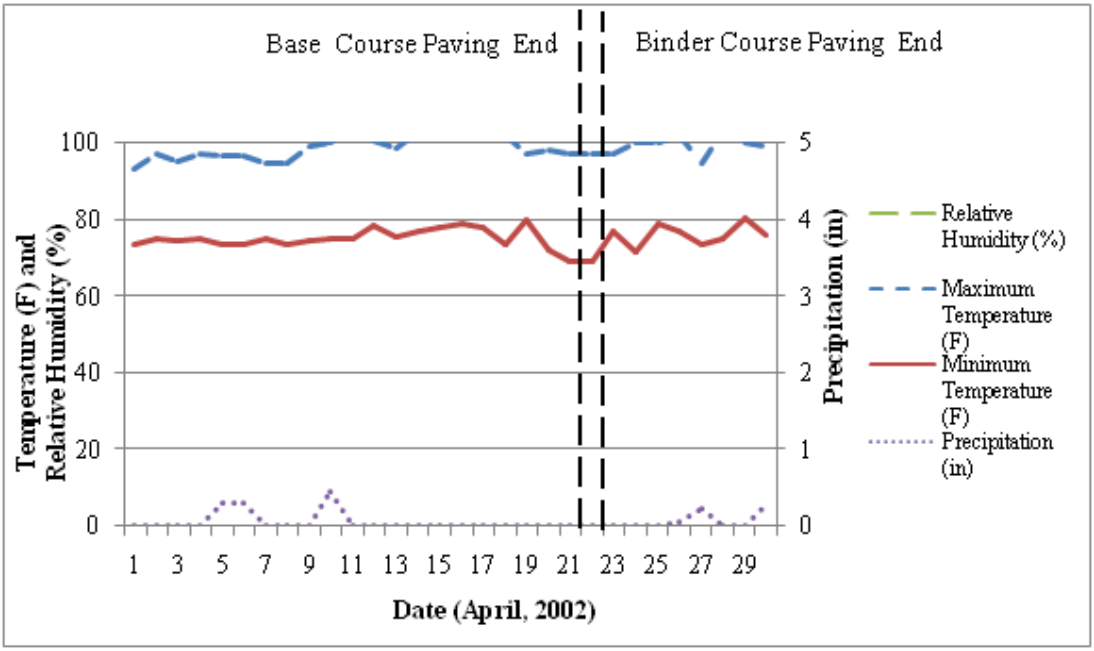

Figure A.14. Weather Data for RAP3 (April, 2002).

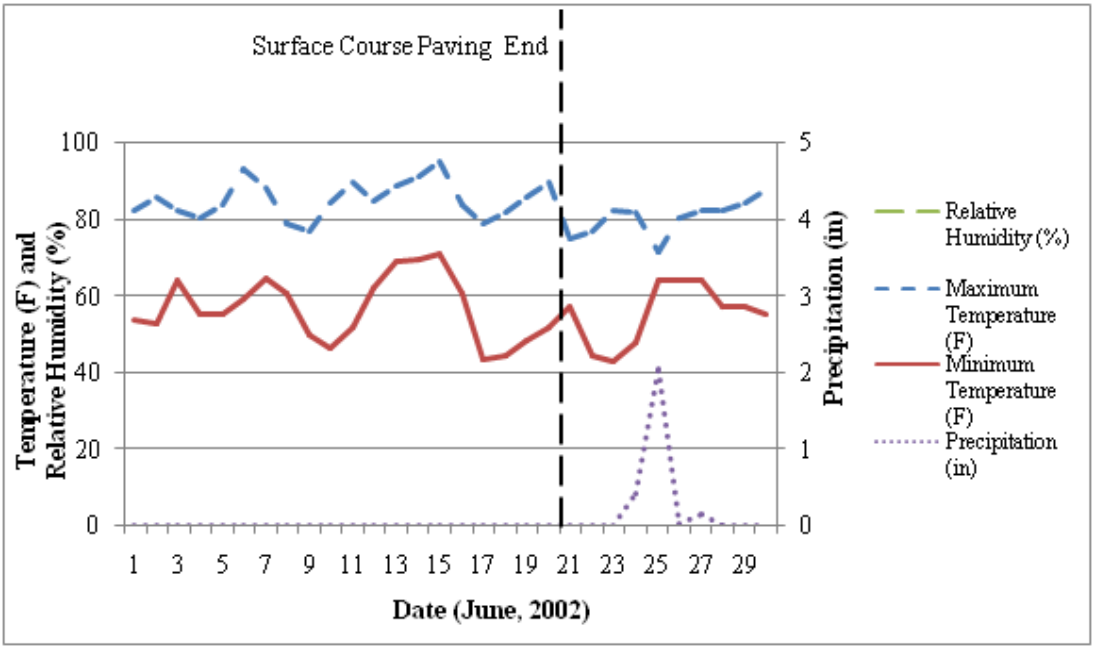

Figure A.15. Weather Data for RAP3 (June, 2002).

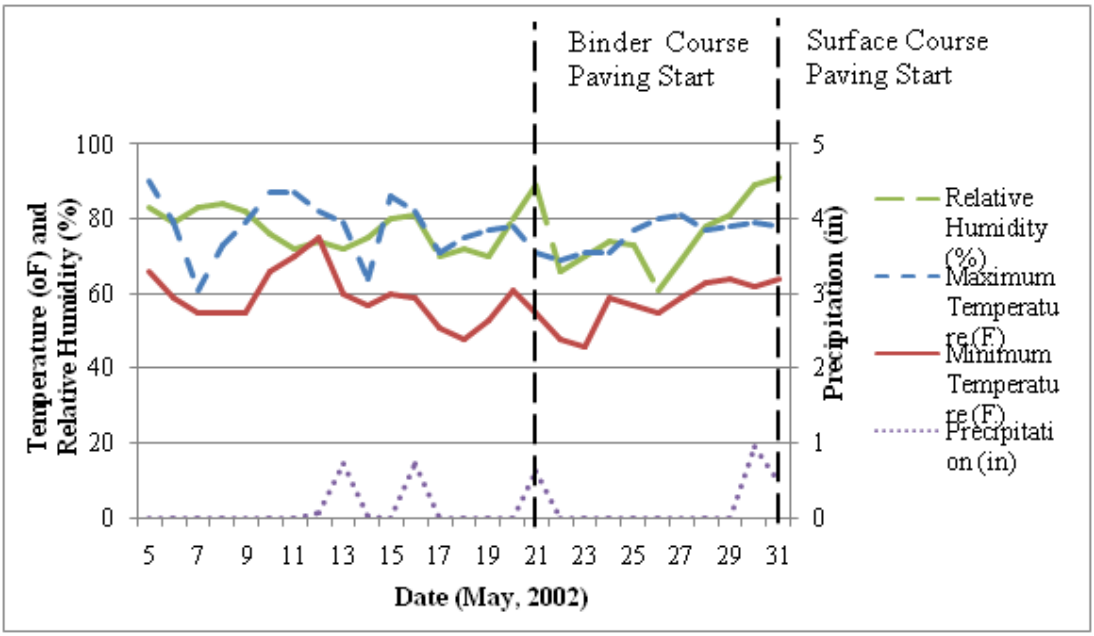

Figure A.16. Weather Data for RAP4 (May, 2002).

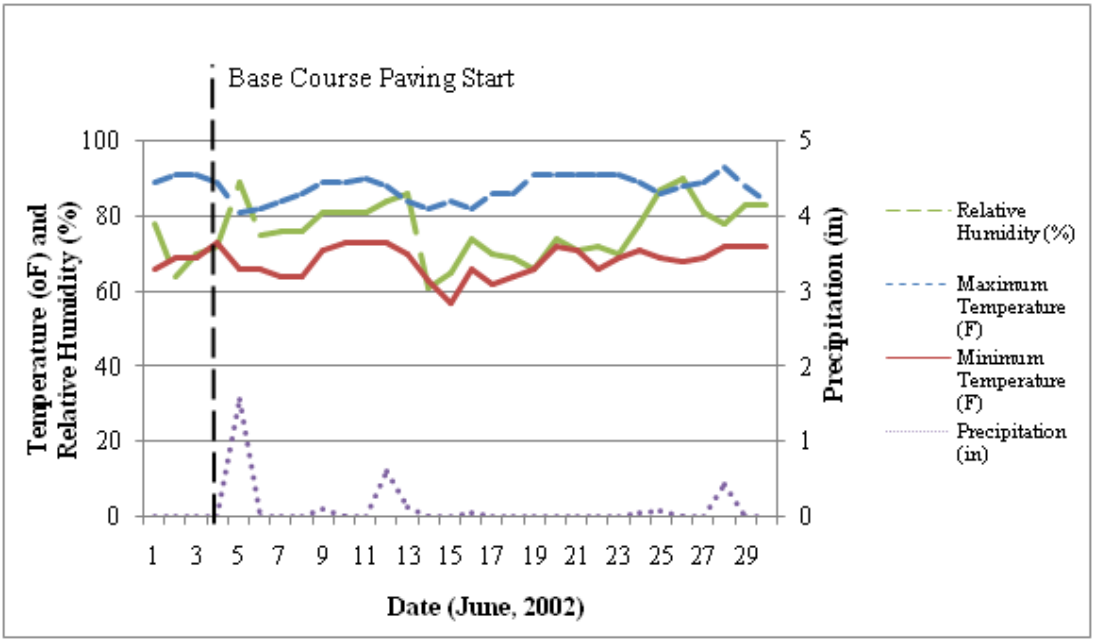

Figure A.17. Weather Data for RAP4 (June, 2002).

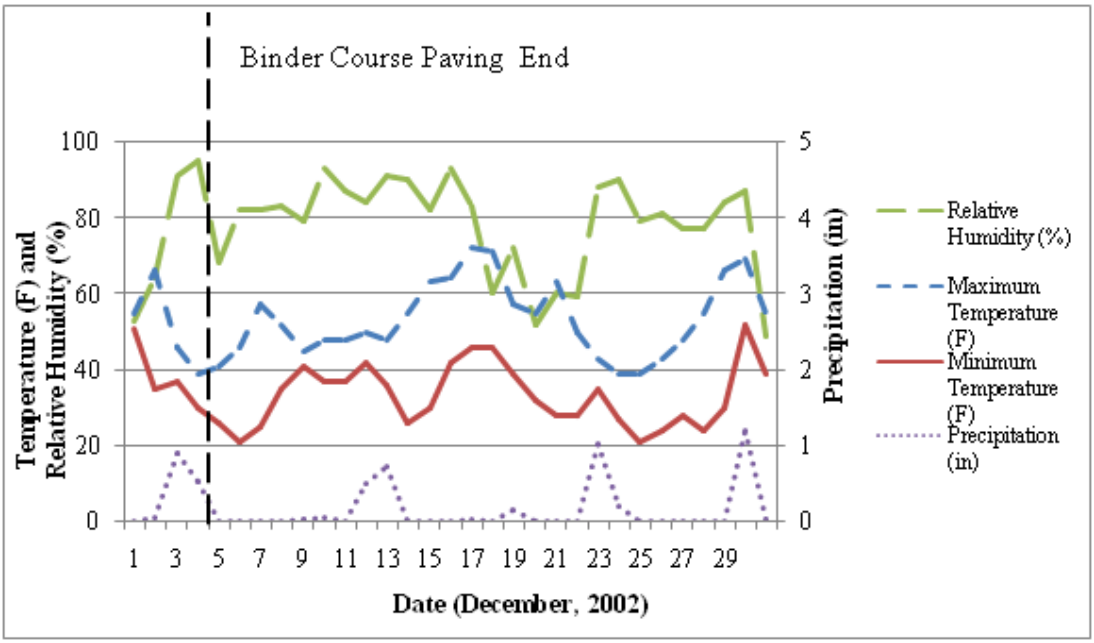

Figure A.18. Weather Data for RAP4 (December, 2002).

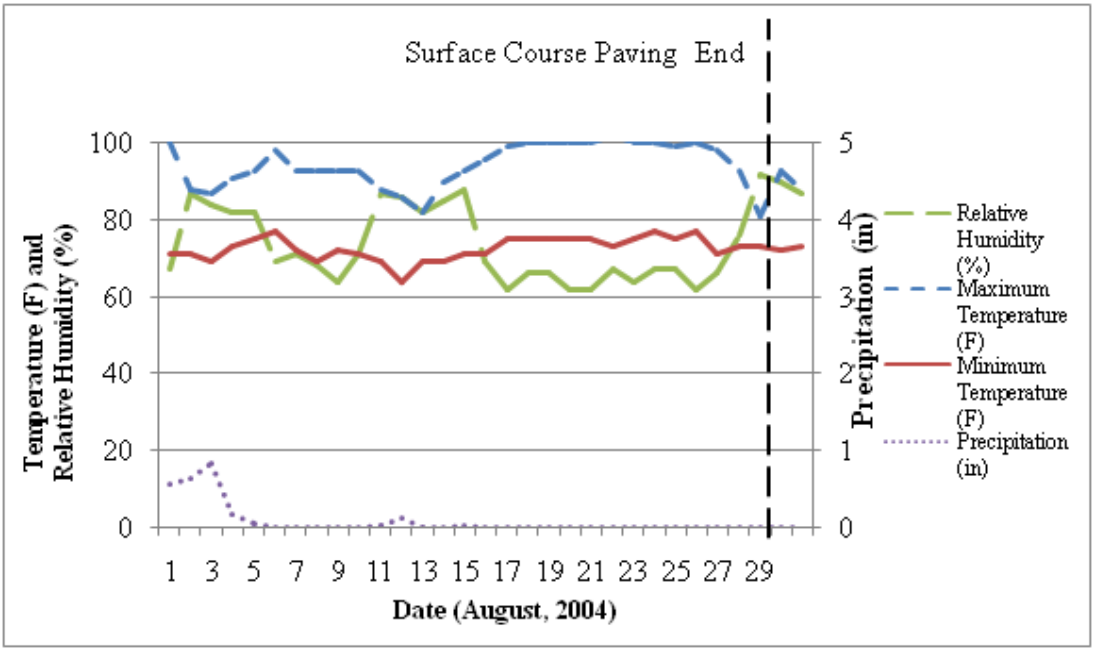

Figure A.19. Weather Data for RAP4 (August, 2004).

APPENDIX B. VISCOSITY DATA

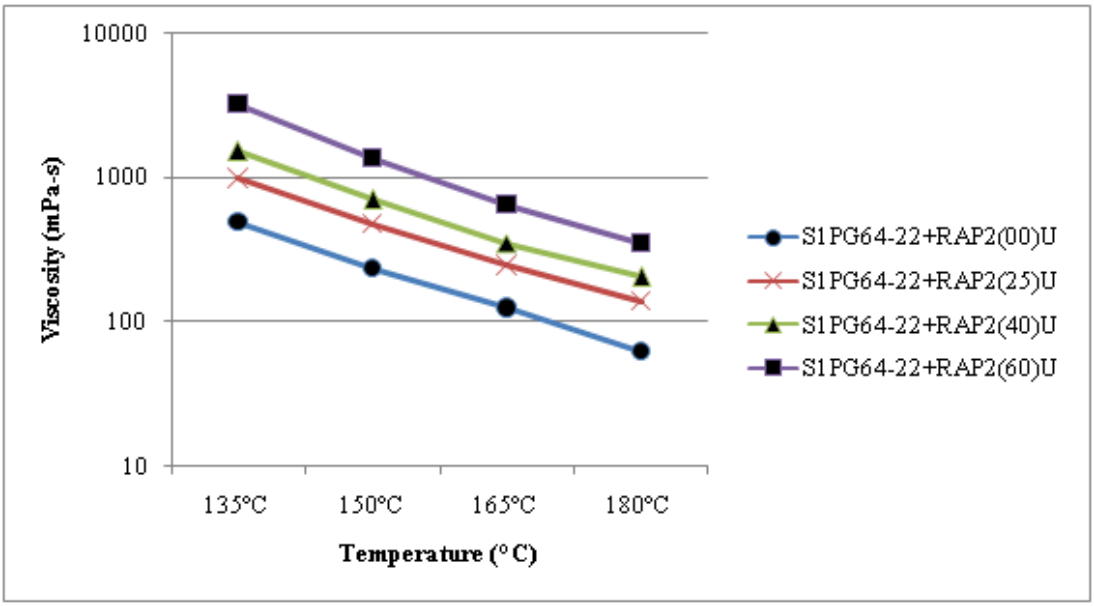

Figure B.20. Viscosity of RAP2 Binder Blends.

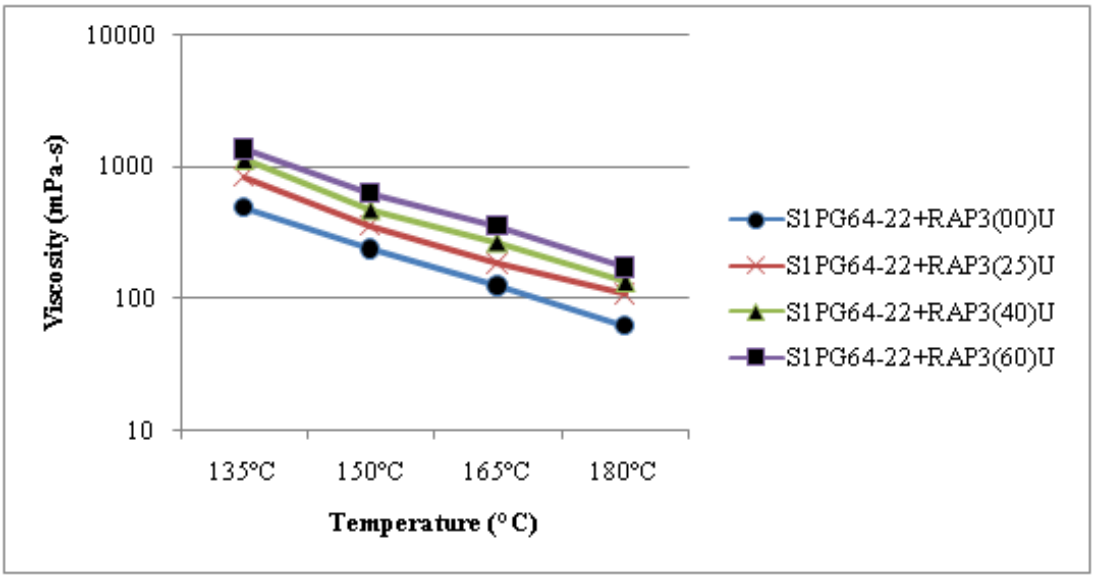

Figure B.21. Viscosity of RAP3 Binder Blends.

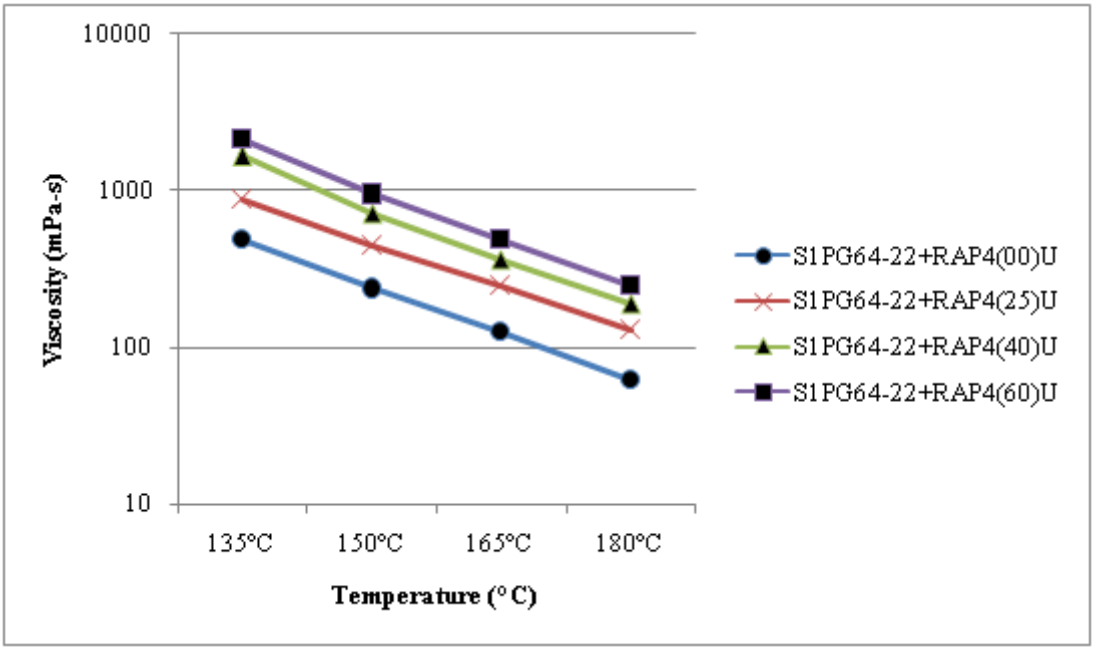

Figure B.22. Viscosity of RAP4 Binder Blends.

APPENDIX C. PG TEMPERATURE CALCULATION

Table C.5. Calculation of Low PG Temperature for 25% RAP1

Temp. (°C)	m-value at 60 s of load		Avg. m-value	Std. dev.	Stiffness at 60 s, MPa		Avg. Stiff., (MPa)	Std. dev.
	Sample 1	Sample 2			Sample 1	Sample 2		
-9	0.329	0.319	0.324	0.007071	124	127	125.5	2.12132
-12	0.3	0.298	0.299	0.001414	188	184	186	2.828427

T at m60 = 0.3	-11.88	Â°C		T at Stiffness, 300 MPa	-17.653	Â°C
Low PG grade Temp = T at m60 - 10	**-21.88**	**Â°C**		**Low PG grade Temp = T at Stiffness, 300 MPa- 10**	**-27.653**	**°C**
	Low PG grade Temp =		**-21.88**	**Â°C**		

Table C.6. Calculation of Low PG Temperature for 40% RAP1

Temp. (°C)	m-value at 60 s of load		Avg. m-value	Std. dev.	Stiffness at 60 s, MPa		Avg. Stiff., (MPa)	Std. dev.
	Sample 1	Sample 2			Sample 1	Sample 2		
-6	0.337	0.321	0.329	0.01131	107	104	105.5	2.12132
-9	0.312	0.309	0.3105	0.00212	148	146	147	1.41421

T at m60 = 0.3	-10.703	Â°C		T at Stiffness, 300 MPa	-20.06	Â°C
Low PG grade Temp = T at m60 - 10	**-20.703**	**Â°C**		**Low PG grade Temp = T at Stiffness, 300 MPa- 10**	**-30.06**	**Â°C**
	Low PG grade Temp =		**-20.703**	**Â°C**		

Table C.7. Calculation of Low PG Temperature for 60% RAP1

Temp. (°C)	m-value at 60 s of load		Avg. m-value	Std. dev.	Stiffness at 60 s, MPa		Avg. Stiff., (MPa)	Std. dev.
	Sample 1	Sample 2			Sample 1	Sample 2		
-6	0.334	0.333	0.3335	0.000707	160	145	152.5	10.6066
-9	0.309	0.313	0.311	0.002828	240	227	233.5	9.192388

T at m60 = 0.3	-10.467	Â°C		T at Stiffness, 300 MPa	-11.46	Â°C
Low PG grade Temp = T at m60 - 10	**-20.467**	**Â°C**		**Low PG grade Temp = T at Stiffness, 300 MPa- 10**	**-21.46**	**Â°C**
	Low PG grade Temp =		**-20.467**	**Â°C**		

Table C.8. Calculation of Low PG Temperature for 25% RAP2

Temp. (°C)	m-value at 60 s of load		Avg. m-value	Std. dev.	Stiffness at 60 s, MPa		Avg. Stiff., (MPa)	Std. dev.
	Sample 1	Sample 2			Sample 1	Sample 2		
-9	0.321	0.343	0.332	0.015556	129	125	127	2.828427
-12	0.302	0.294	0.298	0.005657	186	188	187	1.414214

T at m60 = 0.3	-11.82	Â°C		T at Stiffness, 300 MPa	-17.65	Â°C
Low PG grade Temp = T at m60 - 10	**-21.82**	**Â°C**		**Low PG grade Temp = T at Stiffness, 300 MPa- 10**	**-27.65**	**Â°C**
	Low PG grade Temp =		**-21.824**	**Â°C**		

Table C.9. Calculation of Low PG Temperature for 40% RAP2.

Temp. (°C)	m-value at 60 s of load		Avg. m-value	Std. dev.	Stiffness at 60 s, MPa		Avg. Stiff., (MPa)	Std. dev.
	Sample 1	Sample 2			Sample 1	Sample 2		
-9	0.303	0.305	0.304	0.001414	137	136	136.5	0.707107
-12	0.289	0.282	0.2855	0.00495	187	184	185.5	2.12132

T at m60 = 0.3	-9.65	Â°C		T at Stiffness, 300 MPa	-19.01 Â°C
Low PG grade Temp = T at m60 - 10	**-19.65**	**Â°C**		**Low PG grade Temp = T at Stiffness, 300 MPa- 10**	**-29.01 Â°C**
	Low PG grade Temp =		**-19.649**	**Â°C**	

Table C.10. Calculation of Low PG Temperature for 60% RAP2

Temp. (°C)	m-value at 60 s of load		Avg. m-value	Std. dev.	Stiffness at 60 s, MPa		Avg. Stiff., (MPa)	Std. dev.
	Sample 1	Sample 2			Sample 1	Sample 2		
-9	0.328	0.296	0.312	0.022627	145	149	147	2.828427
-12	0.289	0.284	0.2865	0.003536	239	235	237	2.828427

T at m60 = 0.3	-10.41	Â°C		T at Stiffness, 300 MPa	-14.1	Â°C
Low PG grade Temp = T at m60 - 10	**-20.41**	**Â°C**		**Low PG grade Temp = T at Stiffness, 300 MPa- 10**	**-24.1**	**Â°C**
	Low PG grade Temp =		**-20.412**	**Â°C**		

Table C.11. Calculation of Low PG Temperature for 25% RAP3

Temp. (°C)	m-value at 60 s of load		Avg. m-value	Std. dev.	Stiffness at 60 s, MPa		Avg. Stiff., (MPa)	Std. dev.
	Sample 1	Sample 2			Sample 1	Sample 2		
-9	0.324	0.317	0.3205	0.00495	136	121	128.5	10.6066
-12	0.316	0.314	0.315	0.001414	187	163	175	16.97056

T at m60 = 0.3	-20.18	Â°C		T at Stiffness, 300 MPa	-20.06	Â°C
Low PG grade Temp = T at m60 - 10	**-30.18**	**Â°C**		**Low PG grade Temp = T at Stiffness, 300 MPa- 10**	**-30.06**	**Â°C**
	Low PG grade Temp =		**-30.065**	**Â°C**		

Table C.12. Calculation of Low PG Temperature for 40% RAP3

Temp. (°C)	m-value at 60 s of load		Avg. m-value	Std. dev.	Stiffness at 60 s, MPa		Avg. Stiff., (MPa)	Std. dev.
	Sample 1	Sample 2			Sample 1	Sample 2		
-6	0.332	0.33	0.331	0.001414	104	104	104	0
-9	0.314	0.31	0.312	0.002828	148	144	146	2.828427

T at m60 = 0.3	-10.89	Â°C	T at Stiffness, 300 MPa	-20	Â°C
Low PG grade Temp = T at m60 - 10	**-20.89**	**Â°C**	**Low PG grade Temp = T at Stiffness, 300 MPa- 10**	**-30**	**Â°C**
Low PG grade Temp =	**-20.89**	**Â°C**			

Table C.13. Calculation of Low PG Temperature for 60% RAP3

Temp. (°C)	m-value at 60 s of load		Avg. m-value	Std. dev.	Stiffness at 60 s, MPa		Avg. Stiff., (MPa)	Std. dev.
	Sample 1	Sample 2			Sample 1	Sample 2		
-6	0.32	0.317	0.3185	0.002121	127	134	130.5	4.949747
-9	0.307	0.299	0.303	0.005657	185	191	188	4.242641

T at m60 = 0.3	-9.58	Â°C	T at Stiffness, 300 MPa	-14.84	Â°C
Low PG grade Temp = T at m60 - 10	**-19.58**	**Â°C**	**Low PG grade Temp = T at Stiffness, 300 MPa- 10**	**-24.84**	**Â°C**
Low PG grade Temp =	**-19.581**	**Â°C**			

Table C.14. Calculation of Low PG Temperature for 25% RAP4

Temp. (°C)	m-value at 60 s of load		Avg. m-value	Std. dev.	Stiffness at 60 s, MPa		Avg. Stiff., (MPa)	Std. dev.
	Sample 1	Sample 2			Sample 1	Sample 2		
-9	0.315	0.313	0.314	0.001414	129	127	128	1.414214
-12	0.311	0.287	0.299	0.016971	182	179	180.5	2.12132

T at m60 = 0.3	-11.8	Â°C	T at Stiffness, 300 MPa	-18.83	Â°C
Low PG grade Temp = T at m60 - 10	**-21.8**	**Â°C**	**Low PG grade Temp = T at Stiffness, 300 MPa- 10**	**-28.83**	**Â°C**
Low PG grade Temp =	**-21.8**	**Â°C**			

Table C.15. Calculation of Low PG Temperature for 40% RAP4

Temp. (°C)	m-value at 60 s of load		Avg. m-value	Std. dev.	Stiffness at 60 s, MPa		Avg. Stiff., (MPa)	Std. dev.
	Sample 1	Sample 2			Sample 1	Sample 2		
-6	0.312	0.311	0.3115	0.000707	120	119	119.5	0.707107
-9	0.288	0.286	0.287	0.001414	168	167	167.5	0.707107

T at m60 = 0.3	-7.408	Â°C		T at Stiffness, 300 MPa	-17.281	Â°C
Low PG grade Temp = T at m60 - 10	**-17.408**	**Â°C**		**Low PG grade Temp = T at Stiffness, 300 MPa- 10**	**-27.281**	**Â°C**
	Low PG grade Temp =	**-17.408**	**Â°C**			

Table C.16. Calculation of Low PG Temperature for 60% RAP4

Temp. (°C)	m-value at 60 s of load		Avg. m-value	Std. dev.	Stiffness at 60 s, MPa		Avg. Stiff., (MPa)	Std. dev.
	Sample 1	Sample 2			Sample 1	Sample 2		
-6	0.301	0.298	0.2995	0.002121	130	145	137.5	10.6066
-9	0.282	0.281	0.2815	0.000707	198	215	206.5	12.02082

T at m60 = 0.3	-5.917	Â°C
Low PG grade Temp = T at m60 - 10	**-15.917**	**Â°C**
T at Stiffness, 300 MPa	-13.064	Â°C
Low PG grade Temp = T at Stiffness, 300 MPa- 10	**-23.067**	**Â°C**
Low PG grade Temp =	**-15.917**	**Â°C**